Extended-soft-core Baryon-Baryon Model ESC16
I. Nucleon-Nucleon Scattering

M.M. Nagels and Th.A. Rijken
Institute of Mathematics, Astrophysics, and Particle Physics
Radboud University, Nijmegen, The Netherlands

Y. Yamamoto
Nishina Center for Accelerator-Based Science, Insitute for Physical and Chemical Research (RIKEN). Wako, Saitama, 351-0198, Japan

(Dated: version of: June 17, 2018)

Background: The Nijmegen extended-soft-core (ESC) model ESC16, as well as its predecessors ESC04-ESC08, describe the nucleon-nucleon (NN), hyperon-nucleon (YN), and hyperon-hyperon/nucleon (YY/Ξ N) interactions in a unified way using broken SU(3)-symmetry. SU(3)-symmetry serves to connect the NN with the YN and the YY channels. In the spirit of the Yukawa-approach to the nuclear force problem, the interactions are studied from the meson-exchange picture viewpoint, using generalized soft-core Yukawa-functions. The meson exchanges are supplemented with diffractive contributions due to multiple-gluon-exchanges. The extended-soft-core (ESC) meson-exchange interactions consist of local- and non-local-potentials due to (i) One-boson-exchanges (OBE), which are the members of nonets of pseudoscalar, vector, scalar, and axial-vector mesons, (ii) diffractive exchanges, (iii) two pseudo-scalar exchange (PS-PS), and (iv) meson-pair-exchange (MPE). The OBE- and MPE-vertices are regulated by gaussian form factors producing potentials with a soft behavior near the origin. The assignment of the cut-off masses for the BBM-vertices is dependent on the SU(3)-classification of the exchanged mesons for OBE, and a similar scheme for MPE.

Purpose: The evolution of the ESC approach to the ESC16 model for the baryon-baryon (BB) interactions of the SU(3) flavor-octet of baryons (N, Λ, Σ, and Ξ) is described and presented. In this first of a series of papers, the NN model and results are reported in detail.

Methods: Important non-standard ingredients in the OBE-sector in the ESC-models are (i) the axial-vector meson potentials, and (ii) a zero in the scalar- and axial-vector meson form factors. Furthermore, the strange scalar κ-meson is treated within the scheme of the Gell-Mann-Okubo mass relations, and like the ρ and ϵ treated as a broad meson. The multiple-gluon-exchanges are elaborated further by adding contributions due to odd number of gluon exchanges. A novel contribution is the incorporation of structural effects due to the quark-core of the baryons. In establishing the parameters of the model a simultaneous fit to NN- and YN-channels has been performed. The meson-baryon coupling constants are calculated via SU(3) using the coupling constants of the $NN \oplus YN$-analysis as input. In ESC16 the couplings are kept completely SU(3)-symmetric. About 25 physical coupling parameters and 8 cut-off and diffractive masses, were searched.

Results: In the fit to NN and YN many parameters are essentially fixed by the NN-data. A few, but severely constrained parameters, e.g. $F/(F+D)$-ratio's, are left for determination of the YN-interactions and the YY experimental indications. The simultaneous fit of the ESC-models to the NN- and YN- scattering data with a single set of parameters has achieved excellent results for the NN- and YN-data, and for the YY-data in accordance with the experimental indications for ΛΛ and ΞN. In the case of ESC16, the version discussed here, the achievements are: (i) For the selected 4313 pp and np scattering data with energies $0 \leq T_{lab} \leq 350$ MeV, the model reaches a fit having $\chi^2/N_{data} = 1.10$. (ii) The deuteron binding energy and all the NN scattering lengths are fitted very nicely. (iii) The YN-data are described very well with $\chi^2/N_{data} = 1.03$, giving at the same time a descriptions of the ΞN cross sections in agreement with the experimental indications.

Conclusions: The ESC aproach leads to an excellent description of the NN- and YN-data, and for the scarce YY-data. The added innovations as well as the treatment of mass broken SU(3) make it possible to keep the meson coupling parameters and the $F/(F+D)$-ratio's of the model qualitatively in accordance with the predictions of the $^3P_0$-dominated quark-antiquark pair creation (QPC) model. The information about estimates of (i) the Λ- and Σ-nuclear well-depth, and (ii) the ΛΛ hypernuclei played an important role in the form of using constraints. in particular, the experimental indications for the ΛΛ-attraction and the Σ-nuclear well-depth were directive.

PACS numbers: 13.75.Cs, 12.39.Pn, 21.30.+y

I. INTRODUCTION

In a new series of papers we present the results obtained with the recent ESC16-version of the Extended-Soft-Core (ESC) model [1] for nucleon-nucleon (NN), hyperon-nucleon (YN), and hyperon-hyperon (YY) interactions with $S = 0, -1, -2$. Moreover, we present predictions for the YY-channels with $S = -3, -4$.

The combined study of all baryon-baryon (BB) interactions, exploiting all experimental information hitherto available, both on BB-scattering and (hyper-)nuclear systems, might throw light on the basic mechanisms of these interactions. The program, which in its original form was formulated in Refs. [2, 3], pursuits the aims:

- To study the assumption of broken SU(3)-symmetry. For example we investigate the properties of the scalar mesons ($\varepsilon = f_0(620)$, $f_0(993)$, $\delta = a_0(962)$, $\kappa(861)$).
- To determine the $F/(F+D)$-ratio's [4].
- To study the connection between QCD, the quark-model, and low energy physics.
- To extract, in spite of the scarce experimental YN- and YY-data, information about scattering lengths, effective ranges, the existence of resonances and bound states, etc.
- To provide realistic baryon-baryon potentials, which can be applied in few-body calculations, nuclear- and hyperonic matter studies, neutron-stars;
- To extend the theoretical description to the baryon-baryon channels with strangeness S=-2. This in particular for the $\Lambda\Lambda$ and ΞN channels, where some data already exist, and for which experiments will be realized in the near future.
- Finally, to extend the theoretical description to all baryon-baryon channels with strangeness S=-3,-4. These will be parameter free predictions, and have, like the other BB-channels, relevance for the study of hyperonic matter and compact stars.

With this series of papers this program nears essentially its completion.

As has been amply demonstrated, see Refs. [5–9], the ESC-model interactions give excellent simultaneous descriptions of the NN and YN data. Also it turned out that the ESC-approach gives great improvements for the NN description as compared to the One-Boson-Exchange (OBE) models, e.g. [3, 10], and other existing models in the literature. The ESC16-model presents the culmination in this respect: the NN-model has a quality on equal par with the energy-dependent partial-wave analysis (PWA) [11, 12].

The ESC04-model papers [5–7] contain the first rather extensive exposition of the ESC-approach. As compared to the earlier versions of the ESC-model, we introduced in ESC04-models [5–7] several innovations: Firstly, we introduced a zero in the form factor of the mesons with P-wave quark-antiquark contents, which applies to the scalar and axial-vector mesons. Secondly, we exploited the exchange of the axial-vector mesons with $J^{PC} = 1^{++}$ and $J^{PC} = 1^{+-}$. Thirdly, we employed some $\Lambda\Lambda, \Xi N$ information.

In the ESC16-model on top of these improvements, we introduce in the ESC-approach for the first time: (i) Odderon-exchange $J^{PC} = 1^{--}$. Odderon-exchange represents the exchange of an odd-number of gluons at short-distance. This to complement pomeron-exchange which stands for the exchange of an even-number of gluons. (ii) Quark-core effects. The quark-core effects represent structural effects caused by the occurrence of Pauli-blocked configurations in two-baryon systems. These structural effects depend on the BB-channel and cannot be described by t-channel exchanges.
Furthermore, (iii) the axial-vector ($J^{PC} = 1^{++}$) mesons are treated with the most general vertices, and the $(\boldsymbol{\sigma}_1{\cdot}\mathbf{q})(\boldsymbol{\sigma}_2{\cdot}\mathbf{q})$-operator is evaluated in a superior mannner compared to ESC04. Not included are the potentials from the tensor ($J^{PC} = 2^{++}$) mesons. Attempts including the latter mesons did not lead to substantial potentials from these mesons or qualitative changes in the other contributions to the potentials. The results with the ESC08-model are reported in [8, 9]. With this simultaneous treatment of the NN, YN, and YY channels we have achieved a high quality description of the baryon-baryon interactions. The results, using a single set of meson and quark-core parameters, include: (a) a description of the NN-data with a $\chi^2_{pdp} = 1.10$ and good low energy parameters for the NN-channels including the binding energy E_B of the deuteron, (b) a very good fit to the YN-scattering data. (c) the fitting parameters with a clear physical significance, like e.g. the $NN\pi$-, $NN\rho$-couplings etc. and with realistic values of the $F/(F+D)$-ratio's α_P and α_V^m. The fitting has been done under the constraints of the G-matrix results for the ESC16-interactions. These show (i) satisfactory well-depth values for $U_\Lambda < 0, U_\Sigma > 0$, and $U_\Xi < 0$, (ii) proper spin-spin ($U_{\sigma\sigma} \geq 1$), and small spin-orbit interactions for ΛN. All these features are in agreement with the Hyperball-data [13] and the NAGARA-event [14].

In this first paper of the series, we display and discuss the NN results of the simultaneous fit to the NN- and YN-data, including some $\Lambda\Lambda, \Xi N$ and ΣN information from hypernuclei, using a single set of parameters. In the second paper, henceforth referred to as II [15], we report on the results for strangeness S=-1 YN-channels, using the same simultaneous fit of the NN- and YN-data. This simultaneous fitting procedure was first introduced in [6], and its importance and advantages will be discussed in II. In the third paper, henceforth referred to as III [16], we report on the results and predictions for YY with strangeness $S = -2$. Finally, in the fourth paper (IV), we describe the predictions for YY with strangeness $S = -3, -4$.

The contents of this paper are as follows. In section II a description of the physical background and dynamical contents of the ESC16-model is given. In section III the two-body integral equations in momentum space are discussed. Also, the expansion into Pauli-spinor invariants is reviewed. In section IV the ESC-potentials in momentum and configuration space for non-strange mesons are discussed in detail. In particular the new potentials are given. Section V contains some brief remarks on the ESC-couplings and the QPC-model. In section VI the simultaneous $NN \oplus YN \oplus YY$ fitting procedure is reviewed. Here, also the results for the coupling constants and $F/(F+D)$-ratios for OBE and MPE are given. In section VII the NN-results for the ESC16-model are displayed.

In section VIII we discuss the results and draw some conclusions. In appendix A the B-field formalism for vector- and axial-vector mesons is described. The exact treatment of the non-local-tensor operator is explained in appendix B. In appendix C the realization of the B-field condition, i.e. the conservation of the the axial-vector current, is analyzed in the context of the ESC-model. In appendix D the treatment of the non-local tensor potential is reviewed. In appendix E the basic formulas for the configuration space gaussian-yukawa functions are given.

II. PHYSICAL CONTENT OF THE ESC-MODEL

The general physical basis, within the context of QCD, for the Nijmegen soft-core models has been outlined in the introduction of [5]. The description of baryon-interactions at low energies in terms of baryons and mesons can be reached through the following stages: (i) The strongly interacting sector of the standard-model (SM) contains three families of quarks: (ud), (cs), (tb). (ii) Integrating out the heavy quarks (c,b,t) leads to a QCD-world with effective interactions for the (u,d,s) quarks. (iii) This QCD-world is characterized by a phase transition of the vacuum. Thereby the quarks gets dressed and become the so-called constituent quarks. The emerging picture is that of the constituent-quark-model (CQM) [17]. The phase transition has transformed the effective QCD-world into an complex hadronic-world. (iv) The strong coupling lattice QCD (SCQCD) seems to be a proper model to study the low energy meson-baryon and baryon-baryon physics, see [18] for applications and references. Here the lattice spacing $a \geq 0.11$ fm provides a momentum scale for which the QCD coupling $g \geq 1.1$. Emerging is a picture where the meson-baryon coupling constants get large, and quark-exchange effects are rather small. The latter is due to the suppression due to the gluonic overlaps involved. For a similar reason it has been argued [19] that the pomeron is exchanged between the individual quarks of the baryons. In this picture the Nijmegen soft-core approach to baryon-baryon interactions has a natural motivation. (v) For the mesons we restrict ourselves to mesons with $M \leq 1.5$ GeV$/c^2$, arriving at a so-called *effective field theory* as the arena for our description of the low energy baryon-baryon scattering.

In view of the success of QCD, pseudo-scalar dominance of the divergence of the axial-vector current (PCAC) leading to small light ("current") quark masses [20, 21], the spectroscopic success of the CQM, where the quarks have definite color charges, in generating the masses of the pseudo-scalar and vector nonets, and the masses and magnetic moments of the baryon octet is rather surprising [22, 23]. The transition from "current" to "constituent" quarks comes from dressing the quark fields in the original QCD Lagrangian, see e.g. Refs. [17, 24, 25].

In all works of the Nijmegen group on the baryon-baryon models, (broken) SU(3) flavor-symmetry is explored to connect the NN, YN, and YY channels, making possible a simultaneous fitting of all the available BB-data using a single set of model-parameters. The dynamical basis is the (approximate) permutation symmetry w.r.t. the constituent (u,d,s)-quarks. This has its roots in the approximate equality of the quark-masses, and more importantly that the gluons have no flavor. This enables the calculation of the baryon-baryon-meson coupling constants using as parameters the nucleon-nucleon-meson couplings and the $F/(F+D)$-ratio's. This provides a strong correlation between the (rich) nucleon-nucleon- and the (scarce) hyperon-nucleon-data.

The obtained coupling constants of the BBM-vertices are interpreted studying the predictions of the constituent quark-model (CQM) in the form of the quark-antiquark pair creation model (QPC). It has been argued that the ${}^3P_0$-mechanism [26, 27] is dominant over the ${}^3S_1$-mechanism in lattice QCD [28]. It turned out that the fitted coupling constants in ESC04 and ESC16 indeed follow mainly the pattern of couplings set by the ${}^3P_0$-model. Also, all $\alpha = F/(F+D)$-ratios are required to deviate no more than 0.1 from the QPC-model predictions for the BBM- and the BB-Meson-Pair vertices. Although it is in principle attractive to study the SU(3)-breaking of the BBM-couplings using the QPC-model, as has been explored in ESC04 [6], in ESC16 the couplings are treated as SU(3)-symmetric. In the Nijmegen soft-core OBE- and ESC-models the BBM-vertices are described by coupling constants and gaussian form factors. Given the fact that in the CQM the quark wave functions for the baryons are very much like ground state harmonic oscillator functions, a gaussian behavior of the form factors is most natural. These form factors guarantee a soft behavior of the potentials in configuration space at small distances. The cut-off parameters in the form factors depend only on the type of meson (pseudoscalar, vector, etc.). Within a meson SU(3)-multiplet we distinguish between octet and singlet form factors. Since there is singlet-octet mixing for the I=0 mesons, we attribute the singlet and octet cut-off to the dominant singlet or octet particle respectively. For the considered nonets the singlet and octet cut-off's are the same or close.

In this way we have full predictive power for the $S = -2, -3, -4$ baryon-baryon channels, e.g. $\Lambda\Lambda, \Xi N$-channels which involve the singlet $\{1\}$-irrep that does not occur in the NN and YN channels.

Field theory allows both linear and non-linear realizations of chiral-symmetry (CS) [29–31]. At low-energy phenomenologically the non-linear realization is the most economical and natural. Therefore, we have chosen the pv-coupling and not the ps-coupling for the pseudoscalar mesons. This choice affects some $1/M^2$-terms in the ps-ps-exchange potential, In ESC04 we tested mixtures of the pv- and ps-coupling, but in ESC16 we use only the pv-coupling. In the non-linear realization chiral-symmetry for the couplings of the scalar-, vector-, axial-vector-, etc. mesons is realized through isospin-symmetry SU(2,I) [30, 31].

A. Potentials ESC-model

The potentials of the ESC-model are generated by (i) One-Boson-Exchange (OBE), (ii) uncorrelated Two-Meson-Exchange (TME), (iii) Meson-Pair-Exchange (MPE), (iv) Diffractive/Multi-gluon Exchange, (v) Quark-Core Effects (QCE).

(i) The OBE-part of the dynamical contents of the ESC16-model is determined by the following meson-exchanges:

(a) $J^{PC} = 0^{--}$: The pseudoscalar-meson nonet $\pi,\ \eta,\ \eta',\ K$ with the $\eta-\eta'$ mixing angle $\theta_P = -11.4^0$ [32], close to the Gell-Mann-Okubo (GMO) quadratic mass formula [33].

(b) $J^{PC} = 1^{--}$: The vector-meson nonet $\rho,\ \phi,\ K^\star,\ \omega$ with the $\phi-\omega$ mixing angle $\theta_V = 39.1^0$ [32] This follows from the quadratic GMO mass-formula, and is close to ideal mixing.

(c) $J^{PC} = 1^{++}$: The axial-vector-meson nonet $a_1, f_1,\ K_{1A}, f_1'$ with the $f_1 - f_1'$ mixing angle $\theta_A = 50.0^0$ [34].

(d) $J^{PC} = 0^{++}$: The scalar-meson nonet $a_0(962) = \delta, f_0(993) = S^\star, \kappa(861), f_0(620) = \varepsilon$ [35]. The scalar $S^\star-\varepsilon$ mixing angle $\theta_S = 44.0^0$ is fitted and deviates from the ideal mixing angle $\theta_S = 35.26^0$. The $\kappa(861)$ mass is determined via GMO.

(e) $J^{PC} = 1^{+-}$: The axial-vector-meson nonet $b_1, h_1,\ K_{1B}, h_1'$ with the $h_1 - h_1'$ ideal mixing angle $\theta_B = 35.26^0$. (Furthermore $K_{1,A}$ and $K_{1,B}$ are completely mixed.)

The soft-core approach of the OBE has been given originally for NN in [36], and for YN in [3]. With respect to these OBE-interactions the ESC-models contain the modification of the form factor by introducing a zero for the mesons being P-wave quark-antiquark states in the CQM: the scalar- and axial-vector-mesons. Such a zero is natural in the $^3P_0$-quark-pair-creation (QPC) [26, 27] model for the coupling of the mesonic quark-antiquark ($Q\bar{Q}$) system to baryons. A consequence of such a zero is that a bound state in Λp-scattering is less likely to occur.

(ii) The configuration space soft-core uncorrelated two-meson exchange for NN has been derived in [37, 38]. Similarly to ESC04, also in ESC16 we use these potentials for ps-ps exchange with a complete SU(3)-symmetric treatment in NN, YN and YY. For example, we include double K-exchange in NN-scattering. Since this includes two-pion exchange (TPE) the long-range part of the potentials are represented. Here it is tacitly assumed that other TME potentials, like ps-vc, ps-sc, etc., are either small due to cancellations, or can be described adequately by using effective couplings in the OBE-potentials. When these effective couplings do not deviate from experimentally determined couplings it may be assumed that the corrections from these other SU(3) meson-nonets in the TME potentials are small. This is our working hypothesis for the TME-potentials. From the point of view of SU(3), since OBE contains only $\{8\}$- and $\{1\}$-exchange, TME can not be represented completely in terms of OBE. This because TME also has $\{27\}-, \{10\}$-, and $\{10^*\}$-exchange components. Therefore, the predictions made by the ESC-models could be sensitive to this incompleteness of TME in the ESC-models. At present the BB-data and the hypernuclear-data do not give information at this point.

(iii) Meson-pair exchanges (MPE) have been introduced in [1] for NN and described in detail in [39]. The two-meson-baryon-baryon vertices are the low energy approximations of (a) the heavy-meson and their two-meson decays, and (b) baryon-resonance contributions Δ_{33} etc [34, 39].

(iv) Diffractive contributions to the soft-core potential have been introduced from the beginning, cfr. [36]. The pomeron is thought of being related to an even number of gluon-exchanges. Here we introduce the odderon-potential, which is related to an odd number of gluon exchanges.

(a) $J^{PC} = 0^{++}$: The 'diffractive' contribution from the pomeron (P), which is a unitary singlet. These interactions give a repulsive contribution to the potentials in all channels of a gaussian type.

(b) $J^{PC} = 1^{--}$: The 'diffractive' contribution from the odderon (O). The origin of the odderon is assumed to be purely the exchange of the color-singlets with an odd number of gluons. Similarly to the pomeron, the odderon potential is taken to be an SU(3) singlet and of the gaussian form.

As an explanation of the repulsive character of the pomeron-potential the following: The J^{PC} is identical to that for the scalar-mesons. Naively, one would expect an attractive central potential.

However, considering the two-gluon model for the pomeron [40, 41] the two-gluon parallel and crossed diagram contributions to the BB-interaction can be shown to cancel adiabatically. The remaining non-adiabatic contribution is repulsive [42].

(v) Quark-Core-Effects in the soft-core model can supply extra repulsion, which may be required in some BB-channels. Baryon-baryon studies with the soft-core OBE and ESC-models thus far show that it is difficult to achieve a strongly enough repulsive short-range interactions in (i) the $\Sigma^+p(I = 3/2,^3S_1)$- and (ii) the $\Sigma N(I = 1/2,^1S_0)$-channel. The short-range repulsion in baryon-baryon may in principle come from: (a) meson- and multi-gluon-exchange [5, 6], and/or (b) the occurrence of forbidden six-quark SU(6)-states by the Pauli-principle [43–45]. In view of the mentioned difficulties, we have developed a phenomenological method for the ESC-model, which enables us to incorporate this quark-structural effect. This is an important new ingredient of the here presented ESC16-model. This structural effect we describe phenomenologically by gaussian repulsions, similar to the pomeron. In the ESC16-model we take the strength of this repulsion proportional to the weights of the SU(6)-forbidden [51]-configuration in the various BB-channels. This in contrast to ESC08a,b [8, 9] where the quark-core effect is only included in the BB-channels with a dominant occurrence of the [51]-configuration.

B. Non-local Potentials, SU(3)-breaking, and Coulomb

As is well known, the non-local potentials are inherent to a relativistic theory, and occur in the central, spin-spin, tensor, spin-orbit etc. potentials. In the ESC-models we include the non-local contributions to the central/spin-spin potentials for scalar, vector, axial, and diffractive exchanges, as in the OBE-models [3, 36]. In addition, for all BB-channels we include for the pseudoscalar-type of potentials, which occur from pseudoscalar-, axial A- and B-mesons, the non-local spin-spin and tensor contributions [46]. This, because it turned out that the non-local pion-exchange spin-spin and tensor force is rather important for achieving a very good fit to the NN-data.

The different sources of SU(3)-breaking are discussed in paper II of this series.

As in all Nijmegen models, the Coulomb interaction is included exactly, for which we solve the multichannel Schrödinger equation on the physical particle basis. The nuclear potentials are calculated on the isospin basis. This means that we include only the so-called 'medium strong' SU(3)-breaking and the charge symmetry breaking (CSB) in the potentials.

III. TWO-BODY INTEGRAL EQUATIONS IN MOMENTUM SPACE

A. Three-dimensional Two-Body Equations

We consider the baryon-baryon reactions

$$B(p_a, s_a) + B(p_b, s_b) \rightarrow B(p_{a'}, s_{a'}) + B(p_{b'}, s_{b'}) \quad (3.1)$$

In the following we also refer to a and a' as particles 1 and 1' (or 3), and to b and b' as particles 2 and 2' (or 4). The total four-momenta for the initial and the final states are denoted as $P = p_a + p_b, P' = p_{a'} + p_{b'}$, and similarly the relative momenta by $p = \frac{1}{2}(p_a - p_b), p' = \frac{1}{2}(p_{a'} - p_{b'})$. In the center-of-mass system (CM-system) for a and b on-mass-shell one has $P = (W, \mathbf{0})$, $p = (0, \mathbf{p})$, $p' = (0, \mathbf{p}')$. In the following, the on-mass-shell CM-momenta for the initial and final states are denoted respectively by $\mathbf{p}$ and $\mathbf{p}'$. So, $p^0_a = E_a(\mathbf{p}) = \sqrt{\mathbf{p}^2 + M^2_a}$ and $p^0_{a'} = E_{a'}(\mathbf{p}') = \sqrt{\mathbf{p}'^2 + M^2_{a'}}$, and similarly for b(2) and b'(4). Because of translation-invariance $P = P'$ and $W = W' = E_a(\mathbf{p}) + E_b(\mathbf{p}) = E_{a'}(\mathbf{p}') + E_{b'}(\mathbf{p}')$. The transition amplitude matrix M is related to the S-matrix via

$$\langle f|S|i\rangle = \langle f|i\rangle - i(2\pi)^4\delta^4(P_f - P_i)\langle f|M|i\rangle. \quad (3.2)$$

The two-particle states we normalize in the following way

$$\begin{aligned}\langle \mathbf{p}'_1, \mathbf{p}'_2|\mathbf{p}_1, \mathbf{p}_2\rangle \;=\; & (2\pi)^3 2E(\mathbf{p}_1)\delta^3(\mathbf{p}'_1 - \mathbf{p}_1)\cdot \\ & \times(2\pi)^3 2E(\mathbf{p}_2)\delta^3(\mathbf{p}'_2 - \mathbf{p}_2). \quad (3.3)\end{aligned}$$

Three-dimensional integral equations for the amplitudes $\langle f|M|i\rangle$ have been derived in various ways, see e.g. [2, 47–50]. Here, we follow Ref. [5] which employs the Macke-Klein procedure [51]. After redefining the CM-amplitude $M(\mathbf{p}', \mathbf{p}|W)$ by

$$M(\mathbf{p}', \mathbf{p}|W) \rightarrow \sqrt{\frac{M_a M_b}{E_a(\mathbf{p}')E_b(\mathbf{p}')}} M(\mathbf{p}', \mathbf{p}|W) \sqrt{\frac{M_a M_b}{E_a(\mathbf{p}')E_b(\mathbf{p}')}} \quad (3.4)$$

one arrives, see for details Ref. [5], at the Thompson equation [49]

$$M(\mathbf{p}', \mathbf{p}|W) \;=\; K^{irr}(\mathbf{p}', \mathbf{p}|W) + \int \frac{d^3p''}{(2\pi)^3} K^{irr}(\mathbf{p}', \mathbf{p}''|W)\; E^{(+)}_2(\mathbf{p}''; W)\; M(\mathbf{p}'', \mathbf{p}|W), \quad (3.5)$$

where $E_2^{(+)}(\mathbf{p}'';W) = (W - \mathcal{W}(\mathbf{p}'') + i\delta)^{-1}$, and the two-nucleon irreducible kernel is given by

$$
\begin{aligned}
K^{irr}(\mathbf{p}',\mathbf{p}|W) &= -\frac{1}{(2\pi)^2}\sqrt{\frac{M_a M_b}{E_a(\mathbf{p}')E_b(\mathbf{p}')}}\sqrt{\frac{M_a M_b}{E_a(\mathbf{p})E_b(\mathbf{p})}}\,(W-\mathcal{W}(\mathbf{p}'))\,(W-\mathcal{W}(\mathbf{p})) \\
&\times \int_{-\infty}^{+\infty} dp_0' \int_{-\infty}^{+\infty} dp_0 \left[\left\{ F_W^{(a)}(\mathbf{p}',p_0')F_W^{(b)}(-\mathbf{p}',-p_0') \right\}^{-1} \right. \\
&\times \left. [I(p_0',\mathbf{p}';p_0,\mathbf{p})]_{++,++} \left\{ F_W^{(a)}(\mathbf{p},p_0)F_W^{(b)}(-\mathbf{p},-p_0) \right\}^{-1} \right], \qquad (3.6)
\end{aligned}
$$

where $F_W(\mathbf{p},p_0) = p_0 - E(\mathbf{p}) + W/2 + i\delta$. This same expression for the kernel was exploited in [37–39].

In case one does not assume the strong pair-suppression, one must study instead of equation (3.5) a more general equation with couplings between the positive and negative energy spinorial amplitudes. Also to this more general case one can apply the described three-dimensional reduction, and we refer the reader to Ref. [52] for a treatment of this case.

The M/E-factors in (3.6) are due to the difference between the relativistic and the non-relativistic normalization of the two-particle states. In the following we simply put $M/E(\mathbf{p}) = 1$ in the kernel K^{irr} Eq. (3.6). The corrections to this approximation would give $(1/M)^2$-corrections to the potentials, which we neglect in this paper. In the same approximation there is no difference between the Thompson [49] and the Lippmann-Schwinger equation, when the connection between these equations is made using multiplication factors. Henceforth, we will not distinguish between the two.
1

The contributions to the two-particle irreducible kernel K^{irr} up to second order in the meson-exchange are given in detail in [38, 39].

B. Lippmann-Schwinger Equation

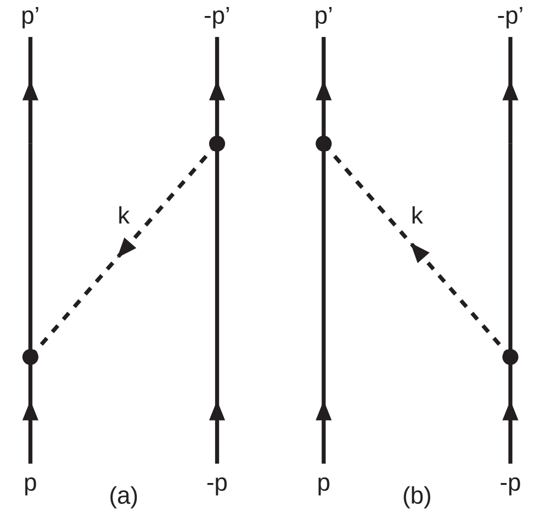

FIG. 1: One-boson-exchange graphs: The dashed lines with momentum $\mathbf{k}$ refers to the bosons: pseudo-scalar, vector, axial-vector, or scalar mesons.

The transformation of (3.5) to the Lippmann-Schwinger equation can be effectuated by defining

$$
\begin{aligned}
T(\mathbf{p}',\mathbf{p}) &= N(\mathbf{p}')\; M(\mathbf{p}',\mathbf{p}|W)\; N(\mathbf{p}), \\
V(\mathbf{p}',\mathbf{p}) &= N(\mathbf{p}')\; K^{irr}(\mathbf{p}',\mathbf{p}|W)\; N(\mathbf{p}), \qquad (3.7)
\end{aligned}
$$

where the transformation function is

$$
N(\mathbf{p}) = \sqrt{\frac{\mathbf{p}_i^2 - \mathbf{p}^2}{2M_N(E(\mathbf{p}_i) - E(\mathbf{p}))}}. \qquad (3.8)
$$

Application of this transformation, yields the Lippmann-Schwinger equation

$$
\begin{aligned}
T(\mathbf{p}',\mathbf{p}) &= V(\mathbf{p}',\mathbf{p}) + \int \frac{d^3p''}{(2\pi)^3} \\
&\times V(\mathbf{p}',\mathbf{p}'')\; g(\mathbf{p}'';W)\; T(\mathbf{p}'',\mathbf{p}) \qquad (3.9)
\end{aligned}
$$

with the standard Green function

$$
g(\mathbf{p};W) = \frac{M_N}{\mathbf{p}_i^2 - \mathbf{p}^2 + i\delta}. \qquad (3.10)
$$

The corrections to the approximation $E_2^{(+)} \approx g(\mathbf{p};W)$ are of order $1/M^2$, which we neglect henceforth.

The transition from Dirac-spinors to Pauli-spinors, is given in Appendix C of Ref. [37], where we write for the the Lippmann-Schwinger equation in the 4-dimensional Pauli-spinor space

$$
\begin{aligned}
\mathcal{T}(\mathbf{p}',\mathbf{p}) &= \mathcal{V}(\mathbf{p}',\mathbf{p}) + \int \frac{d^3p''}{(2\pi)^3} \\
&\times \mathcal{V}(\mathbf{p}',\mathbf{p}'')\; g(\mathbf{p}'';W)\; \mathcal{T}(\mathbf{p}'',\mathbf{p})\ . \qquad (3.11)
\end{aligned}
$$

The $\mathcal{T}$-operator in Pauli spinor-space is defined by

$$
\begin{aligned}
&\chi_{\sigma_a'}^{(a)\dagger}\chi_{\sigma_b'}^{(b)\dagger}\; \mathcal{T}(\mathbf{p}',\mathbf{p})\; \chi_{\sigma_a}^{(a)}\chi_{\sigma_b}^{(b)} = \\
&\bar{u}_a(\mathbf{p}',\sigma_a')\bar{u}_b(-\mathbf{p}',\sigma_b')\; \tilde{T}(\mathbf{p}',\mathbf{p})\; u_a(\mathbf{p},\sigma_a)u_b(-\mathbf{p},\sigma_b). \qquad (3.12)
\end{aligned}
$$

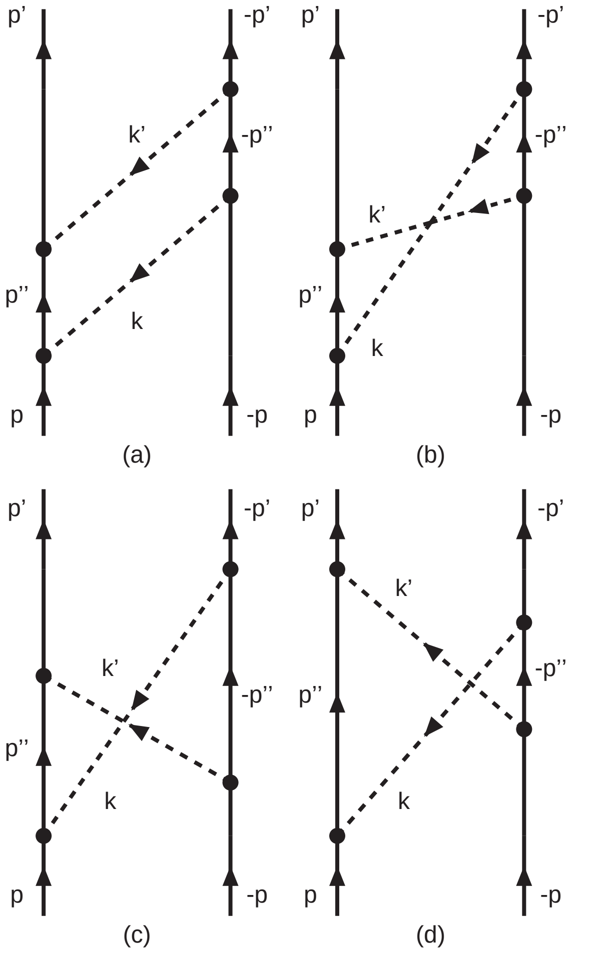

FIG. 2: BW two-meson-exchange graphs: (a) planar and (b)–(d) crossed box. The dashed line with momentum $\mathbf{k}_1$ refers to the pion and the dashed line with momentum $\mathbf{k}_2$ refers to one of the other (vector, scalar, or pseudoscalar) mesons. To these we have to add the "mirror" graphs, and the graphs where we interchange the two meson lines.

and similarly for the $\mathcal{V}$-operator. Like in the derivation of the OBE-potentials [2, 36] we make off-shell and on-shell the approximation, $E(\mathbf{p}) = M + \mathbf{p}^2/2M$ and $W = 2\sqrt{\mathbf{p}_i^2 + M^2} \approx 2M + \mathbf{p}_i^2/M$, everywhere in the interaction kernels, which, of course, is fully justified for low energies only. In contrast to these kinds of approximations, of course the full $\mathbf{k}^2$-dependence of the form factors is kept throughout the derivation of the TME. Notice that the gaussian form factors suppress the high momentum transfers strongly. This means that the contribution to the potentials from intermediate states which are far off-energy-shell can not be very large.

Because of rotational invariance and parity conservation, the $\mathcal{T}$-matrix, which is a 4×4-matrix in Pauli-spinor space, can be expanded into the following set of in general 8 spinor invariants, see for example Ref. [53]. At this point it is suitable to change the notation of the initial and final momenta. We use from now on the notations

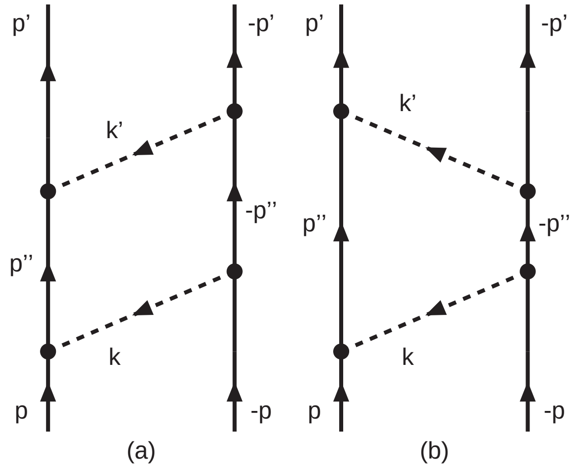

FIG. 3: Planar-box TMO two-meson-exchange graphs. Same notation as in Fig. 2. To these we have to add the "mirror" graphs, and the graphs where we interchange the two meson lines.

$\mathbf{p}_i \equiv \mathbf{p}$, $\mathbf{p}_f \equiv \mathbf{p}'$ for both on-shell and off-shell momenta. Introducing

$$\mathbf{q} = \frac{1}{2}(\mathbf{p}' + \mathbf{p}) \ , \ \mathbf{k} = \mathbf{p}' - \mathbf{p} \ , \ \mathbf{n} = \mathbf{p} \times \mathbf{p}', \tag{3.13}$$

with, of course, $\mathbf{n} = \mathbf{q} \times \mathbf{k}$, we choose for the operators P_j in spin-space

$$\begin{aligned}
&P_1 = 1, \quad P_2 = \boldsymbol{\sigma}_1 \cdot \boldsymbol{\sigma}_2, \\
&P_3 = (\boldsymbol{\sigma}_1 \cdot \mathbf{k})(\boldsymbol{\sigma}_2 \cdot \mathbf{k}) - \frac{1}{3}(\boldsymbol{\sigma}_1 \cdot \boldsymbol{\sigma}_2)\mathbf{k}^2, \\
&P_4 = \frac{i}{2}(\boldsymbol{\sigma}_1 + \boldsymbol{\sigma}_2) \cdot \mathbf{n}, \quad P_5 = (\boldsymbol{\sigma}_1 \cdot \mathbf{n})(\boldsymbol{\sigma}_2 \cdot \mathbf{n}), \\
&P_6 = \frac{i}{2}(\boldsymbol{\sigma}_1 - \boldsymbol{\sigma}_2) \cdot \mathbf{n}, \\
&P_7 = (\boldsymbol{\sigma}_1 \cdot \mathbf{q})(\boldsymbol{\sigma}_2 \cdot \mathbf{k}) + (\boldsymbol{\sigma}_1 \cdot \mathbf{k})(\boldsymbol{\sigma}_2 \cdot \mathbf{q}), \\
&P_8 = (\boldsymbol{\sigma}_1 \cdot \mathbf{q})(\boldsymbol{\sigma}_2 \cdot \mathbf{k}) - (\boldsymbol{\sigma}_1 \cdot \mathbf{k})(\boldsymbol{\sigma}_2 \cdot \mathbf{q}).
\end{aligned} \tag{3.14}$$

Here we follow Ref. [3], where in contrast to Ref. [36], we have chosen P_3 to be a purely 'tensor-force' operator. The expansion in spinor-invariants reads

$$\mathcal{T}(\mathbf{p}', \mathbf{p}) = \sum_{j=1}^{8} \widetilde{T}_j(\mathbf{p}'^2, \mathbf{p}^2, \mathbf{p}' \cdot \mathbf{p}) \ P_j(\mathbf{p}', \mathbf{p}) \ . \tag{3.15}$$

Similarly to (3.15) we expand the potentials V. In the case of the axial-vector meson exchange there will occur terms proportional to

$$P_5' = (\boldsymbol{\sigma}_1 \cdot \mathbf{q})(\boldsymbol{\sigma}_2 \cdot \mathbf{q}) - \frac{1}{3}(\boldsymbol{\sigma}_1 \cdot \boldsymbol{\sigma}_2)\mathbf{q}^2. \tag{3.16}$$

The treatment of such a Pauli-invariant using the Okubo-Marshak identity [54], see also Ref. [53], is not without problems because it involves the division with $\mathbf{k}^2$. Therefore, in the ESC04-models [5, 6] the replacement

$P_5' \to -P_3$ was chosen. For the ESC16-model a satisfactory treatment has been developed, which is described in Appendix B. For the treatment of the potentials with P_8 we use the identity [55]

$$P_8 = -(1 + \boldsymbol{\sigma}_1 \cdot \boldsymbol{\sigma}_2) P_6. \tag{3.17}$$

Under time-reversal $P_7 \to -P_7$ and $P_8 \to -P_8$. Therefore for elastic scattering $V_7 = V_8 = 0$. Anticipating the explicit results for the potentials in section IV we notice the following: (i) For the general BB-reaction we will find no contribution to V_7. The operators P_6 and P_8 give spin singlet-triplet transitions. (ii) In the case of non-strangeness-exchange ($\Delta S = 0$), $V_6 \neq 0$ and V_8=0. The latter follows from our approximation to neglect the mass differences among the nucleons, between the Λ and Σ's, and among the Ξ's. (iii) In the case of strangeness-exchange ($\Delta S = \pm 1$), $V_6, V_8 \neq 0$. The contributions to V_6 come from graphs with both spin- and particle-exchange, i.e. Majorana-type potentials having the $P_f P_\sigma P_6 = -P_x P_6$-operator. Here, $P_f P_\sigma$ reflect our convention for the two-particle wave functions, see [2]. The contributions to V_8 come from graphs with particle-exchange and spin-exchange, because $P_8 = -P_\sigma P_6$. Therefore, we only have to apply P_f in order to map the wave functions after such exchange onto our two-particle wave-functions. So, we have the $P_f P_8 = +P_x P_6$-operator. Here, we used that for BB-systems the allowed physical states satisfy $P_f P_\sigma P_x = -1$.

IV. EXTENDED-SOFT-CORE POTENTIALS IN MOMENTUM SPACE

The potential of the ESC-model contains the contributions from (i) One-boson-exchanges, Fig. 1, (ii) Uncorrelated Two-Pseudo-scalar exchange, Fig. 2 and Fig. 3, and (iii) Meson-Pair-exchange, Fig 4. In this section we review the potentials and indicate the changes with respect to earlier papers on the OBE- and ESC-models. The spin-1 meson-exchange is an important ingredient for the baryon-baryon force. In the ESC16-model we treat the vector-mesons and the axial-vector mesons according to the Proca- [56] and the B-field [57, 58] formalism respectively. For details, we refer to Appendix A.

A. One-Boson-Exchange Interactions in Momentum Space

The OBE-potentials are the same as given in [3, 36], with the exception of (i) the zero in the scalar form factor, and (ii) the axial-vector-meson potentials. Here, we review the OBE-potentials briefly, and give those potentials which are not included in the above references.

Interaction Hamiltonians: The local interaction

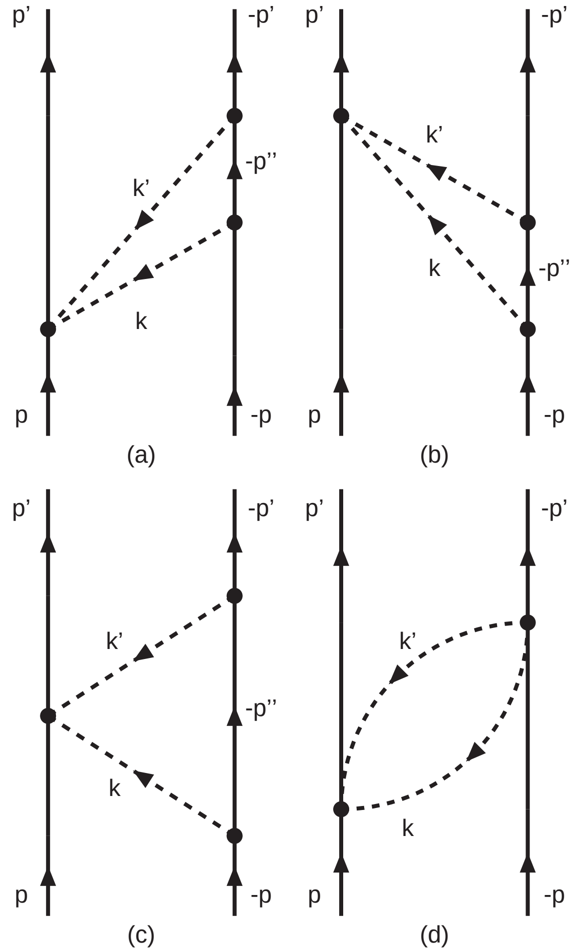

FIG. 4: One- and Two-Pair exchange graphs. To these we have to add the "mirror" graphs, and the graphs where we interchange the two meson lines.

Hamilton densities for the different couplings are [1]

a) Pseudoscalar-meson exchange ($J^{PC} = 0^{-+}$)

$$\mathcal{H}_{PV} = \frac{f_P}{m_{\pi^+}} \bar{\psi} \gamma_\mu \gamma_5 \psi \partial^\mu \phi_P. \tag{4.1}$$

This is the pseudovector coupling, and the relation with the pseudoscalar coupling is $g_P = 2M_B/m_{\pi^+}$, where M_B is the nucleon or hyperon mass.

b) Vector-meson exchange ($J^{PC} = 1^{--}$)

$$\mathcal{H}_V = g_V \bar{\psi} \gamma_\mu \psi \phi_V^\mu + \frac{f_V}{4\mathcal{M}} \bar{\psi} \sigma_{\mu\nu} \psi (\partial^\mu \phi_V^\nu - \partial^\nu \phi_V^\mu), \tag{4.2}$$

where $\sigma_{\mu\nu} = i[\gamma_\mu, \gamma_\nu]/2$, and the scaling mass $\mathcal{M}$, will be taken to be the proton mass.

[1] We follow the conventions of Ref. [59]. We note that in [5, 6] in the definition of the interaction Hamiltonians, we used the conventions of [2, 3].

c) Axial-vector-meson exchange ($J^{PC} = 1^{++}$, 1^{st} kind):

$$\mathcal{H}_A = g_A[\bar{\psi}\gamma_\mu\gamma_5\psi]\phi^\mu_A + \frac{if_A}{\mathcal{M}}[\bar{\psi}\gamma_5\psi]\ \partial_\mu\phi^\mu_A. \quad (4.3)$$

In ESC04 the g_A-coupling was included, but not the derivative f_A-coupling. [2] Also, in ESC04 we used a local-tensor approximation (LTA) for the $(\boldsymbol{\sigma}_1\cdot\mathbf{q})(\boldsymbol{\sigma}_2\cdot\mathbf{q})$ operator. Here, we improve on that considerably by avoiding such rather crude approximation. The details of our new treatment are given in Appendix B.

d) Axial-vector-meson exchange ($J^{PC} = 1^{+-}$, 2^{nd} kind):

$$\mathcal{H}_B = \frac{if_B}{m_B}[\bar{\psi}\sigma_{\mu\nu}\gamma_5\psi]\ \partial_\nu\phi^\mu_B, \quad (4.4)$$

where m_B is the $b_1(1235)$-mass. In ESC04 this coupling was not included. Like for the axial-vector mesons of the 1^{st}-kind we include an SU(3)-nonet with members $b_1(1235), h_1(1170), h_1(1380)$. In the quark-model they are $Q\bar{Q}(^1P_1)$-states.

e) Scalar-meson exchange ($J^{PC} = 0^{++}$):

$$\mathcal{H}_S = g_S[\bar{\psi}\psi]\phi_S + \frac{f_S}{\mathcal{M}}[\bar{\psi}\gamma_\mu\psi]\ \partial^\mu\phi_S, \quad (4.5)$$

which is the most general interaction up to the first derivative. However, charge conjugation gives $\mathcal{C}[\bar{\psi}\gamma_\mu\psi]\mathcal{C}^{-1} = -[\bar{\psi}\gamma_\mu\psi]$, and therefore $f_S = 0$.

f) Pomeron-exchange ($J^{PC} = 0^{++}$): The vertices for this 'diffractive'-exchange have the same Lorentz structure as those for scalar-meson-exchange.

g) Odderon-exchange ($J^{PC} = 1^{--}$):

$$\mathcal{H}_O = g_O[\bar{\psi}\gamma_\mu\psi]\phi^\mu_O + \frac{f_O}{4\mathcal{M}}[\bar{\psi}\sigma_{\mu\nu}\psi](\partial^\mu\phi^\nu_O - \partial^\nu\phi^\mu_O). \quad (4.6)$$

Since the gluons are flavorless, odderon-exchange is treated as an SU(3)-singlet. Furthermore, since the odderon represents a Regge-trajectory with an intercept equal to that of the pomeron, and is supposed not to contribute for small $\mathbf{k}^2$, we include a factor $\mathbf{k}^2/\mathcal{M}^2$ in the coupling.

Form Factors: Including form factors $f(\mathbf{x}'-\mathbf{x})$, the interaction hamiltonian densities are modified to

$$H_X(\mathbf{x}) = \int d^3x'\, f(\mathbf{x}'-\mathbf{x})\mathcal{H}_X(\mathbf{x}'), \quad (4.7)$$

for $X = P,\ V,\ A$, and S (P = pseudo-scalar, V = vector, A = axial-vector, and S = scalar). The potentials in momentum space are the same as for point interactions, except that the coupling constants are multiplied by the Fourier transform of the form factors.

In the derivation of the V_i we employ the same approximations as in [3, 36], i.e.

1. We expand in $1/M$: $E(p) = \left[\mathbf{k}^2/4 + \mathbf{q}^2 + M^2\right]^{\frac{1}{2}} \approx M + \mathbf{k}^2/8M + \mathbf{q}^2/2M$ and keep only terms up to first order in $\mathbf{k}^2/M$ and $\mathbf{q}^2/M$. This except for the form factors where the full $\mathbf{k}^2$-dependence is kept throughout the calculations. Notice that the gaussian form factors suppress the high $\mathbf{k}^2$-contributions strongly.

2. In the meson propagators $(-(p_1-p_3)^2 + m^2) \approx (\mathbf{k}^2 + m^2)$, except for the strangeness carrying mesons, see below.

3. When two different baryons are involved at a BBM-vertex their average mass is used in the potentials and the non-zero component of the momentum transfer is accounted for by using an effective mass in the meson propagator (for details see [3]).

Due to the approximations we get only a linear dependence on $\mathbf{q}^2$ for V_1. In the following, separating the local and the non-local parts, we write

$$V_i(\mathbf{k}^2,\mathbf{q}^2) = V_{ia}(\mathbf{k}^2) + V_{ib}(\mathbf{k}^2)(\mathbf{q}^2 + \frac{1}{4}\mathbf{k}^2), \quad (4.8)$$

where in principle $i = 1, 8$.

The OBE-potentials are now obtained in the standard way (see e.g. [3, 36]) by evaluating the BB-interaction in Born-approximation. We write the potentials V_i of Eqs. (3.15) and (4.8) in the form

$$V_i(\mathbf{k}^2,\mathbf{q}^2) = \sum_X \Omega_i^{(X)}(\mathbf{k}^2)\cdot\Delta^{(X)}(\mathbf{k}^2, m^2, \Lambda^2). \quad (4.9)$$

Furthermore for $X = P, V$

$$\Delta^{(X)}(\mathbf{k}^2, m^2, \Lambda^2) = e^{-\mathbf{k}^2/\Lambda^2}/\left(\mathbf{k}^2 + m^2\right), \quad (4.10)$$

and for $X = S, A$ a zero in the form factor

$$\Delta^{(S)}(\mathbf{k}^2, m^2, \Lambda^2) = \left(1 - \mathbf{k}^2/U^2\right)\ e^{-\mathbf{k}^2/\Lambda^2}/\left(\mathbf{k}^2 + m^2\right), \quad (4.11)$$

and for $X = D, O$

$$\Delta^{(D)}(\mathbf{k}^2, m^2, \Lambda^2) = \frac{1}{\mathcal{M}^2}e^{-\mathbf{k}^2/(4m^2_{P,O})}. \quad (4.12)$$

In the last expression $\mathcal{M}$ is a universal scaling mass, which is again taken to be the proton mass. The mass parameter m_P controls the $\mathbf{k}^2$-dependence of the pomeron. Similarly, m_O controls the $\mathbf{k}^2$-dependence of the odderon.

In the following we give the OBE-potentials in momentum-space for the nucleon/hyperon-nucleon systems for the non-strange mesons. From these those

[2] Note that in this paper we suppose that f_A does not contain the one-pion-pole etc. In momentum space $f_A(\mathbf{k}^2)$ is a smooth function of $\mathbf{k}^2$.

for NN and YY can be deduced easily. We assign the particles 1 and 3 to be hyperons, and particles 2 and 4 to be nucleons. Mass differences among the hyperons and among the nucleons will be neglected.

For pseudo-scalar mesons, the graph's of Fig. 1 give for the potential $V(\mathbf{k},\mathbf{q}) \approx K^{(2)}_{PS}(\mathbf{p}',\mathbf{p}|W)$

$$\begin{aligned} V_{PS}(\mathbf{k},\mathbf{q}) &= -\frac{f_{13}f_{24}}{m_\pi^2}\left(1-\frac{(\mathbf{q}^2+\mathbf{k}^2/4)}{2M_YM_N}\right)\cdot\left[\frac{1}{2\omega}\left\{\frac{1}{\omega+a}+\frac{1}{\omega-a}\right\}(\boldsymbol{\sigma}_1\cdot\mathbf{k})(\boldsymbol{\sigma}_2\cdot\mathbf{k})\right. \\ &\left.+\frac{1}{M_Y+M_N}\left\{\frac{1}{\omega+a}-\frac{1}{\omega-a}\right\}(\boldsymbol{\sigma}_1\cdot\mathbf{q}\,\boldsymbol{\sigma}_2\cdot\mathbf{k}-\boldsymbol{\sigma}_1\cdot\mathbf{k}\,\boldsymbol{\sigma}_2\cdot\mathbf{q})\right]\exp\left(-\mathbf{k}^2/\Lambda^2\right). \end{aligned} \tag{4.13}$$

Here, $\omega=\sqrt{\mathbf{k}^2+m^2}$, and using the on-energy-shell approximation $E_1+E_2=E_3+E_4$, we have

$$\begin{aligned} a &= E_1+E_4-W=\frac{1}{2}\left(E_1+E_4-E_2-E_3\right) \\ &\approx \Delta M+\frac{1}{4}\Delta M\left(\frac{1}{M_1M_3}+\frac{1}{M_2M_4}\right)\left(\mathbf{q}^2+\mathbf{k}^2/4\right), \end{aligned}$$

where $\Delta M=(M_1+M_4-M_3-M_2)/2$, and we neglected the $\mathbf{q}\cdot\mathbf{k}$-term which is of order $(M_Y-M_N)/2M_YM_N$. Henceforth we neglect the non-adiabatic effects, i.e. $a\approx\Delta M$, in the OBE-potentials, except for the P_8-terms, where the leading term is proportional to a. One notices that the P_8-term in (4.13) is only non-zero for K-exchange.

B. Non-strange Meson-exchange

For the non-strange mesons the mass differences at the vertices are neglected, we take at the YYM- and the NNM-vertex the average hyperon and the average nucleon mass respectively. This implies that we do not include contributions to the Pauli-invariants P_7 and P_8. Below the contributions to the different $\Omega^{(X)}_i$'s for baryon-baryon scattering are given in detail.

(a) Pseudoscalar-meson exchange:

$$\Omega^{(P)}_{2a} = -f^{PV}_{13}f^{PV}_{24}\left(\frac{\mathbf{k}^2}{3m^2_{\pi^+}}\right)\ ,\ \Omega^{(P)}_{3a}=-f^{PV}_{13}f^{PV}_{24}\left(\frac{1}{m^2_{\pi^+}}\right), \tag{4.14a}$$

$$\Omega^{(P)}_{2b} = +f^{PV}_{13}f^{PV}_{24}\left(\frac{\mathbf{k}^2}{6m^2_{\pi^+}M_YM_N}\right)\ ,\ \Omega^{(P)}_{3b}=+f^{PV}_{13}f^{PV}_{24}\left(\frac{1}{2m^2_{\pi^+}M_YM_N}\right),. \tag{4.14b}$$

(b) Vector-meson exchange:

$$\begin{aligned} \Omega^{(V)}_{1a} &= \left\{g^V_{13}g^V_{24}\left(1-\frac{\mathbf{k}^2}{2M_YM_N}\right)-g^V_{13}f^V_{24}\frac{\mathbf{k}^2}{4\mathcal{M}M_N}-f^V_{13}g^V_{24}\frac{\mathbf{k}^2}{4\mathcal{M}M_Y}\right. \\ &\left.+f^V_{13}f^V_{24}\frac{\mathbf{k}^4}{16\mathcal{M}^2M_YM_N}\right\},\ \ \Omega^{(V)}_{1b}=g^V_{13}g^V_{24}\left(\frac{3}{2M_YM_N}\right), \\ \Omega^{(V)}_{2a} &= -\frac{2}{3}\mathbf{k}^2\,\Omega^{(V)}_{3a},\ \ \Omega^{(V)}_{2b}=-\frac{2}{3}\mathbf{k}^2\,\Omega^{(V)}_{3b}, \\ \Omega^{(V)}_{3a} &= \left\{(g^V_{13}+f^V_{13}\frac{M_Y}{\mathcal{M}})(g^V_{24}+f^V_{24}\frac{M_N}{\mathcal{M}})-f^V_{13}f^V_{24}\frac{\mathbf{k}^2}{8\mathcal{M}^2}\right\}/(4M_YM_N), \\ \Omega^{(V)}_{3b} &= -(g^V_{13}+f^V_{13}\frac{M_Y}{\mathcal{M}})(g^V_{24}+f^V_{24}\frac{M_N}{\mathcal{M}})/(8M_Y^2M_N^2), \\ \Omega^{(V)}_{4} &= -\left\{12g^V_{13}g^V_{24}+8(g^V_{13}f^V_{24}+f^V_{13}g^V_{24})\frac{\sqrt{M_YM_N}}{\mathcal{M}}-f^V_{13}f^V_{24}\frac{3\mathbf{k}^2}{\mathcal{M}^2}\right\}/(8M_YM_N) \\ \Omega^{(V)}_{5} &= -\left\{g^V_{13}g^V_{24}+4(g^V_{13}f^V_{24}+f^V_{13}g^V_{24})\frac{\sqrt{M_YM_N}}{\mathcal{M}}+8f^V_{13}f^V_{24}\frac{M_YM_N}{\mathcal{M}^2}\right\}/(16M_Y^2M_N^2) \\ \Omega^{(V)}_{6} &= -\left\{(g^V_{13}g^V_{24}+f^V_{13}f^V_{24}\frac{\mathbf{k}^2}{4\mathcal{M}^2})\frac{(M_N^2-M_Y^2)}{4M_Y^2M_N^2}-(g^V_{13}f^V_{24}-f^V_{13}g^V_{24})\frac{1}{\sqrt{\mathcal{M}^2M_YM_N}}\right\}. \end{aligned} \tag{4.15}$$

(c) Scalar-meson exchange:

$$\Omega_{1a}^{(S)} = -g_{13}^S g_{24}^S \left(1+\frac{\mathbf{k}^2}{4M_Y M_N}\right), \quad \Omega_{1b}^{(S)} = +g_{13}^S g_{24}^S \frac{1}{2M_Y M_N}$$
$$\Omega_4^{(S)} = -g_{13}^S g_{24}^S \frac{1}{2M_Y M_N}, \quad \Omega_5^{(S)} = g_{13}^S g_{24}^S \frac{1}{16M_Y^2 M_N^2}$$
$$\Omega_6^{(S)} = -g_{13}^S g_{24}^S \frac{(M_N^2-M_Y^2)}{4M_Y M_N}. \tag{4.16}$$

(d) Axial-vector-exchange $J^{PC}=1^{++}$:

$$\Omega_{2a}^{(A)} = -g_{13}^A g_{24}^A \left[1-\frac{2\mathbf{k}^2}{3M_Y M_N}\right] + \left[\left(g_{13}^A f_{24}^A \frac{M_N}{\mathcal{M}} + f_{13}^A g_{24}^A \frac{M_Y}{\mathcal{M}}\right) - f_{13}^A f_{24}^A \frac{\mathbf{k}^2}{2\mathcal{M}^2}\right] \frac{\mathbf{k}^2}{6M_Y M_N}$$
$$\Omega_{2b}^{(A)} = -g_{13}^A g_{24}^A \left(\frac{3}{2M_Y M_N}\right)$$
$$\Omega_3^{(A)} = -g_{13}^A g_{24}^A \left[\frac{1}{4M_Y M_N}\right] + \left[\left(g_{13}^A f_{24}^A \frac{M_N}{\mathcal{M}} + f_{13}^A g_{24}^A \frac{M_Y}{\mathcal{M}}\right) - f_{13}^A f_{24}^A \frac{\mathbf{k}^2}{2\mathcal{M}^2}\right] \frac{1}{2M_Y M_N}$$
$$\Omega_4^{(A)} = -g_{13}^A g_{24}^A \left[\frac{1}{2M_Y M_N}\right], \quad \Omega_5^{(A)'} = -g_{13}^A g_{24}^A \left[\frac{2}{M_Y M_N}\right]$$
$$\Omega_6^{(A)} = -g_{13}^A g_{24}^A \left[\frac{(M_N^2-M_Y^2)}{4M_Y^2 M_N^2}\right] \tag{4.17}$$

Here, we used the B-field description with $\alpha_r = 1$, see Appendix A. The detailed treatment of the potential proportional to P_5', i.e. with $\Omega_5^{(A)'}$, is given in Appendix B.

(e) Axial-vector mesons with $J^{PC}=1^{+-}$:

$$\Omega_{2a}^{(B)} = +f_{13}^B f_{24}^B \frac{(M_N+M_Y)^2}{m_B^2}\left(1-\frac{\mathbf{k}^2}{4M_Y M_N}\right)\left(\frac{\mathbf{k}^2}{12M_Y M_N}\right), \quad \Omega_{2b}^{(B)} = +f_{13}^B f_{24}^B \frac{(M_N+M_Y)^2}{m_B^2}\left(\frac{\mathbf{k}^2}{8M_Y^2 M_N^2}\right)$$
$$\Omega_{3a}^{(B)} = +f_{13}^B f_{24}^B \frac{(M_N+M_Y)^2}{m_B^2}\left(1-\frac{\mathbf{k}^2}{4M_Y M_N}\right)\left(\frac{1}{4M_Y M_N}\right), \quad \Omega_{3b}^{(B)} = +f_{13}^B f_{24}^B \frac{(M_N+M_Y)^2}{m_B^2}\left(\frac{3}{8M_Y^2 M_N^2}\right). \tag{4.18}$$

(f) Diffractive-exchange (pomeron):
The Ω_i^D are the same as for scalar-meson-exchange Eq.(4.16), but with $\pm g_{13}^S g_{24}^S$ replaced by $\mp g_{13}^D g_{24}^D$, and except for the zero in the form factor.

(g) Odderon-exchange: The Ω_i^O are the same as for vector-meson-exchange Eq. (4.15), but with $g_{13}^V \to g_{13}^O$, $f_{13}^V \to f_{13}^O$ and similarly for the couplings with the 24-subscript.

As in Ref. [3] in the derivation of the expressions for $\Omega_i^{(X)}$, given above, M_Y and M_N denote the mean hyperon and nucleon mass, respectively $M_Y = (M_1+M_3)/2$ and $M_N = (M_2+M_4)/2$, and m denotes the mass of the exchanged meson. Moreover, the approximation $1/M_N^2 + 1/M_Y^2 \approx 2/(M_N M_Y)$, is used, which is rather good since the mass differences between the baryons are not large.

C. One-Boson-Exchange Interactions in Configuration Space I

In configuration space the BB-interactions are described by potentials of the general form [3]

$$\begin{aligned} V &= V_C(r) + V_\sigma(r)\boldsymbol{\sigma}_1\cdot\boldsymbol{\sigma}_2 + V_T(r)S_{12} + V_{SO}(r)\mathbf{L}\cdot\mathbf{S} + V_Q(r)Q_{12} \\ &\quad + V_{ASO}(r)\ \frac{1}{2}(\boldsymbol{\sigma}_1-\boldsymbol{\sigma}_2)\cdot\mathbf{L} - \frac{1}{2M_YM_N}\left(\boldsymbol{\nabla}^2 V^{n.l.}(r) + V^{n.l.}(r)\boldsymbol{\nabla}^2\right), \end{aligned} \tag{4.19a}$$

$$V^{n.l.} = \left\{\varphi_C(r) + \varphi_\sigma(r)\boldsymbol{\sigma}_1\cdot\boldsymbol{\sigma}_2 + \varphi_T(r)S_{12}\right\}, \tag{4.19b}$$

where

$$S_{12} = 3(\boldsymbol{\sigma}_1\cdot\hat{r})(\boldsymbol{\sigma}_2\cdot\hat{r}) - (\boldsymbol{\sigma}_1\cdot\boldsymbol{\sigma}_2), \tag{4.20a}$$

$$Q_{12} = \frac{1}{2}\left[(\boldsymbol{\sigma}_1\cdot\mathbf{L})(\boldsymbol{\sigma}_2\cdot\mathbf{L}) + (\boldsymbol{\sigma}_2\cdot\mathbf{L})(\boldsymbol{\sigma}_1\cdot\mathbf{L})\right]. \tag{4.20b}$$

For the basic functions for the Fourier transforms with gaussian form factors, we refer to Refs. [3, 36]. For the details of the Fourier transform for the potentials with P_5', which occur in the case of the axial-vector mesons with $J^{PC}=1^{++}$, we refer to Appendix B.

(a) Pseudoscalar-meson-exchange:

$$V_{PS}(r) = \frac{m}{4\pi}\left[f^P_{13}f^P_{24}\left(\frac{m}{m_{\pi^+}}\right)^2\left(\frac{1}{3}(\boldsymbol{\sigma}_1\cdot\boldsymbol{\sigma}_2)\ \phi^1_C + S_{12}\phi^0_T\right)\right], \tag{4.21a}$$

$$V^{n.l.}_{PS}(r) = -\frac{m}{4\pi}\left[f^P_{13}f^P_{24}\left(\frac{m^2}{2m^2_{\pi^+}}\right)\left(\frac{1}{3}(\boldsymbol{\sigma}_1\cdot\boldsymbol{\sigma}_2)\ \phi^1_C + S_{12}\phi^0_T\right)\right]. \tag{4.21b}$$

(b) Vector-meson-exchange:

$$\begin{aligned} V_V(r) &= \frac{m}{4\pi}\left[\left\{g^V_{13}g^V_{24}\left[\phi^0_C + \frac{m^2}{2M_YM_N}\phi^1_C\right]\right.\right. \\ &+ \left.\left[g^V_{13}f^V_{24}\frac{m^2}{4\mathcal{M}M_N} + f^V_{13}g^V_{24}\frac{m^2}{4\mathcal{M}M_Y}\right]\phi^1_C + f^V_{13}f^V_{24}\frac{m^4}{16\mathcal{M}^2M_YM_N}\phi^2_C\right\} \\ &+ \frac{m^2}{6M_YM_N}\left\{\left[\left(g^V_{13}+f^V_{13}\frac{M_Y}{\mathcal{M}}\right)\cdot\left(g^V_{24}+f^V_{24}\frac{M_N}{\mathcal{M}}\right)\right]\phi^1_C + f^V_{13}f^V_{24}\frac{m^2}{8\mathcal{M}^2}\phi^2_C\right\}(\boldsymbol{\sigma}_1\cdot\boldsymbol{\sigma}_2) \\ &- \frac{m^2}{4M_YM_N}\left\{\left[\left(g^V_{13}+f^V_{13}\frac{M_Y}{\mathcal{M}}\right)\cdot\left(g^V_{24}+f^V_{24}\frac{M_N}{\mathcal{M}}\right)\right]\phi^0_T + f^V_{13}f^V_{24}\frac{m^2}{8\mathcal{M}^2}\phi^1_T\right\}S_{12} \\ &- \frac{m^2}{M_YM_N}\left\{\left[\frac{3}{2}g^V_{13}g^V_{24} + \left(g^V_{13}f^V_{24}+f^V_{13}g^V_{24}\right)\frac{\sqrt{M_YM_N}}{\mathcal{M}}\right]\phi^0_{SO} + \frac{3}{8}f^V_{13}f^V_{24}\frac{m^2}{\mathcal{M}^2}\phi^1_{SO}\right\}\mathbf{L}\cdot\mathbf{S} \\ &+ \frac{m^4}{16M_Y^2M_N^2}\left\{\left[g^V_{13}g^V_{24} + 4\left(g^V_{13}f^V_{24}+f^V_{13}g^V_{24}\right)\frac{\sqrt{M_YM_N}}{\mathcal{M}} + 8f^V_{13}f^V_{24}\frac{M_YM_N}{\mathcal{M}^2}\right]\right\}\cdot \\ &\times \frac{3}{(mr)^2}\phi^0_TQ_{12} - \frac{m^2}{M_YM_N}\left\{\left[\left(g^V_{13}g^V_{24} - f^V_{13}f^V_{24}\frac{m^2}{\mathcal{M}^2}\right)\frac{(M_N^2-M_Y^2)}{4M_YM_N}\right.\right. \\ &- \left.\left.\left.\left(g^V_{13}f^V_{24}-f^V_{13}g^V_{24}\right)\frac{\sqrt{M_YM_N}}{\mathcal{M}}\right]\phi^0_{SO}\right\}\cdot\frac{1}{2}\left(\boldsymbol{\sigma}_1-\boldsymbol{\sigma}_2\right)\cdot\mathbf{L}\right], \end{aligned} \tag{4.22a}$$

$$\begin{aligned} V^{n.l.}_V(r) &= \frac{m}{4\pi}\left[\frac{3}{2}g^V_{13}g^V_{24}\ \phi^0_C\right. \\ &+ \frac{m^2}{6M_YM_N}\left\{\left[\left(g^V_{13}+f^V_{13}\frac{M_Y}{\mathcal{M}}\right)\cdot\left(g^V_{24}+f^V_{24}\frac{M_N}{\mathcal{M}}\right)\right]\phi^1_C\right\}(\boldsymbol{\sigma}_1\cdot\boldsymbol{\sigma}_2) \\ &- \left.\frac{m^2}{4M_YM_N}\left\{\left[\left(g^V_{13}+f^V_{13}\frac{M_Y}{\mathcal{M}}\right)\cdot\left(g^V_{24}+f^V_{24}\frac{M_N}{\mathcal{M}}\right)\right]\phi^0_T\right\}S_{12}\right]. \end{aligned} \tag{4.22b}$$

---

[3] The relation with the non-local $\phi(r)$-function defined in Ref. [36], Eq. (35), and the $V^{n,l.}(r)$ is $\phi(r) = [2M_{red}/(2M_YM_N)]\ V^{n.l.}(r)$.

Note: the spin-spin and tensor non-local terms are not included in ESC16.

(c) Scalar-meson-exchange:

$$
\begin{aligned}
V_S(r) &= -\frac{m}{4\pi}\left[g^S_{13}g^S_{24}\left\{\left[\phi^0_C - \frac{m^2}{4M_YM_N}\phi^1_C\right] + \frac{m^2}{2M_YM_N}\phi^0_{SO}\ \mathbf{L}\cdot\mathbf{S} + \frac{m^4}{16M_Y^2M_N^2}\cdot\right.\right. \\
&\quad \left.\left. \times\frac{3}{(mr)^2}\phi^0_T Q_{12} + \frac{m^2}{M_YM_N}\left[\frac{(M_N^2-M_Y^2)}{4M_YM_N}\right]\phi^0_{SO}\cdot\frac{1}{2}\left(\boldsymbol{\sigma}_1-\boldsymbol{\sigma}_2\right)\cdot\mathbf{L}\right\}\right], \qquad (4.23a) \\
V^{n.l.}_S(r) &= \frac{m}{4\pi}\left[\frac{1}{2}g^S_{13}g^S_{24}\ \phi^0_C\right]. \qquad (4.23b)
\end{aligned}
$$

(d) Axial-vector-meson exchange $J^{PC}=1^{++}$:

$$
\begin{aligned}
V_A(r) = &-\frac{m}{4\pi}\left[\left\{g^A_{13}g^A_{24}\left(\phi^0_C + \frac{2m^2}{3M_YM_N}\phi^1_C\right) + \frac{m^2}{6M_YM_N}\left(g^A_{13}f^A_{24}\frac{M_N}{\mathcal{M}} + f^A_{13}g^A_{24}\frac{M_Y}{\mathcal{M}}\right)\phi^1_C\right.\right. \\
&+ f^A_{13}f^A_{24}\frac{m^4}{12M_YM_N\mathcal{M}^2}\phi^2_C\Big\}\left(\boldsymbol{\sigma}_1\cdot\boldsymbol{\sigma}_2\right) - \frac{m^2}{4M_YM_N}\left\{\left[g^A_{13}g^A_{24}\right.\right. \\
&-2\left(g^A_{13}f^A_{24}\frac{M_N}{\mathcal{M}} + f^A_{13}g^A_{24}\frac{M_Y}{\mathcal{M}}\right)\Big]\phi^0_T - f^A_{13}f^A_{24}\frac{m^2}{\mathcal{M}^2}\phi^1_T\Big\}S_{12} \\
&+\frac{m^2}{2M_YM_N}g^A_{13}g^A_{24}\left.\left\{\phi^0_{SO}\ \mathbf{L}\cdot\mathbf{S} + \frac{m^2}{M_YM_N}\left[\frac{(M_N^2-M_Y^2)}{4M_YM_N}\right]\phi^0_{SO}\cdot\frac{1}{2}\left(\boldsymbol{\sigma}_1-\boldsymbol{\sigma}_2\right)\cdot\mathbf{L}\right\}\right], \qquad (4.24a) \\
V^{n.l.}_A(r) = &-\frac{m}{4\pi}\left[\frac{3}{2}g^A_{13}g^A_{24}\ \phi^0_C(\boldsymbol{\sigma}_1\cdot\boldsymbol{\sigma}_2)\right]. \qquad (4.24b)
\end{aligned}
$$

(e) Axial-vector-meson exchange $J^{PC}=1^{+-}$:

$$
\begin{aligned}
V_B(r) &= -\frac{m}{4\pi}\frac{(M_N+M_Y)^2}{m^2}\left[f^B_{13}f^B_{24}\left\{\frac{m^2}{12M_YM_N}\left(\phi^1_C + \frac{m^2}{4M_YM_N}\phi^2_C\right)\left(\boldsymbol{\sigma}_1\cdot\boldsymbol{\sigma}_2\right)\right.\right. \\
&\quad \left.\left. +\frac{m^2}{4M_YM_N}\left(\phi^0_T + \frac{m^2}{4M_YM_N}\phi^1_T\right)S_{12}\right\}\right], \qquad (4.25a) \\
V^{n.l.}_B(r) &= -\frac{m}{4\pi}\frac{3(M_N+M_Y)^2}{8m^2}\left[f^B_{13}f^B_{24}\left\{\left(\frac{1}{3}\boldsymbol{\sigma}_1\cdot\boldsymbol{\sigma}_2\ \phi^1_C + S_{12}\ \phi^0_T\right)\right\}\right]. \qquad (4.25b)
\end{aligned}
$$

(f) Pomeron exchange:

$$
\begin{aligned}
V_P(r) = &\frac{m_P}{4\pi}\left[g^P_{13}g^P_{24}\frac{4}{\sqrt{\pi}}\frac{m_P^2}{\mathcal{M}^2}\cdot\left[\left\{1 + \frac{m_P^2}{2M_YM_N}(3-2m_P^2r^2) + \frac{m_P^2}{M_YM_N}\mathbf{L}\cdot\mathbf{S}\right.\right.\right. \\
&\left.\left.\left. +\left(\frac{m_P^2}{2M_YM_N}\right)^2 Q_{12} + \frac{m_P^2}{M_YM_N}\left[\frac{(M_N^2-M_Y^2)}{4M_YM_N}\right]\cdot\frac{1}{2}\left(\boldsymbol{\sigma}_1-\boldsymbol{\sigma}_2\right)\cdot\mathbf{L}\right\}\ e^{-m_P^2r^2}\right\}\right], \qquad (4.26a) \\
V^{n.l.}_D(r) = &-\frac{m}{4\pi}\left[\frac{1}{2}e^{-m_P^2r^2}\right]. \qquad (4.26b)
\end{aligned}
$$

(g) Odderon-exchange:

$$\begin{aligned}
V_{O,C}(r) &= +\frac{g^O_{13}g^O_{24}}{4\pi}\frac{8}{\sqrt{\pi}}\frac{m_O^5}{\mathcal{M}^4}\left[\left(3-2m_O^2r^2\right)\right. \\
&\left. -\frac{m_O^2}{M_YM_N}\left(15-20m_O^2r^2+4m_O^4r^4\right)\right]\exp(-m_O^2r^2)\ , \qquad (4.27a)\\
V_O^{n.l.}(r) &= -\frac{g^O_{13}g^O_{24}}{4\pi}\frac{8}{\sqrt{\pi}}\frac{m_O^5}{\mathcal{M}^4}\frac{3}{4M_YM_N}\left\{\boldsymbol{\nabla}^2\left[(3-2m_O^2r^2)\exp(-m_O^2r^2)\right]+\right.\\
&\left.+\left[(3-2m_O^2r^2)\exp(-m_O^2r^2)\right]\boldsymbol{\nabla}^2\right\}\ , \qquad (4.27b)\\
V_{O,\sigma}(r) &= -\frac{g^O_{13}g^O_{24}}{4\pi}\frac{8}{3\sqrt{\pi}}\frac{m_O^5}{\mathcal{M}^4}\frac{m_O^2}{M_YM_N}\left[15-20m_O^2r^2+4m_O^4r^4\right]\exp(-m_O^2r^2)\cdot\\
&\times\left(1+\kappa^O_{13}\frac{M_Y}{\mathcal{M}}\right)\left(1+\kappa^O_{24}\frac{M_N}{\mathcal{M}}\right), \qquad (4.27c)\\
V_{O,T}(r) &= -\frac{g^O_{13}g^O_{24}}{4\pi}\frac{8}{3\sqrt{\pi}}\frac{m_O^5}{\mathcal{M}^4}\frac{m_O^2}{M_YM_N}\cdot m_O^2r^2\left[7-2m_O^2r^2\right]\exp(-m_O^2r^2)\cdot\\
&\times\left(1+\kappa^O_{13}\frac{M_Y}{\mathcal{M}}\right)\left(1+\kappa^O_{24}\frac{M_N}{\mathcal{M}}\right), \qquad (4.27d)\\
V_{O,SO}(r) &= -\frac{g^O_{13}g^O_{24}}{4\pi}\frac{8}{\sqrt{\pi}}\frac{m_O^5}{\mathcal{M}^4}\frac{m_O^2}{M_YM_N}\left[5-2m_O^2r^2\right]\exp(-m_O^2r^2)\cdot\\
&\times\left\{3+\left(\kappa^O_{13}+\kappa^O_{24}\right)\frac{\sqrt{M_YM_N}}{\mathcal{M}}\right\}, \qquad (4.27e)\\
V_{O,Q}(r) &= +\frac{g^O_{13}g^O_{24}}{4\pi}\frac{2}{\sqrt{\pi}}\frac{m_O^5}{\mathcal{M}^4}\frac{m_O^4}{M_Y^2M_N^2}\left[7-2m_O^2r^2\right]\exp(-m_O^2r^2)\cdot\\
&\times\left\{1+4\left(\kappa^O_{13}+\kappa^O_{24}\right)\frac{\sqrt{M_YM_N}}{\mathcal{M}}+8\kappa_{13}\kappa_{24}\frac{M_YM_N}{\mathcal{M}^2}\right\}, \qquad (4.27f)\\
V_{O,ASO}(r) &= -\frac{g^O_{13}g^O_{24}}{4\pi}\frac{4}{\sqrt{\pi}}\frac{m_O^5}{\mathcal{M}^4}\frac{m_O^2}{M_YM_N}\left[5-2m_O^2r^2\right]\exp(-m_O^2r^2)\cdot\\
&\times\left\{\frac{M_N^2-M_Y^2}{M_YM_N}-4\left(\kappa^O_{24}-\kappa^O_{13}\right)\frac{\sqrt{M_YM_N}}{\mathcal{M}}\right\}\ . \qquad (4.27g)
\end{aligned}$$

Here, $\kappa^O_{13}=g^O_{13}/f^O_{13}$ and $\kappa^O_{24}=g^O_{24}/f^O_{24}$.

D. One-Boson-Exchange Interactions in Configuration Space II

Here we give the extra potentials due to the zero's in the scalar and axial-A vector form factors:

a) Scalar-mesons:

$$\Delta V_S(r)=-\frac{m}{4\pi}\ \frac{m^2}{U^2}\ \left[g^S_{13}g^S_{24}\left\{\left[\phi^1_C-\frac{m^2}{4M_YM_N}\phi^2_C\right]+\frac{m^2}{2M_YM_N}\phi^1_{SO}\ \mathbf{L}\cdot\mathbf{S}\right.\right.$$
$$\left.\left.+\frac{m^4}{16M_Y^2M_N^2}\phi^1_T\ Q_{12}+\frac{m^2}{4M_YM_N}\frac{M_N^2-M_Y^2}{M_YM_N}\ \phi^{(1)}_{SO}\cdot\frac{1}{2}(\boldsymbol{\sigma}_1-\boldsymbol{\sigma}_2)\cdot\mathbf{L}\right\}\right]\ . \qquad (4.28)$$

b) Axial-mesons: The extra contribution to the potentials coming from the zero in the axial-vector meson form factor are obtained from the expression (4.17) by making substitutions as follows

$$\Delta V^{(1)}_A(r)\ =\ V^{(1)}_A\left(\phi^0_C\to\phi^1_C,\phi^0_T\to\phi^1_T,\phi^0_{SO}\to\phi^1_{SO}\right)\cdot\frac{m^2}{U^2}\ . \qquad (4.29)$$

Note that we do not include the similar $\Delta V_A^{(2)}(r)$ since they involve $\mathbf{k}^4$-terms in momentum-space. Then,

$$
\begin{aligned}
V_A^{(1)}(r) = -\frac{g_{13}^A g_{24}^A}{4\pi}\ m \Big[& \phi_C^0\ (\boldsymbol{\sigma}_1\cdot\boldsymbol{\sigma}_2) - \frac{1}{12 M_Y M_N}\left(\nabla^2\phi_C^0 + \phi_C^0\nabla^2\right)(\boldsymbol{\sigma}_1\cdot\boldsymbol{\sigma}_2) \\
& + \frac{3m^2}{4M_Y M_N}\ \phi_T^0\ S_{12} + \frac{m^2}{2M_Y M_N}\ \phi_{SO}^0\ \mathbf{L}\cdot\mathbf{S} \\
& + \frac{m^2}{4M_Y M_N}\frac{M_N^2 - M_Y^2}{M_Y M_N}\ \phi_{SO}^{(0)}\cdot\frac{1}{2}(\boldsymbol{\sigma}_1 - \boldsymbol{\sigma}_2)\cdot\mathbf{L}\Big]\ .
\end{aligned}
\tag{4.30}
$$

E. PS-PS-exchange Interactions in Configuration Space

In Fig. 2 and Fig. 3 the included two-meson exchange graphs are shown schematically. Explicit expressions for $K^{irr}(BW)$ and $K^{irr}(TMO)$ were derived [37], where also the terminology BW and TMO is explained. The TPS-potentials for nucleon-nucleon have been given in detail in [38, 39] The generalization to baryon-baryon is similar to that for the OBE-potentials. So, we substitute $M \to \sqrt{M_Y M_N}$, and include all PS-PS possibilities with coupling constants as in the OBE-potentials. As compared to nucleon-nucleon in [38, 39] here we have in addition the potentials with double K-exchange. The masses are the physical pseudo-scalar meson masses. For the intermediate two-baryon states we take into account of the different thresholds. We have not included uncorrelated PS-vector, PS-scalar, or PS-diffractive exchange. This because the range of these potentials is similar to that of the vector-,scalar-,and axial-vector-potentials. Moreover, for potentially large potentials, in particular those with scalar mesons involved, there will be very strong cancellations between the planar- and crossed-box contributions.

F. MPE-exchange Interactions

In Fig. 4 both the one-pair graphs and the two-pair graphs are shown. In this work we include only the one-pair graphs. The argument for neglecting the two-pair graph is to avoid some 'double-counting'. Viewing the pair-vertex as containing heavy-meson exchange means that the contributions from $\rho(750)$ and $\epsilon = f_0(620)$ to the two-pair graphs is already accounted for by our treatment of the broad ρ and ϵ OBE-potential. For a more complete discussion of the physics behind MPE we refer to our previous papers [1, 38, 39]. The MPE-potentials for nucleon-nucleon have been given in Refs. [38, 39]. The generalization to baryon-baryon is similar to that for the TPS-potentials. For the intermediate two-baryon states we neglect the different two-baryon thresholds. This because, although in principle possible, it complicates the computation of the potentials considerably. For a proper appreciation of the physics it is useful to scale the phenomenological meson-pair baryon-baryon interaction Hamiltonians different from the originally used scalings [38, 39]. Below we give these Hamiltonians:

$$
\mathcal{H}_S = \bar{\psi}\psi\left[g_{(\pi\pi)_0}\boldsymbol{\pi}\cdot\boldsymbol{\pi} + g_{(\sigma\sigma)}\sigma^2\right]/\mathcal{M}, \tag{4.31a}
$$

$$
\begin{aligned}
\mathcal{H}_V = {} & g_{(\pi\pi)_1}\left[\bar{\psi}\gamma_\mu\boldsymbol{\tau}\psi\right]\cdot\left(\boldsymbol{\pi}\times\partial^\mu\boldsymbol{\pi}/m_\pi\right)/\mathcal{M} \\
& -\frac{f_{(\pi\pi)_1}}{2M}\left[\bar{\psi}\sigma_{\mu\nu}\boldsymbol{\tau}\psi\right]\partial^\nu\cdot\left(\boldsymbol{\pi}\times\partial^\mu\boldsymbol{\pi}/m_\pi\right)/\mathcal{M},
\end{aligned}
\tag{4.31b}
$$

$$
\mathcal{H}_A = g_{(\pi\rho)_1}\left[\bar{\psi}\gamma_5\gamma_\mu\boldsymbol{\tau}\psi\right]\cdot\boldsymbol{\pi}\times\boldsymbol{\rho}/\mathcal{M}, \tag{4.31c}
$$

$$
\mathcal{H}_B = i g_{(\pi\omega)}\left[\bar{\psi}\gamma_5\sigma_{\mu\nu}\boldsymbol{\tau}\psi\right]\cdot\partial^\nu\left(\boldsymbol{\pi}\phi_\omega^\mu\right)/(m_\pi\mathcal{M}), \tag{4.31d}
$$

$$
\mathcal{H}_P = g_{(\pi\sigma)}\left[\bar{\psi}\gamma_5\gamma_\mu\boldsymbol{\tau}\psi\right]\cdot\left(\boldsymbol{\pi}\partial^\mu\sigma - \sigma\partial^\mu\boldsymbol{\pi}\right)/(m_\pi\mathcal{M}). \tag{4.31e}
$$

Here, we systematically scaled the partial derivatives with m_π.
The generalization of the pair-couplings to baryon-baryon is described in Ref. [6], section III. Also here in NN, we have in addition to [38, 39] included the pair-potentials with KK-, KK*-, and Kκ-exchange. The convention for the MPE coupling constants is the same as in Refs. [38, 39].

G. The Schrödinger equation with Non-local potential

The non-local potentials are of the central-, spin-spin, and tensor type. The method of solution of the Schrödinger equation for nucleon-nucleon central (and spin-spin) potentials has been described in Ref. [36]. In [46] the extension of the method to non-local tensor potentials has been presented. The method is reviewed briefly in Appendix D. Here, the non-local tensor is in momentum space of the form $(\mathbf{q}^2+\mathbf{k}^2/4)\ \tilde{v}_T(\mathbf{k})$.

V. ESC-COUPLINGS AND THE QPC-MODEL

In the ESC-model for baryon-baryon the meson-baryon couplings are in principle only restricted by the requirements of relativistic covariance, time-reversal and parity. However, dynamical input based on e.g. QCD, the QM, chiral-symmetry, and flavor SU(3), is essential in order to be able to link the NN-, YN-, and YY-systems. It appeared that in the ESC-model the $^3P_0$ quark-antiquark pair-creation model [26, 27] leads to a scheme for the meson-baryon-baryon couplings which is very similar to that found in the fits of the ESC-model [5, 6]. The couplings found in the ESC16-model fit very well in the $(^3P_0 +^3 S_1)$-scheme with a ratio $^3P_0/^3S_1 = 2:1$.

A. QPC-model Coupling Non-strange Mesons

According to the Quark-Pair-Creation (QPC) model, in the $^3P_0$-version [26, 27], the baryon-baryon-meson couplings are given in terms of the quark-pair creation constant γ_M, and the radii of the (constituent) gaussian quark wave functions, by [27, 60]

$$g_{BBM}(\pm) = \gamma_{q\bar{q}}\ \frac{3}{\sqrt{2}}\ \pi^{-3/4}\ X_M\left(I_M, L_M, S_M, J_M\right)\ F_M^{(\pm)}\ , \tag{5.1}$$

where $\pm = -(-)^{L_f}$ with L_f is the orbital angular momentum of the final BM-state, $X_M(\ldots)$ is a isospin, spin etc. recoupling coefficient, and

$$\begin{aligned} F^{(+)} &= \frac{3}{2}\ (m_M R_M)^{+1/2}\ (\Lambda_{QPC}R_M)^{-2}, \\ F^{(-)} &= \frac{3}{2}\ (m_M R_M)^{-1/2}\ (\Lambda_{QPC}R_M)^{-2}\cdot 3\sqrt{2}(M_M/M_B). \end{aligned} \tag{5.2}$$

are coming from the overlap integrals, see Appendix F. Here, the superscripts $\mp$ refer to the parity of the mesons M: $(-)$ for $J^{PC}=0^{+-},1^{--}$, and $(+)$ for $J^{PC}=0^{++},1^{++}$. The radii of the baryons, in this case nucleons, and the mesons are respectively denoted by R_B and R_M.

The QPC($^3P_0$)-model gives several interesting relations, such as $g_\omega = 3g_\rho, g_\epsilon = 3g_{a_0}$, and $g_{a_0}\approx g_\rho, g_\epsilon \approx g_\omega$. These relations can be seen most easily by applying the Fierz-transformation to the $^3P_0$-pair-creation Hamiltonian, see Appendix F.

From $\rho \to e^+e^-$, employing the current-field-identities (C.F.I's) one can derive, see for example [61], the following relation with the QPC-model

$$f_\rho = \frac{m_\rho^{3/2}}{\sqrt{2}|\psi_\rho(0)|} \Leftrightarrow \gamma\left(\frac{2}{3\pi}\right)^{1/2} \frac{m_\rho^{3/2}}{|'\psi_\rho(0)'|}\ , \tag{5.3}$$

which, neglecting the difference between the wave functions on the left and right hand side, gives for the pair creation constant $\gamma \to \gamma_0 = \frac{1}{2}\sqrt{3\pi} = 1.535$. However, since in the QPC-model gaussian wave functions are used, the $q\bar{q}$-potential is a harmonic-oscillator one. This does not account for the $1/r$-behavior, due to one-gluon-exchange (OGE), at short distance. This implies a OG-correction [62] to the wave function, which gives for γ [63]

$$\gamma = \gamma_0\left(1-\frac{16}{3}\frac{\alpha(m_M)}{\pi}\right)^{-1/2}\ . \tag{5.4}$$

In Table I $\gamma(\mu)$ is shown, Using from [64] the parameterization

$$\alpha_s(\mu) = 4\pi/\left(\beta_0\ln(\mu^2/\Lambda_{QCD}^2)\right)\ , \tag{5.5}$$

with $\Lambda_{QCD}=100$ MeV and $\beta_0 = 11-\frac{2}{3}n_f$ for $n_f=3$, and taking the typical scale $m_M\approx 1$ GeV, the above formula gives $\gamma = 2.19$. This value we will use later when comparing the QPC-model predictions and the ESC16-model coupling constants.

The formulas (5.2) are valid for the most simple QPC-model. For a realistic description of the coupling constants of

TABLE I: Pair-creation constant γ as a function of μ.

μ [GeV]	$\alpha_s(\mu)$	$\gamma(\mu)$
∞	0.00	1.535
80.0	0.10	1.685
35.0	0.20	1.889
1.05	0.30	2.191
0.55	0.40	2.710
0.40	0.50	3.94
0.35	0.55	5.96

the ESC16-model we include two sophistocations: (i) inclusion of both the $^3P_0$- and the $^3S_1$-mechanism, (ii) inclusion of SU(6)-breaking. For details, see [65]. For the latter we use the ($\underline{56}$) and ($\underline{70}$) SU(6)-irrep mixing [60], and a short-distance quark-gluon form factor. In Table II we show the $^3P_0 -^3 S_1$-model results and the values obtained in the ESC16-fit. In this table we fixed $\gamma_M = 2.19$ for the vector-, scalar-, and axial-vector-mesons. From Table I one sees that at the scale of $m_M \approx 1$ GeV such a value is reasonable. Here, one has to realize that the QPC-predictions are kind of "bare" couplings, which allows vertex corrections from meson-exchange. For the pseudo-scalar, a different value has to be used, showing indeed some 'running'-behavior as expected from QCD. In [63], for the decays $\rho, \epsilon \rightarrow 2\pi$ etc. it was found $\gamma = 3.33$, whereas we have $\gamma_\pi = 5.51$. For the mesonic decays of the charmonium states $\gamma = 1.12$. One notices the similarity between the QPC($^3P_0$)-model predictions and the fitted couplings. Of course, these results are sensitive to the r_M values. We found that for all solutions with a very good χ^2_{NN} the r_M values varied by ± 0.2 fm.
The ESC16-couplings and the QPC-couplings agree very well. In particular, the SU(6)-breaking is improving the agreement significantly. All this strengthens the claim that the ESC16-couplings are realistic ones.

B. ESC-potentials and the Constituent Quark-model

The calculation of Table II uses the constituent quark model (CQM) in the SU(6)-version of [27]. Since this calculation implicity uses the direct coupling of the mesons to the quarks, it defines the QQM-vertex. Then, OBE-potentials can be derived by folding meson-exchange with the quark wave functions of the baryons. prescribed by the Dirac-structure, at the baryon level the vertices have in Pauli-spinor space the 1/M$_B$-expansion

$$\begin{aligned} \bar{u}(p',s')\Gamma u(p,s) &= \chi'^{\dagger}_{s'} \left\{ \Gamma_{bb} + \Gamma_{bs} \frac{\boldsymbol{\sigma}\cdot\mathbf{p}}{E+M} - \frac{\boldsymbol{\sigma}\cdot\mathbf{p}'}{E'+M'}\Gamma_{sb} - \frac{\boldsymbol{\sigma}\cdot\mathbf{p}}{E+M}\Gamma_{ss}\frac{\boldsymbol{\sigma}\cdot\mathbf{p}'}{E'+M'}\Gamma_{sb} \right\} \chi_s \\ &\equiv \sum_l c^{(l)}_{BB} \left[\chi'^{\dagger}_{s'} O_l(\mathbf{p}',\mathbf{p})\ \chi_s \right] \ (\sqrt{M'M})^{\alpha_l} \quad (l = bb, bs, sb, ss). \end{aligned} \tag{5.6}$$

This expansion is general and does not depend on the internal structure of the baryon. A similar expansion can be made on the quark-level, but now with quark masses m_Q and coefficients $c^{(l)}_{QQ}$. It appears that in the CQM, i.e. $m_Q = M_B/3$, the QQM-vertices can be chosen such that the ratio's $c^{(l)}_{QQ}/c^{(l)}_{BB}$ are constant for each type of meson [66]. Then, by scaling the couplings these coefficients can be made equal. (Ipso facto this defines a meson-exchange quark-quark interaction.) This shows that the use of the QPC-model is consistent with the 1/M-expansion.

VI. ESC16-MODEL: FITTING $NN \oplus YN \oplus YY$-DATA

In the simultaneous χ^2-fit of the NN-, YN-, and YY-data a *single set of parameters* was used, which means the same parameters for all BB-channels. The input NN-data are the same as in Ref. [5], and we refer the reader to

TABLE II: SU(6)-breaking in coupling constants, using (56) and (70)-irrep mixing with angle $\varphi = -22^o$ for the $^3P_0$- and $^3S_1$-model. Gaussian Quark-gluon cut-off $\Lambda_{QQG} = 986.6$ MeV. Ideal mixing for vector and scalar meson nonets. For pseudoscalar- and axial-nonets the mixing angles are -11.4^0 and -42.7^o respectively, imposing the OZI-rule. Here, $\Lambda_{QPC} = 259.6$ MeV, $\gamma(\alpha_s = 0.30) = 2.19$ etc. The weights are A=0.789 and B=0.211 for the $^3P_0$ and $^3S_1$ respectively. The values in parentheses in the column QPC denote the results for $\varphi = 0^o$.

Meson	$r_M[fm]$	γ_M	$^3S_1$	$^3P_0$	QPC	ESC16
$\pi(140)$	0.30	5.51	$g = -1.37$	$g = +5.12$	3.76 (3.99)	3.65
$\eta'(957)$	0.60	2.22	$g = -1.61$	$g = +6.02$	4.41 (5.38)	4.32
$\rho(770)$	0.80	2.37	$g = -0.09$	$g = +0.65$	0.57 (0.68)	0.58
$\omega(783)$	0.70	2.35	$g = -0.48$	$g = +3.60$	3.12 (3.09)	3.11
$a_0(962)$	0.80	2.22	$g = +0.12$	$g = +0.46$	0.59 (0.61)	0.54
$\epsilon(620)$	0.70	2.37	$g = +0.63$	$g = +2.35$	2.98 (2.98)	2.98
$a_1(1270)$	0.60	2.09	$g = -0.09$	$g = -0.67$	-0.76 (-0.77)	-0.82
$f_1(1285)$	0.60	2.09	$g = -0.08$	$g = -0.60$	-0.68 (-0.69)	-0.76

this paper for a description of the employed phase shift analysis [11, 12]. Note that in addition to the NN-phases, including their correlations, in the ESC16-model also the NN-low energy parameters and the deuteron binding energy are fitted. The YN-data are those used in Ref. [6] with the addition of higher energy data, see paper II. Of course, it is to be expected that the accurate and very numerous NN-data essentially fix most of the parameters. Only some of the parameters, for example certain $F/(F+D)$-ratios, are quite influenced by the YN-data. In the fitting procedure the following constraints are applied: (i) A strong restriction imposed on YN-models is the absence of S=-1 bound states. (ii) During the fitting process sometimes constraints are imposed in the form of 'pseudo-data' for some YN scattering lengths. These constraints are based on experiences with Nijmegen YN-models in the past or to impose constraints from the G-matrix results. In some cases it is necessary to add some extra weight of the YN-scattering data w.r.t. the NN-data in the fitting process. (iii) After obtaining a solution for the scattering data the corresponding model is tested by checking the corresponding G-matrix results for the well-depths for $U_\Sigma > 0$ and $U_\Xi < 0$, and sufficient s-wave spin splitting in the U_Λ. If not satisfactory we refit the scattering data etc. This iterative process implements the constraints from the G-matrix well-depth's results, and plays a vital role in obtaining the final results of the combined fit. (For the G-matrix approach to hyperon-nucleus systems, see e.g. Ref. [67].) The fitting process is discussed more elaborately in paper II.

The χ^2 is a very shallow function of the quark-core parameter, which influences only the YN- and YY-channels. Accordingly solutions have been obtained using different assumptions about the quark-core-effects, all with a strength of about 25% of the total diffractive contribution. In previous work [9], models ESC08a and ESC08a", the solutions were obtained by assuming quark-core effects only for the channels where the [51]-component is dominant: $\Sigma^+p(^3S_1, I = 3/2), \Sigma N(^1S_0, I = 1/2)$, and $\Xi N(^1S_0, I = 1)$. The solution ESC16 is obtained by application of the quark-core effects according to equation (8.4) in [9], see paper II for a full description of the Pauli-blocking scheme.

Like in the NN-fit, described in Ref. [5], also in the simultaneous χ^2-fit of the NN- and YN-data, it appeared again that the OBE-couplings could be constrained successfully by the 'naive' predictions of the QPC-model [26, 27]. Although these predictions, see section V, are 'bare' ones, we tried to keep during the searches many OBE-couplings in the neighborhood of the QPC-values. Also, it appeared that we could either fix the $F/(F+D)$-ratios to those as suggested by the QPC-model, or apply the same restraining strategy as for the OBE-couplings.

A. Fitted BB-parameters

The treatment of the broad mesons ρ and ϵ is similar to that in the OBE-models [3, 36]. For the ρ-meson the same parameters are used as in these references. However, for the $\epsilon = f_0(620)$ we take in this work the mass $m_\epsilon = 620$ MeV and width $\Gamma_\epsilon = 464$ MeV. Using the the Bryan-Gersten "dipole" parameters [68] for the two-pole approximation we get: $m_1 = 455.15919$ MeV, $m_2 = 1158.56219$ MeV, and $\beta_1 = 0.28193, \beta_2 = 0.71807$. Other meson masses are given in Table III. The sensitivity for the values of the cut-off masses of the η and η' is very weak. Therefore we have set the $\{1\}$-cut-off mass for the pseudoscalar nonet equal to that for the $\{8\}$. Likewise, for the two nonets of the axial-vector mesons, see table III. Furthermore we experience a rather shallow dependence on the value of α_P in the range 0.33-0.40. Therefore, we put it at the Cabibbo-theory value 0.365.

Summarizing the parameters we have for baryon-baryon (BB): (i) NN Meson-couplings: $f_{NN\pi}, f_{NN\eta'}, g_{NN\rho}, g_{NN\omega}$, $f_{NN\rho}, f_{NN\omega}$, $g_{NNa_0}, g_{NN\epsilon}$, g_{NNa_1}, f_{NNa_1}, $g_{NNf_1'}$, $f_{NNf_1'}$, f_{NNb_1}, $f_{NNh_1'}$, (ii) $F/(F+D)$-ratios: α_V^m, α_A, (iii) NN Pair couplings: $g_{NN(\pi\pi)_1}, f_{NN(\pi\pi)_1}$, $g_{NN(\pi\rho)_1}$, $g_{NN\pi\omega}, g_{NN\pi\eta}, g_{NN\pi\epsilon}$, (iv) Diffractive couplings and masslike parameters g_{NNP}, g_{NNO}, f_{NNO}, m_P, m_O, (v) Cut-off masses: $\Lambda_8^P = \Lambda_1^P = \Lambda_8^B = \Lambda_1^B$, Λ_8^V, Λ_1^V, Λ_8^S, Λ_1^S, and $\Lambda_8^A = \Lambda_1^A$.

The pair coupling $g_{NN(\pi\pi)_0}$ was kept fixed at zero. Note that in the interaction Hamiltonians of the pair-couplings (4.31b)-(4.31e) the partial derivatives are scaled by m_π, and there is a scaling mass M_N.

The ESC-model described here, is fully consistent with SU(3)-symmetry using a straightforward extension of the NN-model to YN and YY. This the case for the OBE- and TPS-potentials, as well as for the Pair-potentials. For example $g_{(\pi\rho)_1} = g_{A_8VP}$, and besides $(\pi\rho)$-pairs one sees also that $KK^*(I=1)$- and $KK^*(I=0)$-pairs contribute to the NN potentials. All $F/(F+D)$-ratio's are taken as fixed with heavy-meson saturation in mind. The approximation we have made in this paper is to neglect the baryon mass differences in the TPS-potentials, i.e. we put $m_\Lambda = m_\Sigma = m_N$. This because we have not yet worked out the formulas for the inclusion of these mass differences, which is straightforward in principle.

B. Coupling Constants, $F/(F+D)$ Ratios, and Mixing Angles

In Table III we give the ESC16 meson masses, and the fitted couplings and cut-off parameters. Note that the axial-vector couplings for the B-mesons are scaled with m_{B_1}. The mixing for the pseudo-scalar, vector, and scalar mesons, as well as the handling of the diffractive potentials, has been described elsewhere, see e.g. Refs. [3, 10]. The mixing scheme of the axial-vector mesons is completely similar as for the vector etc. mesons, except for the mixing angle. In the paper II [15] the SU(3) singlet and octet couplings are listed, and also the $F/(F+D)$-ratios and mixing angles. Also the Pauli-blocking effect parameter a_{PB}, described in [9], section 8, for ESC16 is given. As mentioned above, we searched for solutions where all OBE-couplings are compatible with the QPC-predictions. This time the QPC-model contains a mixture of the $^3P_0$ and $^3S_1$ mechanism, whereas in Ref. [5] only the $^3P_0$-mechanism was considered. For the pair-couplings all $F/(F+D)$-ratios were fixed to the predictions of the QPC-model.

One notices that all the BBM α's have values rather close to that which are expected from the QPC-model. In the ESC16 solution $\alpha_A \approx 0.383$, which is close to $\alpha_A \sim 0.4$. As in previous works, e.g. Ref. [36], $\alpha_V^e = 1$ is kept fixed. Above, we remarked that the axial-nonet parameters may be sensitive to whether or not the heavy pseudoscalar nonet with the $\pi(1300)$ are included.

In Table IV we listed the fitted Pair-couplings for the MPE-potentials. We recall that only One-pair graphs are included, in order to avoid double counting, see Ref. [5]. The $F/(F+D)$-ratios are all fixed, assuming heavy-boson domination of the pair-vertices. The ratios are taken from the QPC-model for $Q\bar{Q}$-systems with the same quantum numbers as the dominating boson. For example, the α-parameter for the axial $(\pi\rho)_1$-pair could fixed at the quark-model prediction 0.40, see Table IV. The BB-Pair couplings are calculated, assuming unbroken SU(3)-symmetry, from the NN-Pair coupling and the $F/(F+D)$-ratio using SU(3). Unlike in Refs. [38, 39], we did not fix pair couplings using a theoretical model, e.g. based on heavy-meson saturation and chiral-symmetry. So, in addition to the 14 parameters used in Refs. [38, 39] we now have 6 pair-coupling fit parameters. In Table IV the fitted pair-couplings are given. Note that the $(\pi\pi)_0$-coupling gets a non-zero contribution from the $\{8_s\}$-pairs, giving $g_{(\pi\pi)_0} = -0.688/2 \approx -0.34$, which is opposite in sign compared to the result in [38, 39]. The $f_{(\pi\pi)_1}$-pair coupling has opposite sign as compared to Refs. [38, 39]. In a model with a more complex and realistic meson-dynamics [34] this coupling is predicted as found in the present ESC-fit. The $(\pi\rho)_1$-coupling is large as expected from A_1-saturation, see Refs. [38, 39]. We conclude that the pair-couplings are in general not well understood quantitatively, and deserve more study.

In Table III we show the OBE-coupling constants and the gaussian cut-off's Λ. The used $\alpha =: F/(F+D)$-ratio's for the OBE-couplings are: pseudoscalar mesons $\alpha_P = 0.365$, vector mesons $\alpha_V^e = 1.0, \alpha_V^m = 0.4655$, scalar-mesons $\alpha_S = 1.0$, axial mesons $\alpha_A = 0.3830$ and $\alpha_B = 0.4$. In Table IV we show the MPE-coupling constants. The used $\alpha =: F/(F+D)$-ratio's for the MPE-couplings are: $(\pi\eta)$ pairs $\alpha(\{8_s\}) = 1.0$, $(\pi\pi)_1$ pairs $\alpha_V^e(\{8\}_a) = 1.0, \alpha_V^m(\{8\}_a) =$

TABLE III: Meson couplings and parameters employed in the ESC16-potentials. Coupling constants are at $\mathbf{k}^2 = 0$. An asterisk denotes that the coupling constant is constrained via SU(3). The masses and Λ's are given in MeV.

meson	mass	$g/\sqrt{4\pi}$	$f/\sqrt{4\pi}$	Λ
π	138.04		0.2684	1030.96
η	547.45		0.1368*	,,
η'	957.75		0.3181	,,
ρ	768.10	0.5793	3.7791	680.79
ϕ	1019.41	–1.2384*	2.8878*	,,
ω	781.95	3.1149	–0.5710	734.21
a_1	1270.00	–0.8172	–1.6521	1034.13
f_1	1420.00	0.5147	4.4754	,,
f_1'	1285.00	–0.7596	–4.4179	,,
b_1	1235.00		–2.2598	1030.96
h_1	1380.00		–0.0830*	,,
h_1'	1170.00		–1.2386	,,
a_0	962.00	0.5393		830.42
f_0	993.00	–1.5766*		,,
ε	620.00	2.9773		1220.28
Pomeron	212.06	2.7191		
Odderon	268.81	4.1637	–3.8859	

TABLE IV: Pair-meson coupling constants employed in the ESC16 MPE-potentials. Coupling constants are at $\mathbf{k}^2 = 0$. The F/(F+D)-ratio are QPC-predictions, except that $\alpha_{(\pi\omega)} = \alpha_P$, which is very close to QPC.

J^{PC}	SU(3)-irrep	$(\alpha\beta)$	$g/4\pi$	$F/(F+D)$
0^{++}	$\{1\}$	$g(\pi\pi)_0$	—	—
0^{++}	,,	$g(\sigma\sigma)$	—	—
0^{++}	$\{8\}_s$	$g(\pi\eta)$	-0.6894	1.000
1^{--}	$\{8\}_a$	$g(\pi\pi)_1$	0.2519	1.000
		$f(\pi\pi)_1$	–1.7762	0.400
1^{++}	,,	$g(\pi\rho)_1$	5.7017	0.400
1^{++}	,,	$g(\pi\sigma)$	–0.3899	0.400
1^{++}	,,	$g(\pi P)$	—	—
1^{+-}	$\{8\}_s$	$g(\pi\omega)$	–0.3287	0.365

0.400, and the $(\pi\rho)_1$ pairs $\alpha_A(\{8\}_a) = 0.400$. The $(\pi\omega)$ pairs $\alpha(\{8_s\})$ has been set equal to $\alpha_P = 0.365$.

VII. ESC16-MODEL , *NN*-RESULTS

A. Nucleon-nucleon Fit, Low-energy and Phase Parameters

For a more detailed discussion on the NN-fitting we refer to Ref. [5]. Here, we fit to the 1993 Nijmegen representation of the χ^2-hypersurface of the NN scattering data below $T_{lab} = 350$ MeV [11, 12], and also the low-energy parameters are fitted for pp, np and nn. In this simultaneous fit of NN and YN, we obtained for ESC16 for the phase shifts $\chi^2/Ndata = 1.10$. For a comparison with Ref. [5], and for use of this model for the description of NN, we give in

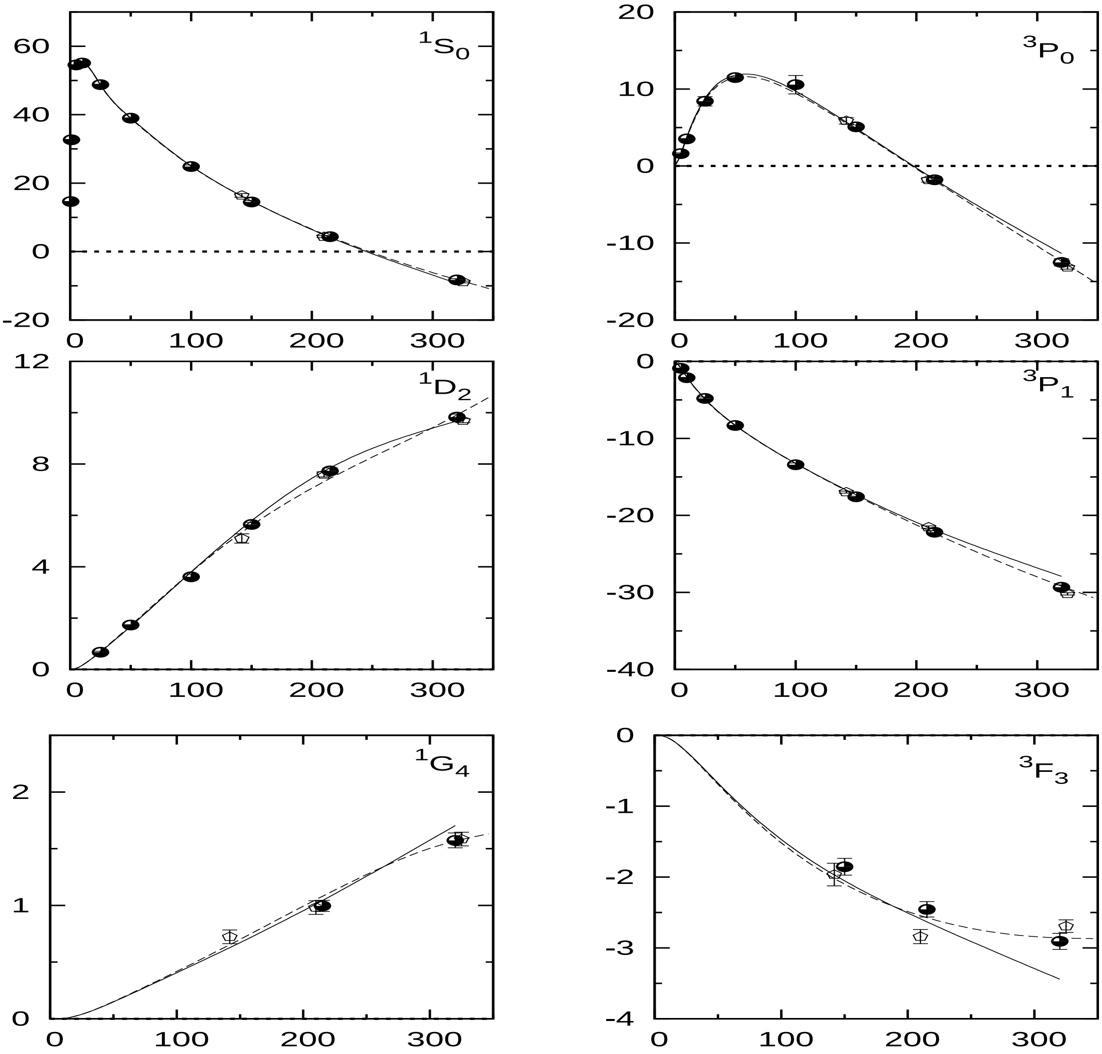

FIG. 5: Solid line: proton-proton I=1 phase shifts in degrees vs. T_{lab} in MeV for the ESC16-model. The dashed line: the m.e. phases of the Nijmegen93 PW-analysis [11]. The black dots: the s.e. phases of the Nijmegen93 PW-analysis. The diamonds: Bugg s.e. [69].

Table V the nuclear-bar phases for pp in case $I = 1$, and for np in the case of $^1S_0(I = 1)$ and the $I = 0$-phases. Here, $\Delta\chi^2$ denotes the accrescence in χ^2 of the ESC-model w.r.t. the phase shift analysis [11, 12].

The deuteron has been included in the fitting procedure, as well as the low-energy parameters. The fitted binding energy $E_B = 2.224636$ MeV, which is very close to $E_B(experiment) = 2.224644$ MeV. The charge-symmetry breaking is described phenomenologically by having next to $g_{\rho nn}$ free couplings for $g_{\rho np}$, and $g_{\rho pp}$. This phenomenological treatment is successful for the various NN-channels, especially for the $np(^1S_0, I = 1)$-phases, which were included in the NN-fit.

We emphasize that we use the single-energy (s.e.) phases and χ^2-surface [12] as a means to fit the NN-data. The multi-energy (m.e.) phases of the PW-analysis [11] in Fig. 5-Fig. 7 are the dashed lines in these figures. One notices that the central value of the s.e. phases do not correspond to the m.e. phases in general, illustrating that there has been a certain amount of noise fitting in the s.e. PW-analysis, see e.g. ϵ_1 and $^1P_1$ at $T_{lab} = 100$ MeV. The m.e. PW-analysis reaches $\chi^2/N_{data} = 0.99$, using 39 phenomenological parameters plus normalization parameters. The related phenomenological PW-potentials NijmI,II and Reid93 [70], with respectively 41, 47, and 50 parameters, turn out all with $\chi^2/Ndata = 1.03$. This should be compared to the ESC-model, which has $\chi^2/N_{data} = 1.10$ using for NN 32 meson related parameters. These are 14 QPC-constrained meson-nucleon-nucleon couplings, 6 meson-pair-nucleon-nucleon couplings, 6 gaussian cut-off parameters, 3 diffractive couplings, and 2 diffractive mass parameters. The 3 remaining fitting parameters (2 F/(F+D) ratios and the Pauli blocking fraction) are mainly or totally determined by

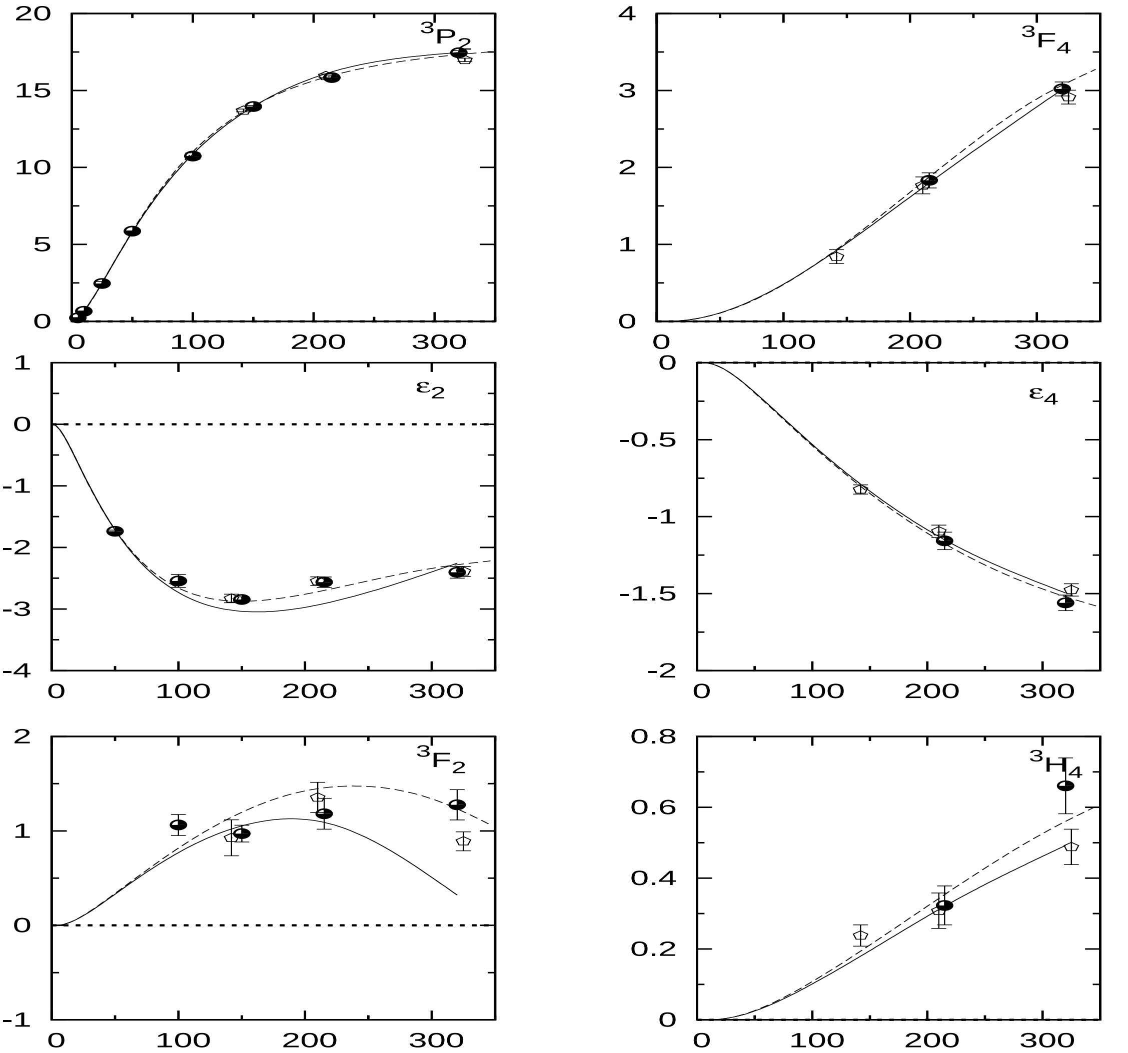

FIG. 6: Solid line: proton-proton I=1 phase shifts in degrees vs. T_{lab} in MeV for the ESC16-model. The dashed line: the m.e. phases of the Nijmegen93 PW-analysis [11]. The black dots: the s.e. phases of the Nijmegen93 PW-analysis. The diamonds: Bugg s.e. [69].

the YN-fit. From the figures it is obvious that the ESC-model deviates from the m.e. PW-analysis in particular at the highest energy.

In Table VI the results for the low energy parameters are given. In order to discriminate between the $^1S_0$-wave for pp, np, and nn, we introduced some charge independence breaking by taking $g_{pp\rho} \neq g_{np\rho} \neq g_{nn\rho}$. With this device we fitted the difference between the $^1S_0(pp)$ and $^1S_0(np)$ phases, and the different scattering lengths and effective ranges as well. We found $g_{np\rho} = 0.5427,\ g_{pp\rho} = 0.5932$, which are not far from $g_{nn\rho} = 0.5793$, see Table III. The NN low-energy parameters are described very well, see Table VI. Here, with the exception of a_{nn} and r_{nn} the experimental values are taken from the compilation given in Ref. [71]. For $a_{nn}(^1S_0)$ we have used in the fitting the value from an investigation of the n-p and n-n final state interaction in the $^2H(n,nnp)$ reaction at 13 MeV [72]. The value for $a_{nn}(^1S_0)$ is still somewhat in discussion. Another recent determination [73] obtained e.g. $a_{nn}(^1S_0) = -16.27 \pm 0.40$ fm. The ESC16-model has the value -17.78 fm which is in between these values. Although the values from [71] are not recent, here they still give an adequate presentation since this ESC-model is not detailed study of the low-energy parameters. For a discussion of the theoretical and experimental situation w.r.t. these low energy parameters, see [74]. The binding energy of the deuteron is fitted excellently. The electric quadrupole moment result is typical for models without meson-exchange current effects. Further properties of the deuteron in this model are: $P_D = 6.15\%, D/S = 0.025698, N_G^2 = 0.771658$, and $\rho_{-\epsilon,-\epsilon} = 1.725857$.

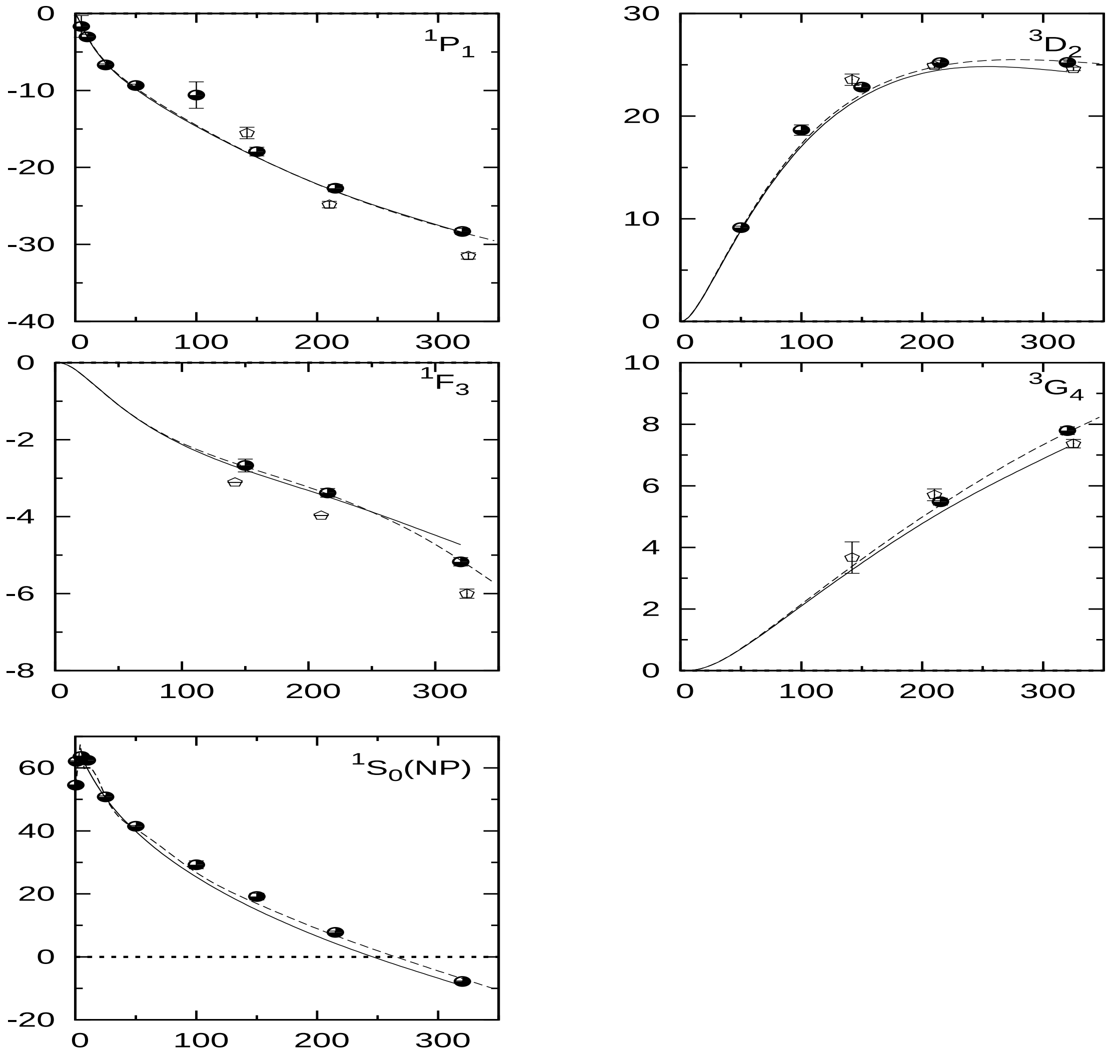

FIG. 7: Solid line: neutron-proton I=0, and the I=1 $^1S_0(NP)$ phase shifts in degrees vs. T$_{lab}$ in MeV for the ESC16-model. The dashed line: the m.e. phases of the Nijmegen93 PW-analysis [11]. The black dots: the s.e. phases of the Nijmegen93 PW-analysis. The diamonds: Bugg s.e. [69].

B. Nucleon-nucleon Potentials [4]

The nucleon-nucleon OBE-, TPS-, and Pair-potentials are qualitatively rather similar in character as the hyperon-nucleon potentials, which are shown in Ref. [6] for the ESC04 model. Therefore we refer the reader to this cited YN-paper for pictures of the potentials. The odderon and the derivative axial-vector coupling, and the non-local pseudoscalar type i spin-spin and tensor potentials are added.

The odderon potential is a novel feature of ESC16-model. In Fig. 9 the central and spin-orbit potentials are shown. The spin-spin, tensor, and quadratic spin-orbit potentials are very small. One notices from this figure that the pomeron potential is like an 'anti-scalar' potential whereas the odderon is a normal vector-exchange potential. Note the strong cancellation in the spin-orbit giving a negligible summed contribution. The upshot is a universal central repulsion from the pomeron+odderon. In ESC models the strength of the pomeron is related to that of the ε. The pomeron curve in Fig. 9 corresponds to a fit with $\varepsilon = f_0(760)$, whereas in this paper we have $\varepsilon = f_0(620)$. This results in weaker couplings of ε, ω, and pomeron, reducing the strength of the pomeron by $\approx 2/3$.

[4] The fortran code NNPOTESC16.f is put on the permanent open access website, NN-Online facility:*http://nn-online.org*.

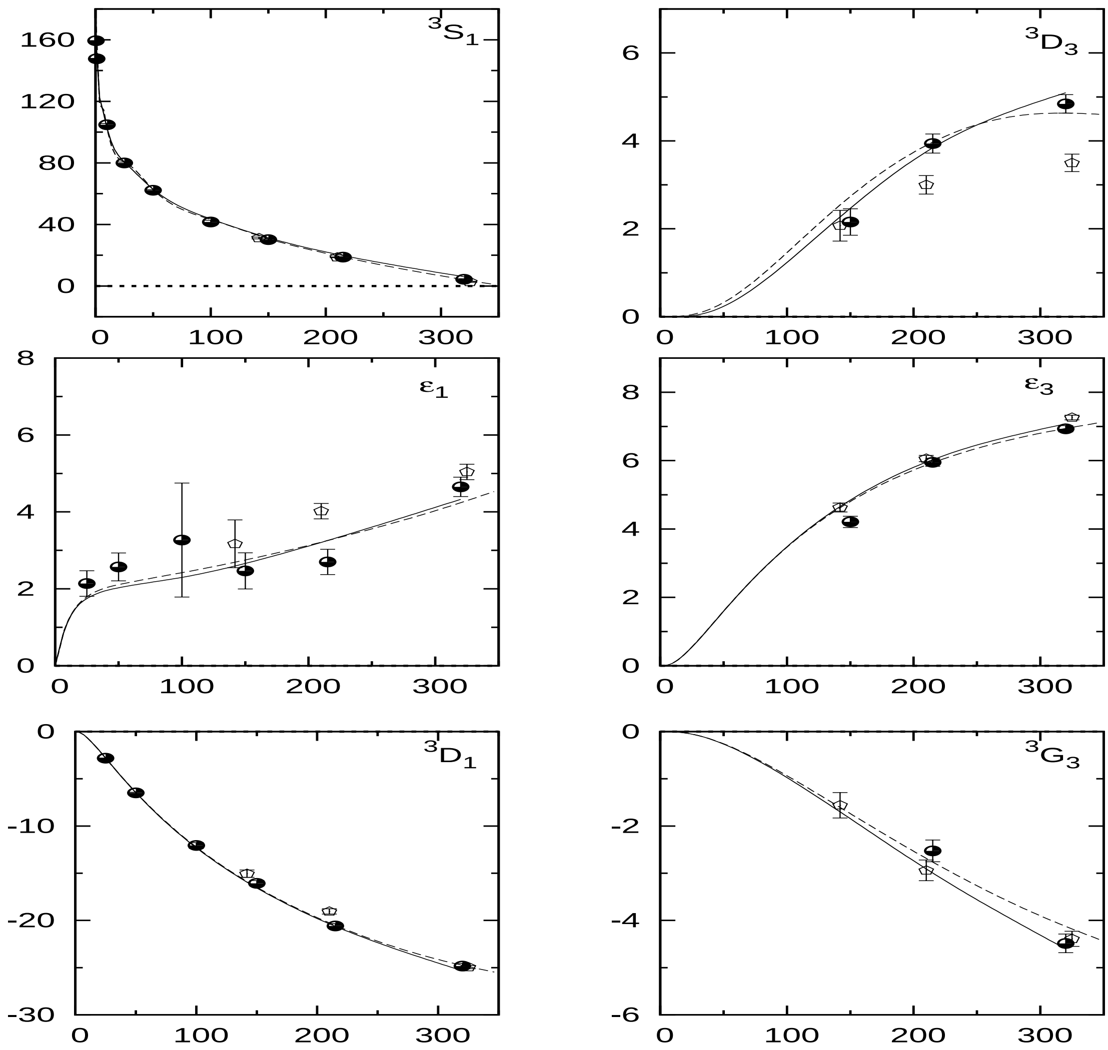

FIG. 8: Solid line: neutron-proton I=0 phase shifts in degrees vs. T_{lab} in MeV for the ESC16-model. The dashed line: the m.e. phases of the Nijmegen93 PW-analysis [11]. The black dots: the s.e. phases of the Nijmegen93 PW-analysis. The diamonds: Bugg s.e. [69].

VIII. DISCUSSION AND CONCLUSIONS

The ESC-approach to baryon-baryon (BB) interactions is a meson-exchange model with (physical) form factors. Here, besides pseudoscalar also vector-, scalar-, and axial-vector-mesons are included, which is important for an accurate description of the phase shifts at the higher energies. Also, in this approach flavor SU(3) (broken) symmetry can be incorporated in order to connect the different BB-channels. A presentation of the potentials, valid at low energies, can be obtained by making a low-t expansion of the vector etc. meson propagators and form factors giving contact terms. This would be similar to the EFT-approach [75].

The presentation in this paper reports on the present stage of the ESC-model. Compared to ESC04 [5–7] the model has been developed further. The new version ESC16 has in addition to meson-exchange also incorporated quark-core effects. Furthermore, the multi-gluon sector has been completed by the inclusion of the odderon. Moreover, the treatment of the axial-vector mesons is now in a very satisfactory shape by employing the B-field formalism. The ESC-approach to the nuclear force is a promising one. It opens the possibility to make a connection between the at present available baryon-baryon experimental data on the one hand, and with the underlying quark structure of the baryons and mesons on the other hand. Namely, a successful description of both the NN- and YN-scattering data is obtained with meson-baryon coupling parameters which all comply with the QPC-model. Here, we note that in particular the QPC-model treats the vector and scalar mesons on an equal footing. Apart from its role in $\pi\pi$ and πK scattering,

TABLE V: ESC16 nuclear-bar pp and np phases in degrees.

$T_{\rm lab}$	0.38	1	5	10	25	50	100	150	215	320
$^1S_0(np)$	54.57	62.02	63.47	59.72	50.48	39.82	25.45	15.11	4.65	–8.34
$^1S_0$	14.62	32.62	54.75	55.16	48.67	38.97	25.06	14.85	4.44	–8.53
$^3S_1$	159.39	147.77	118.25	102.72	80.81	63.03	43.62	31.27	19.58	5.83
ϵ_1	0.03	0.11	0.68	1.17	1.82	2.15	2.50	2.94	3.64	4.93
$^3P_0$	0.02	0.14	1.61	3.81	8.81	11.80	9.68	4.83	–1.86	–11.73
$^3P_1$	–0.01	–0.08	–0.89	–2.04	–4.89	–8.29	–13.28	–17.35	–21.87	–27.90
$^1P_1$	–0.05	–0.19	–1.50	–3.07	–6.39	–9.81	–14.65	–18.75	–23.38	–29.44
$^3P_2$	0.00	0.02	0.22	0.67	2.51	5.80	10.90	14.04	16.24	17.07
ϵ_2	–0.00	–0.00	–0.05	–0.20	–0.81	–1.71	–2.71	–2.99	–2.84	–2.18
$^3D_1$	–0.00	–0.01	–0.18	–0.68	–2.83	–6.51	–12.40	–16.69	–20.72	–25.04
$^3D_2$	0.00	0.01	0.22	0.85	3.70	8.93	17.22	22.15	24.99	25.05
$^1D_2$	0.00	0.00	0.04	0.17	0.69	1.70	3.78	5.70	7.64	9.20
$^3D_3$	0.00	0.00	0.00	0.00	0.03	0.24	1.17	2.31	3.61	4.86
ϵ_3	0.00	0.00	0.01	0.08	0.55	1.59	3.46	4.81	5.97	6.99
$^3F_2$	0.00	0.00	0.00	0.01	0.11	0.34	0.80	1.10	1.14	0.39
$^3F_3$	–0.00	–0.00	–0.01	–0.03	–0.23	–0.67	–1.46	–2.06	–2.66	–3.50
$^1F_3$	–0.00	–0.00	–0.01	–0.06	–0.41	–1.10	–2.11	–2.77	–3.46	–4.69
$^3F_4$	0.00	0.00	0.00	0.00	0.02	0.12	0.51	1.04	1.80	3.00
ϵ_4	–0.00	–0.00	–0.00	–0.00	–0.05	–0.19	–0.53	–0.83	–1.13	–1.46
$^3G_3$	–0.00	–0.00	–0.00	–0.00	–0.05	–0.26	–0.93	–1.73	–2.77	–4.17
$^3G_4$	0.00	0.00	0.00	0.01	0.17	0.71	2.11	3.52	5.17	7.28
$^1G_4$	0.00	0.00	0.00	0.00	0.04	0.15	0.41	0.69	1.06	1.70
$^3G_5$	–0.00	–0.00	–0.00	–0.00	–0.01	–0.05	–0.16	–0.25	–0.28	–0.19
ϵ_5	0.00	0.00	0.00	0.00	0.04	0.20	0.70	1.22	1.83	2.62

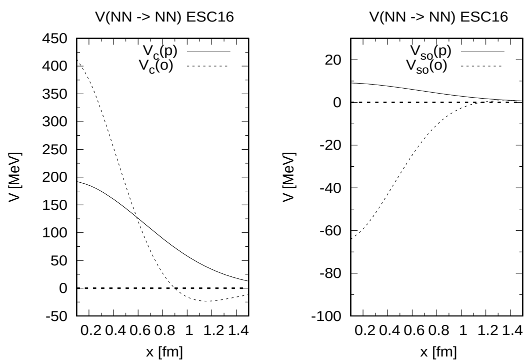

FIG. 9: Pomeron(p) and Odderon(o) central- and spin-orbit potentials.

the $f_0(620)$ has been shown to be present in relativistic nuclear scattering as well [76]. We note that by studying the relation between the QPC-processes and the BBM-couplings, we determined the ratio $\gamma(^3P_0)/\gamma(^3S_1) = 2:1$. In the literature, the $^3P_0$-QPC and the $^3S_1$-QPC in the SCQCD [18] has been studied in [77] and [78] respectively. In this paper we give therefore an estimation of the relative importance of the QPC processes. At the same time we comply with the strong constraint of no bound states in the $S=-1$ systems. Therefore, the ESC-models, ESC04 and ESC16, are an important step in the determination of the baryon-baryon interactions for low energy scattering and the description of hypernuclei in the context of broken SU(3)-symmetry. The values for many parameters, which

TABLE VI: ESC16 Low energy parameters: S-wave scattering lengths and effective ranges, deuteron binding energy E_B, and electric quadrupole Q_e. Experimental values and references, see [71, 72]. The asterisk denotes that the low-energy parameters were not searched.

	experimental data			ESC16
$a_{pp}(^1S_0)$	–7.828	±	0.008	–7.7718
$r_{pp}(^1S_0)$	2.800	±	0.020	2.7612*
$a_{np}(^1S_0)$	–23.748	±	0.010	–23.7346
$r_{np}(^1S_0)$	2.750	±	0.050	2.6992*
$a_{nn}(^1S_0)$	–18.63	±	0.48	–17.783
$r_{nn}(^1S_0)$	2.860	±	0.15	2.8301*
$a_{np}(^3S_1)$	5.424	±	0.004	5.4396*
$r_{np}(^3S_1)$	1.760	±	0.005	1.7488*
E_B	–2.224644	±	0.000046	–2.224636
Q_e	0.286	±	0.002	0.2727

TABLE VII: ESC16 χ^2 and χ^2 per datum at the ten energy bins for the Nijmegen93 Partial-Wave-Analysis. N_{data} lists the number of data within each energy bin. The bottom line gives the results for the total $0-350$ MeV interval. The χ^2-accrescence for the ESC model is denoted by $\Delta\chi^2$ and $\Delta\hat{\chi}^2$, respectively.

$T_{\rm lab}$	♯ data	χ_0^2	$\Delta\chi^2$	$\hat{\chi}_0^2$	$\Delta\hat{\chi}_0^2$
0.383	144	137.555	18.7	0.960	0.130
1	68	38.019	57.3	0.560	0.843
5	103	82.226	7.5	0.800	0.073
10	290	257.995	29.8	1.234	0.103
25	352	272.197	32.6	0.773	0.093
50	571	538.522	33.5	0.957	0.059
100	399	382.499	20.9	0.959	0.052
150	676	673.055	82.6	0.996	0.122
215	756	754.525	132.7	0.998	0.176
320	954	945.379	254.1	0.991	0.266
Total	4313	4081.971	669.8	0.948	0.153

in previous Nijmegen work were considered to be free to a large extent, follow now rather well the pattern shown in quark-model predictions. This is particularly the case for the $F/(F+D)$-ratios of the OBE- and MPE-interactions.

In fitting the NN-data the Nijmegen PWA(1993) is used. Although phase shift analyses, with a more extended data base comprising more recent data, e.g. [79] are available in principle, we expect apart from fine tuning no major changes. For example, it appeared that measured spin correlations like A_{xx} and A_{yy} from [80] respectively [81] are successfully described by PWA(1993). In Fig. 2 of Ref. [79] the Granada phase shifts are compared to the Nijmegen PWA(1993). From this figure it is clear that both analyses overlap very strongly.

As is well known, the experimental nuclear saturation properties, the density ρ_N, the binding energy per nucleon E/A, and the compression modulus K, cannot be reproduced quantitatively with nuclear two-body interactions only, see e.g. Ref. [82]. The inclusion of many-nucleon interactions is essential for giving the correct energy curve $E(\rho_N)$. Here, the three-nucleon interaction, composed of an attractive (TNA) and a repulsive (TNR) part, seems to be most important. Soft-core two-baryon potentials lead to a too soft equation of state (EoS). For example, ESC16 gives for the mass of the neutron star $1.35M_\odot$ [83], implying for this model the necessity for a TNR contribution. Furthermore, at high densities hyperon-mixing in neutron-star matter brings about a significant softening of the EoS, which gives a reduction of the TNR effect for the maximum mass [84–86]. To compensate for this adverse effect Nishizaki, Takatsuka and one of the authors (Y.Y.) [86] made the conjecture that there is a three-baryon repulsion (TBR) that operates universally for YNN and YYN as well as for NNN. In QCD the gluons are flavor blind and therefore it is natural to relate this universal TBR to multi-gluon exchange. Because in QCD the pomeron is a (non-perturbative) multi-gluon effect, which gives repulsion at low energies, we associate TBR with triple and quartic pomeron exchange [87, 88], as illustrated in Fig. 10.

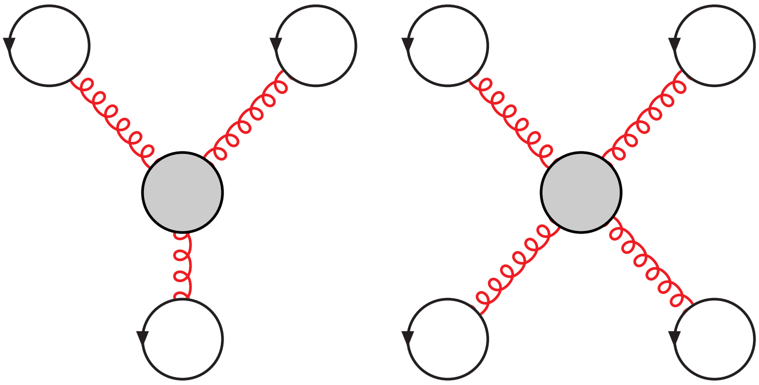

FIG. 10: Triple- and quartic-pomeron 3- and 4-body interaction.

Then, in order to stiffen the EoS, together with a phenomenological TNA, we include in the G-matrix matter calculations with ESC16 the universal repulsive multi-gluon three-body (and four-body) forces in the form of the multi-pomeron exchange potential (MPP) [9, 89, 90]. As demonstrated in [91–94], the inclusion of TNA+MPP gives the proper nuclear saturation point, and makes the EoS of neutron matter stiff enough to assure the large observed values of two massive neutron stars with mass $1.97 \pm 0.04M_\odot$ for PSR J1614-2230 [95] and $2.01 \pm 0.04M_\odot$ for PSR J0348+0432 [96]. So, with the introduction of TNA+MPP three things are achieved: (i) the right nuclear saturation point, (ii) the proper description of the neutron star masses, and moreover (iii) better hyperonic well depth's U_Y for $Y = \Lambda, \Sigma$ (see the companion paper II).

The combined fit for NN and YN is extremely good in ESC16. It is for the first time that the quality of the NN-fit does not suffer from the inclusion of the YN-data. The ΛN p-waves seem to be better, which is the result of the truly simultaneous $NN + YN$-fitting. This is also reflected in the better Scheerbaum K_Λ-value [97], making the well-known small spin-orbit splitting smaller, see Ref. [98].

The G-matrix results showed for ESC04 that basic features of hypernuclear data are reproduced nicely, improving on the soft-core OBE-models NSC89 [3] and NSC97 [10]. In spite of this superiority of ESC04 for hypernuclear data, some problems remained. In particular the well depth U_Σ was attractive, which is very unlikely in view of several other studies e.g. Refs. [99–102] Furthermore, it has been shown [86] that the EoS for nuclear matter is too soft for the soft-core models. From this we learn that a good fit to the present scattering data not necessarily means success in the G-matrix results. To explain this one can think of two reasons: (i) the G-matrix results are sensitive to the two-body interactions below 1 fm, whereas the present YN-scattering data are not, (ii) other than two-body forces play an important role. The problem with U_Σ hints at a special feature in the $\Sigma^+ p(^3S_1)$-channel. As we show in ESC16 paper II of this series, it can be solved partly by the inclusion of quark-core effects. Furthermore, for the stiffening of the EoS a natural possibility is the presence of TBF in nuclear and hyperonic matter, see Ref. [86]. This also solves the nuclear saturation problem [6].

It is important to stress the role of the information on hypernuclei in our analysis. We imposed for the ESC16-solution (i) no BB-bound states, (ii) $U_{ss} > 1$, and $U_\Sigma > 0$.

Summarizing the results of the ESC-approach to baryon-baryon interactions, it can be stated that this is a very successful one. It has been shown that ESC-models are able to give with a single parameter-set extremely satisfactory descriptions of the NN⊕YN-data, and at the same time lead to successful G-matrix results. For the coupling constants (i) flavor SU(3)-symmetry can be maintained, and (ii) they show rather well the pattern as predicted by the QPC-model. We conclude that these ESC-model predictions, as well as the applications to the S=-3,-4 systems and hyperonic matter, have a rather sound physical basis.

We close by remarking that the determination of the MPE-couplings opens the possibility to compute the TBF-potentials for baryon-systems where all meson-pair vertices are fixed by the ESC-model.

Acknowledgements

We wish to thank E. Hiyama, K. Itonaga, T. Motoba and H.-J. Schulze for many stimulating discussions. Th.A.R. is grateful for the interest and collaboration with R.A. Bryan on the scalar mesons.

APPENDIX A: B-FIELD FORMALISM FOR VECTOR- AND AXIAL-VECTOR MESONS

As an alternative to the usual Proca-formalism for vector mesons, Nakanishi and collaborators [57, 58] introduced the B-field formalism. In the non-abelian theory, e.g. isospin SU(2,I), one introduces the B-field through the Lagrangian

$$\mathcal{L}_A = -\frac{1}{4}\mathcal{F}^i_{\mu\nu}\mathcal{F}^{\mu\nu i} + \frac{1}{2}m^2 A^i_\mu A^{\mu i} + B^i\partial_\mu A^{\mu i} + \frac{\alpha}{2}B^i B^i \ , \tag{A1}$$

where the field tensor and the covariant derivative D_μ are given by

$$\mathcal{F}^i_{\mu\nu} = \partial_\mu A^i_\nu - \partial_\nu A^i_\mu + g_A\epsilon^{ijk}A^j_\mu A^k_\nu, \tag{A2a}$$

$$D_\mu = \partial_\mu - ig_A t_i\ A^i_\mu \ . \tag{A2b}$$

We assume that the A^i_μ-field is coupled to the conserved, or almost conserved, hadronic 'strong' current $J_{H,\mu}$. The field equations, neglecting the non-abelian term in the axial field tensor, become

$$A^i_\mu\ :\ \partial^\mu\mathcal{F}^i_{\mu\nu} + m^2 A^i_\mu = -J^i_{H,\mu} + \partial_\mu B^i \ , \tag{A3a}$$

$$B^i\ :\ \partial^\mu A^i_\mu + \alpha B^i = 0 \ . \tag{A3b}$$

Exploiting now that approximately $\partial^\mu J^i_\mu = 0$, one derives from the field equation for A^i_μ, upon taking the derivative ∂_μ etc., that B^i is a free field, i.e.

$$\left(\Box + \alpha m^2\right) B^i = 0 \ . \tag{A4}$$

This theory can be quantized in a satisfactory way, giving an axial-vector-meson propagator which is covariant, see Nakanishi & Ojima [58] It implies that in the propagator one has for the spectral function of the propagator projection operator

$$\Pi^{\mu\nu}(k) = \left[-\eta^{\mu\nu} + \frac{k^\mu k^\nu}{m^2}\right]\delta(k^2-m^2) - \frac{k^\mu k^\nu}{m^2}\ \delta(k^2-\alpha_r m^2) \ , \tag{A5}$$

where $\alpha_r > 0$ is the renormalized B-field parameter α giving it a mass $\sqrt{\alpha_r}m$ [58]. The propagator becomes

$$\begin{aligned} P^{\mu\nu}(k) &= -\frac{\eta^{\mu\nu}}{k^2-m^2+i\epsilon} + (1-\alpha_r)\frac{k^\mu k^\nu}{(k^2-m^2+i\epsilon)(k^2-\alpha_r m^2+i\epsilon)} \\ &\Rightarrow -\frac{\eta^{\mu\nu}}{k^2-m^2+i\epsilon} \ , \ \text{ for } \ \alpha_r = 1 \ . \end{aligned} \tag{A6}$$

The case $\alpha_r = 1$ reminds one of the Feynman-gauge in the massless case. Now, in the case of coupling to a conserved current, the potential will be independent of α_r. Therefore, we will use the "Feynman-gauge" in this paper. It implies that the $k^\mu k^\nu$-terms in the vector-meson propagators will not contribute to the potentials in the B-field formalism. This in contrast to the Proca-formalism, see e.g. Ref. [56]. For the axial-vector mesons we will use the B-field formalism, whereas for the vector mesons we continue to use the Proca formalism, like in Refs. [3, 6, 10].

APPENDIX B: EXACT TREATMENT NON-LOCAL-TENSOR (NLT) OPERATOR

From results given in Ref. [103], we derive a new method for the treatment of the non-local-tensor (NLT) $\boldsymbol{\sigma}_1\cdot\mathbf{q}\boldsymbol{\sigma}_2\cdot\mathbf{q}$-operator. Starting from

$$\widetilde{V}(\mathbf{k},\mathbf{q}) = \int d^3r' \int d^3r\ e^{i\mathbf{p}'\cdot\mathbf{r}'}V(\mathbf{r}',\mathbf{r})e^{-i\mathbf{p}\cdot\mathbf{r}} \ , \tag{B1}$$

where

$$V(\mathbf{r}',\mathbf{r}) = \delta^3(\mathbf{r}'-\mathbf{r})\ f(r)\ Q_{12}\ , \tag{B2}$$

with the quadratic-spin-orbit operator $Q_{12} = (\boldsymbol{\sigma}_1\cdot\mathbf{L}\boldsymbol{\sigma}_2\cdot\mathbf{L}+\boldsymbol{\sigma}_2\cdot\mathbf{L}\boldsymbol{\sigma}_1\cdot\mathbf{L})/2$. Introducing the functions $g(r)$ and $h(r)$ by

$$r_i f(r) = -\nabla_i g(r)\ \ ,\ \ r_i r_j f(r) = \left[-\nabla_i\nabla_j + \delta_{ij}\left(\frac{1}{r}\frac{d}{dr}\right)\right]\ h(r)\ , \tag{B3}$$

executing the Fourier transformation in (B1) leads to the identity

$$\begin{aligned}\widetilde{V}(\mathbf{k},\mathbf{q}) &= [\boldsymbol{\sigma}_1\cdot\mathbf{q}\times\mathbf{k}]\,[\boldsymbol{\sigma}_2\cdot\mathbf{q}\times\mathbf{k}]\ \widetilde{h}(\mathbf{k}^2)\\ &-\left[\boldsymbol{\sigma}_1\cdot\mathbf{q}\boldsymbol{\sigma}_2\cdot\mathbf{q}-\mathbf{q}^2\boldsymbol{\sigma}_1\cdot\boldsymbol{\sigma}_2\right]\ \widetilde{g}(\mathbf{k}^2)\\ &+\frac{1}{4}\left[\boldsymbol{\sigma}_1\cdot\mathbf{k}\boldsymbol{\sigma}_2\cdot\mathbf{k}-\mathbf{k}^2\boldsymbol{\sigma}_1\cdot\boldsymbol{\sigma}_2\right]\ \widetilde{g}(\mathbf{k}^2)\ ,\end{aligned} \tag{B4}$$

where $\widetilde{h}(\mathbf{k}^2)$ and $\widetilde{g}(\mathbf{k}^2)$ are the Fourier transforms of respectively $h(r)$ and $g(r)$.

The strategy is now to derive the configuration potentials with the $\boldsymbol{\sigma}_1\cdot\mathbf{q}\boldsymbol{\sigma}_2\cdot\mathbf{q}$-operator by utilizing (B4), which we rewrite as

$$\begin{aligned}&\left[\boldsymbol{\sigma}_1\cdot\mathbf{q}\boldsymbol{\sigma}_2\cdot\mathbf{q}-\mathbf{q}^2\boldsymbol{\sigma}_1\cdot\boldsymbol{\sigma}_2\right]\ \widetilde{g}(\mathbf{k}^2) =\\ &\left\{[\boldsymbol{\sigma}_1\cdot\mathbf{q}\times\mathbf{k}]\,[\boldsymbol{\sigma}_2\cdot\mathbf{q}\times\mathbf{k}]\ \widetilde{h}(\mathbf{k}^2)-\widetilde{V}(\mathbf{k},\mathbf{q})\right\}\\ &+\frac{1}{4}\left[\boldsymbol{\sigma}_1\cdot\mathbf{k}\boldsymbol{\sigma}_2\cdot\mathbf{k}-\mathbf{k}^2\boldsymbol{\sigma}_1\cdot\boldsymbol{\sigma}_2\right]\ \widetilde{g}(\mathbf{k}^2)\ ,\end{aligned} \tag{B5}$$

In our application

$$\widetilde{g}(\mathbf{k}^2) = \frac{\exp(-\mathbf{k}^2/\Lambda^2)}{\mathbf{k}^2+m^2}\ \ ,\ \ g(r) = \frac{m}{4\pi}\phi^0_C(r,m,\Lambda)\ . \tag{B6}$$

Then, from (B3) one derives that

$$f(r) = -\frac{1}{r}\frac{d}{dr}g(r) = -\frac{m}{4\pi}\frac{1}{r}\frac{d}{dr}\phi^0_C(r,m,\Lambda) = \frac{m^3}{4\pi}\phi^0_{SO}(r,m,\Lambda)\ . \tag{B7}$$

In momentum space, one easily derives the relation $d\widetilde{f}(\mathbf{k}^2)/d\mathbf{k}^2 = -\widetilde{g}(\mathbf{k}^2)/2$, which leads to

$$\widetilde{f}(\mathbf{k}^2) = \frac{1}{2}\exp\left(m^2/\Lambda^2\right)\ E_1\left[(\mathbf{k}^2+m^2)/\Lambda^2\right]\ , \tag{B8}$$

where $E_1(x)$ is the standard exponential integral function.

Next, we turn to the determination of $h(r)$. From (B3) one readily derives the momentum space differential equation

$$\boldsymbol{\nabla}^2_k\ \widetilde{g}(\mathbf{k}^2) = (\mathbf{k}\cdot\boldsymbol{\nabla}_k+3)\ \widetilde{h}(\mathbf{k}^2)\ . \tag{B9}$$

Trying the form

$$\widetilde{h}(\mathbf{k}^2) = \left(A+\frac{B}{\mathbf{k}^2+m^2}\right)\widetilde{g}(\mathbf{k}^2)\ , \tag{B10}$$

one obtains from (B9) the solution $A=-2/\Lambda^2$ and $B=-2$. So,

$$\widetilde{h}(\mathbf{k}^2) = -2\left(\frac{1}{\Lambda^2}+\frac{1}{\mathbf{k}^2+m^2}\right)\widetilde{g}(\mathbf{k}^2) = -2\left(\frac{1}{\Lambda^2}-\frac{d}{dm^2}\right)\widetilde{g}(\mathbf{k}^2) = 2\frac{d\widetilde{g}(\mathbf{k}^2)}{d\mathbf{k}^2} \tag{B11}$$

Using the (approximate) axial-current conservation, and the "Feynman gauge" in the B-field formalism, we have from the $\Omega_i^{(A)}$ in (4.17) the following expression for $\mathcal{V}_A^{(1)}$

$$\begin{aligned}\tilde{\mathcal{V}}_A^{(1)} &= -g_A^2\left[\left(1-\frac{1}{3MM'}\mathbf{k}^2+\frac{3(\mathbf{q}^2+\mathbf{k}^2/4)}{2M'M}\right)\boldsymbol{\sigma}_1\cdot\boldsymbol{\sigma}_2+\frac{2}{MM'}\left((\boldsymbol{\sigma}_1\cdot\mathbf{q})(\boldsymbol{\sigma}_2\cdot\mathbf{q})\right.\right.\\ &\quad\left.-\mathbf{q}^2\boldsymbol{\sigma}_1\cdot\boldsymbol{\sigma}_2\right)-\frac{1}{4M'M}\left((\boldsymbol{\sigma}_1\cdot\mathbf{k})(\boldsymbol{\sigma}_2\cdot\mathbf{k})-\frac{1}{3}\mathbf{k}^2\boldsymbol{\sigma}_1\cdot\boldsymbol{\sigma}_2\right)\\ &\quad\left.+\frac{i}{4M'M}(\boldsymbol{\sigma}_1+\boldsymbol{\sigma}_2)\cdot\mathbf{q}\times\mathbf{k}\right]\cdot\widetilde{g}(\mathbf{k}^2)\ , \end{aligned} \tag{B12}$$

Here, the superscript (1) refers to the circumstance that this comes from the $g_{\mu\nu}$-term in the axial-vector-meson propagator. Then, using the identity (B5) we get from (B12)

$$\begin{aligned}\tilde{\mathcal{V}}_A^{(1)} &= -g_A^2\left[\left(1-\frac{2\mathbf{k}^2}{3MM'}+\frac{3(\mathbf{q}^2+\mathbf{k}^2/4)}{2M'M}\right)\boldsymbol{\sigma}_1\cdot\boldsymbol{\sigma}_2\right.\\ &\quad+\frac{1}{4M'M}\left((\boldsymbol{\sigma}_1\cdot\mathbf{k})(\boldsymbol{\sigma}_2\cdot\mathbf{k})-\frac{1}{3}\mathbf{k}^2\boldsymbol{\sigma}_1\cdot\boldsymbol{\sigma}_2\right)\\ &\quad\left.+\frac{i}{4M'M}(\boldsymbol{\sigma}_1+\boldsymbol{\sigma}_2)\cdot\mathbf{q}\times\mathbf{k}\right]\cdot\widetilde{g}(\mathbf{k}^2)\\ &\quad-g_A^2\left[\frac{2}{MM'}\left\{[\boldsymbol{\sigma}_1\cdot\mathbf{q}\times\mathbf{k}]\,[\boldsymbol{\sigma}_2\cdot\mathbf{q}\times\mathbf{k}]\ \widetilde{h}(\mathbf{k}^2)-\widetilde{V}(\mathbf{k},\mathbf{q})\right\}\right]\ . \end{aligned} \tag{B13}$$

Making now our standard approximation of the Fourier transformation of the $[\boldsymbol{\sigma}_1\cdot\mathbf{q}\times\mathbf{k}]\,[\boldsymbol{\sigma}_2\cdot\mathbf{q}\times\mathbf{k}]$-operator, cfr. Ref. [36], the configuration space potentials corresponding with (B13) read

$$\begin{aligned}\mathcal{V}_A^{(1)} &= -\frac{g_A^2}{4\pi}\,m\left[\left(\phi_C^0+\frac{2m^2}{3M'M}\,\phi_C^1\right)(\boldsymbol{\sigma}_1\cdot\boldsymbol{\sigma}_2)-\frac{3}{4M'M}\left(\nabla^2\phi_C^0+\phi_C^0\nabla^2\right)(\boldsymbol{\sigma}_1\cdot\boldsymbol{\sigma}_2)\right.\\ &\quad\left.-\frac{m^2}{4M'M}\,\phi_T^0\,S_{12}+\frac{m^2}{2M'M}\,\phi_{SO}^0(m,r)\,\mathbf{L}\cdot\mathbf{S}\right]\\ &\quad+\frac{g_A^2}{4\pi}\,\frac{2m^2}{M'M}\left[\phi_{SO}^0(r)+\frac{3}{(mr)^2}\left\{3-\frac{2m^2}{\Lambda^2}+\left(m\frac{d}{dm}\right)\right\}\,\phi_T^0(r)\right]\,Q_{12}\ . \end{aligned} \tag{B14}$$

Now it happens that the second term in the coefficient of Q_{12} in (B14) becomes by virtue of the properties of the Gaussian Yukawa-functions, see Appendix E,

$$\frac{3}{(mr)^2}\left\{\ldots\right\}=-\frac{3}{(mr)^2}\,\psi_T^0(r)=-\phi_{SO}^0(r)\ , \tag{B15}$$

and so the coefficient of Q_{12} in (B14) vanishes!

APPENDIX C: AXIAL-DERIVATIVE COUPLING AND CAC

In the B-field theory the conservation of the axial-current conservation (CAC) is an important ingredient. Therefore, an analysis of the realization of CAC in the ESC-model is opportune. Isolating the derivative coupling terms in the axial-vector meson-exchange potential we have

$$V_{A,a}(r)=-\frac{m}{4\pi}\frac{m^2}{2M_YM_N}\left(g_{13}^Af_{24}^A\frac{M_N}{\mathcal{M}}+f_{13}^Ag_{24}^A\frac{M_Y}{\mathcal{M}}\right)\left[\frac{1}{3}(\boldsymbol{\sigma}_1\cdot\boldsymbol{\sigma}_2)\,\phi_C^1+S_{12}\,\phi_T^0\right], \tag{C1a}$$

$$V_{A,b}(r)=-\frac{m}{4\pi}\,f_{13}^Af_{24}^A\frac{m^2}{\mathcal{M}^2}\frac{m^2}{4M_YM_N}\left[\frac{1}{3}(\boldsymbol{\sigma}_1\cdot\boldsymbol{\sigma}_2)\,\phi_C^2+S_{12}\,\phi_T^1\right]. \tag{C1b}$$

Depending on the sign of g_Af_A the first potential $V_{A,a}(r)$ is a B-type ($g_Af_A>0$) or a P-type ($g_Af_A<0$) potential, and the second potential $V_{A,b}(r)$ is a B-type potential.

Axial-vector current conservation at the meson-pole requires

$$\partial_\mu J^\mu_A = 0: \;\; \frac{f^A}{g^A} = -2\frac{M_N \mathcal{M}}{m_A^2} \approx -1. \tag{C2}$$

For NN the response of the axial potentials upon the change $f^A \to f^A_0 + \Delta f^A$ from (C1b) is

$$\begin{aligned} \Delta V_A(r) \;&=\; \Delta V_{A,a}(r) + \Delta V_{A,b}(r) = -\frac{m}{4\pi}\frac{m^2}{2M_N^2}\left[2\left(g_A + \frac{m^2}{2M_N^2} f_A\right)\Delta f^A \right. \\ &\left. + \frac{m^2}{2M_N^2}(\Delta f^A)^2\right] \cdot \left[\frac{1}{3}(\boldsymbol{\sigma}_1\cdot\boldsymbol{\sigma}_2)\ \phi^1_C + S_{12}\ \phi^0_T\right]. \end{aligned} \tag{C3}$$

Now, it turns out that for ESC16, with the parameters presented in this paper, the expression $[\ldots] > 0$ for the axial mesons $a_1(1270), f_1(1420), f_1(1285)$. The coupling constant for the compensating B-meson potential is

$$f^2_B(A) = \frac{3m^2}{2M_N^2}\left[2\left(g_A + \frac{m^2}{2M_N^2} f_A\right)\Delta f^A + \frac{m^2}{2M_N^2}(\Delta f^A)^2\right] \tag{C4}$$

From the results for the couplings it appears that changes in the derivative couplings can be made in order to satisfy (C2), which can be compensated by changing the B-meson couplings.

APPENDIX D: NON-LOCAL TENSOR-CORRECTION

In this appendix we repeat the treatment of the non-local correction correction to the tensor-potential similar to that for the central non-local potential

$$\Delta\widetilde{V}_T = \left(\mathbf{q}^2 + \frac{1}{4}\mathbf{k}^2\right)\widetilde{v}_T\ S_{12}. \tag{D1}$$

This incorporation of this kind of potential in the solution of the Schrödinger equation is given in [46], see Appendix D. For completeness we repeat here the treatment of this type of potential, which is exact when there is no non-local spin-orbit potential. For definiteness we consider the contribution to the π-exchange potential

$$\widetilde{v}_T = \frac{f_P^2}{2MM'\ m_\pi^2}\left(\mathbf{q}^2 + \frac{1}{4}\mathbf{k}^2\right)/(\mathbf{k}^2 + m^2). \tag{D2}$$

In configuration space this leads to the potential

$$\begin{aligned} V_T(r) \;&=\; \frac{f_P^2}{4\pi}\frac{m}{4MM'}\left[\frac{1}{3}(\boldsymbol{\sigma}_1\cdot\boldsymbol{\sigma}_2)\left(\nabla^2\phi^1_C + \phi^1_C\nabla^2\right) + \left(\nabla^2\phi^0_T S_{12} + \phi^0_T S_{12}\nabla^2\right)\right] \\ &\equiv\; -\left[\left(\nabla^2\phi(r) + \phi(r)\nabla^2\right) + \left(\nabla^2\chi(r)S_{12} + \chi(r)S_{12}\nabla^2\right)\right]. \end{aligned} \tag{D3}$$

Here we put $\boldsymbol{\sigma}_1\cdot\boldsymbol{\sigma}_2 = 1$, because this potential contributes for spin-triplet states only. The radial Schrödinger equation reads

$$\begin{aligned} &\left\{(1+2\phi) + 2\chi\ S_12\right\}\ u'' + \left(2\phi' + 2\chi'\ S_{12}\right)\ u' + \left[k^2_{cm} - 2M_{red}V\right. \\ &\left. -\left\{(1+2\phi) + \chi\ S_{12}\right\}\frac{\mathbf{L}^2}{r^2} - \frac{\mathbf{L}^2}{r^2}\chi\ S_{12} + \phi'' + \chi''\ S_{12}\right]\ u = 0. \end{aligned} \tag{D4}$$

Under the substitution $u = A^{-1/2}v$, where

$$A \equiv (1+2\phi) + 2\chi\ S_{12}, \tag{D5}$$

over into the radial equation for $v(r)$

$$v''(r) + \left[k^2_{cm} - \frac{l(l+1)}{r^2} - 2M_{red}W\right]\ v(r) = 0 \tag{D6}$$

with the (pseudo) potential

$$\begin{aligned} 2M_{red}W &= 2M_{red}A^{-1/2}V\ A^{-1/2} - A^{-2}\left(\phi' + \chi'\ S_{12}\right)^2 - \left(A^{-1} - 1\right)\ k_{cm}^2 \\ &\quad + \left\{A^{1/2}\left[L^2, A^{-1/2}\right] + A^{-1/2}\left[L^2, A^{1/2}\right]\right\}/(2r^2). \end{aligned} \tag{D7}$$

In passing we note that A and S_{12} commute, and therefore

$$A^{-2}\left(\phi' + \chi'\ S_{12}\right)^2 = \left[A^{-1/2}\left(\phi' + \chi'\ S_{12}\right)A^{-1/2}\right]^2 = \frac{1}{4}\left[A^{-1/2}\ A'\ A^{-1/2}\right]^2.$$

Defining

$$X = (1 + 2\phi + 4\chi)^{1/2} \quad , \quad Y = (1 + 2\phi - 8\chi)^{1/2}, \tag{D8}$$

the transformation A is given as

$$\begin{aligned} A^{1/2} &= \frac{1}{3}(2X + Y) + \frac{1}{6}(X - Y)\ S_{12} \\ A^{-1/2} &= \left\{\frac{1}{3}(X + 2Y) + \frac{1}{6}(-X + Y)\ S_{12}\right\}/(XY). \end{aligned} \tag{D9}$$

Using (D10) one readily derives

$$\begin{aligned} &\left\{A^{1/2}\left[L^2, A^{-1/2}\right]_- + A^{-1/2}\left[L^2, A^{1/2}\right]_-\right\} = \\ &-2\frac{(X-Y)^2}{XY}\ \frac{\sqrt{J(J+1)}}{2J+1}\ \begin{pmatrix} 2\sqrt{J(J+1)} & -1 \\ -1 & -2\sqrt{J(J+1)} \end{pmatrix}. \end{aligned} \tag{D10}$$

Writing $A^{-1} = \alpha + \beta\ S_{12}$ one finds

$$\begin{aligned} \alpha &= +(1 + 2\phi - 4\chi)\left[(1 + 2\phi + 4\chi)(1 + 2\phi - 8\chi)\right]^{-1}, \\ \beta &= -2\chi\ \left[(1 + 2\phi + 4\chi)(1 + 2\phi - 8\chi)\right]^{-1}, \end{aligned} \tag{D11}$$

leading to

$$\begin{aligned} -\left(A^{-1} - 1\right) &= \left[\left\{(2\phi - 8\chi)(1 + 2\phi + 4\chi) - 8\chi\right\} + 2\chi\ S_{12}\right]\cdot \\ &\quad \times\left[(1 + 2\phi + 4\chi)(1 + 2\phi - 8\chi)\right]^{-1}. \end{aligned} \tag{D12}$$

APPENDIX E: GAUSSIAN YUKAWA-FUNCTIONS

The basic Fourier transforms for the soft-core potentials is Refs. [3, 36]

$$\int \frac{d^3k}{(2\pi)^3}\frac{e^{i\mathbf{k}\cdot\mathbf{r}}}{\mathbf{k}^2 + m^2}(\mathbf{k}^2)^n \exp\left(-\mathbf{k}^2/\Lambda^2\right) \equiv \frac{m}{4\pi}(-m^2)^n \phi_C^n(r) = (-\boldsymbol{\nabla}^2)^n \frac{m}{4\pi}\phi_C^0(r), \tag{E1}$$

and similar ones for the tensor-, spin-orbit-, and the quadratic-spin-orbit potentials. The basic central, tensor, and spin-orbit functions are

(i) central potentials:

$$\phi_C^0(r) = \exp(m^2/\Lambda^2)\left[e^{-mr}\mathcal{E}rfc\left(-\frac{\Lambda r}{2} + \frac{m}{\Lambda}\right) - e^{mr}\mathcal{E}rfc\left(\frac{\Lambda r}{2} + \frac{m}{\Lambda}\right)\right]/2mr\ , \tag{E2a}$$

$$\phi_C^1(r) = \phi_C^0(r) - \frac{1}{2\sqrt{\pi}}\left(\frac{\Lambda}{m}\right)^3 \exp\left[-\left(\frac{\Lambda r}{2}\right)^2\right], \tag{E2b}$$

$$\phi_C^2(r) = \phi_C^1(r) + \frac{1}{2\sqrt{\pi}}\left(\frac{\Lambda}{m}\right)^5\left[\frac{3}{2} - \left(\frac{\Lambda r}{2}\right)^2\right] \exp\left[-\left(\frac{\Lambda r}{2}\right)^2\right], \tag{E2c}$$

(ii) tensor potentials:

$$\phi^0_T(r) = \frac{1}{3}\frac{1}{m^2} r\frac{\partial}{\partial r}\frac{1}{r}\frac{\partial}{\partial r}\phi^0_C(r) = \Big\{\exp(m^2/\Lambda^2)\Big[[1+mr+(mr)^2/3]e^{-mr}\cdot$$
$$\times\mathcal{E}rfc\left(-\frac{\Lambda r}{2}+\frac{m}{\Lambda}\right) - [1-mr+(mr)^2/3]e^{mr}\mathcal{E}rfc\left(\frac{\Lambda r}{2}+\frac{m}{\Lambda}\right)\Big]$$
$$-\frac{4}{\sqrt{\pi}}\left(\frac{\Lambda r}{2}\right)\left[1+\frac{2}{3}\left(\frac{\Lambda r}{2}\right)^2\right]\exp\left[-\left(\frac{\Lambda r}{2}\right)^2\right]\Big\}/2(mr)^3\ , \tag{E3a}$$
$$\phi^1_T(r) = \phi^0_T - \frac{1}{6\sqrt{\pi}}\left(\frac{\Lambda}{m}\right)^5\left(\frac{\Lambda r}{2}\right)^2\exp\left[-\left(\frac{\Lambda r}{2}\right)^2\right]. \tag{E3b}$$

(iii) spin-orbit potentials:

$$\phi^0_{SO}(r) = -\frac{1}{m^2}\frac{1}{r}\frac{\partial}{\partial r}\phi^0_C(r) = \Big\{\exp(m^2/\Lambda^2)\Big[[1+mr]e^{-mr}\cdot$$
$$\times\mathcal{E}rfc\left(-\frac{\Lambda r}{2}+\frac{m}{\Lambda}\right) - [1-mr]e^{mr}\mathcal{E}rfc\left(\frac{\Lambda r}{2}+\frac{m}{\Lambda}\right)\Big]$$
$$-\frac{4}{\sqrt{\pi}}\left(\frac{\Lambda r}{2}\right)\left(\frac{\Lambda r}{2}\right)\exp\left[-\left(\frac{\Lambda r}{2}\right)^2\right]\Big\}/2(mr)^3\ , \tag{E4a}$$
$$\phi^1_{SO}(r) = \phi^0_{SO} - \frac{1}{4\sqrt{\pi}}\left(\frac{\Lambda}{m}\right)^5\left(\frac{\Lambda r}{2}\right)^2\exp\left[-\left(\frac{\Lambda r}{2}\right)^2\right]. \tag{E4b}$$

(iv) quadratic-spin-orbit potentials:

$$\phi^0_Q(r) = -\frac{m^5}{4\pi}\frac{3}{(mr)^2}\phi^0_T(r). \tag{E5}$$

The Fourier transforms of the Pomeron-type of potentials are gaussian-integrals, which can be obtained from the above formulas by the substitutions

$$\frac{1}{2}\Lambda \equiv m_P,\quad m=0,\quad \phi_i^{P,n} = \phi_i^{n+1}. \tag{E6}$$

For explicit formulas see Refs. [3, 36].

APPENDIX F: NEW VERSION QUARK-PAIR-CREATION MODEL [65]

In this appendix we give a short description of the evaluation of the BBM coupling constants in the QPC-model using the Fierz-transformation technique. For details we refer to Ref. [65]. Here, apart from the Fierz-transformation, the techniques used are those of [27, 60, 63]. In Fig. 11 the two kind of processes, direct (a) and exchange (b), are shown. The derivation of the BBM-couplings starts from the generalized $^3P_0$ (S) and $^3S_1$ (V) Pair-creation Hamiltonians

$$\mathcal{H}_I^{(S)} = -4\gamma^{(S)}_{q\bar{q}}\left(\sum_i \bar{q}_i q_i\right)\cdot\left(\sum_j \bar{q}_j q_j\right),$$
$$\mathcal{H}_I^{(V)} = -\gamma^{(V)}_{q\bar{q}}\left(\sum_i \bar{q}_{i,\alpha}(\boldsymbol{\lambda})^\alpha{}_\beta\gamma^\mu q_{i,\beta}\right)\otimes\left(\sum_j \bar{q}_{j,\gamma}(\boldsymbol{\lambda})^\gamma{}_\delta\gamma_\mu q_{j,\delta}\right) \tag{F1}$$

where $\gamma^{(V)}_{q\bar{q}}$ is a phenomenological constant, and the summations run as $i,j = u,d,s$. In this QPC-model in the fundamental process there is a (confined) scalar or gluon propagator. This implies, assuming a constant propagator,

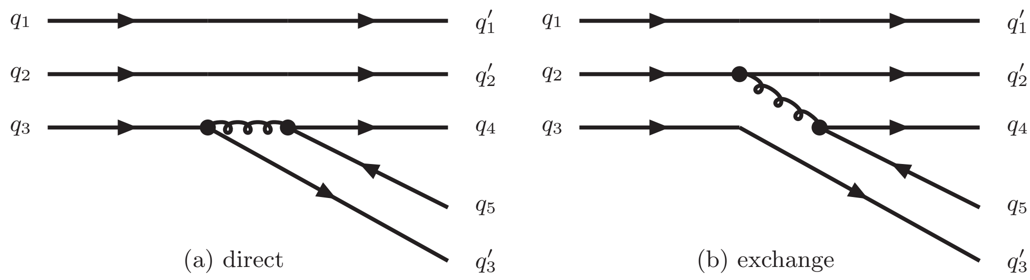

FIG. 11: $^3P_0$- *and* $^3S_1$*-quark-pair-creation (QPC)*

an extra factor depending on a scalar or (massive) gluon exchange $(-i)^2.(\mp i/m_G^2) \sim \pm i/\Lambda_{QPC}^2$. meaning $\sim \pm i H_{int}$. Rearrangement is supposed to take place when a quark-antiquark pair is created by some mechanism in a baryon, where one quark from the baryon combines into a mesonic state with the anti-quark from the pair. The quark from the pair recombines with the two remaining quarks of the baryon to make the baryon in the final state. This rearrangements into mesons of different kind can be understood from a Fierz-transformation applied to (F1). One has the identity [104]

$$\begin{aligned}
\mathcal{H}_I^{(S)} &= \gamma_{q\bar{q}}^{(S)} \sum_{i,j} \Biggl[+\ \bar{q}_i\ q_j \cdot \bar{q}_i\ q_j + \bar{q}_i \gamma_\mu q_j \cdot \bar{q}_j \gamma^\mu q_i \\
&-\frac{1}{2}\ \bar{q}_i \sigma_{\mu\nu} q_j \cdot \bar{q}_j \sigma^{\mu\nu} q_i - \bar{q}_i \gamma_\mu \gamma_5 q_j \cdot \bar{q}_j \gamma^\mu \gamma^5 q_i +\ \bar{q}_i \gamma_5 q_j \cdot \bar{q}_j \gamma^5 q_i \Biggr], \\
\mathcal{H}_I^{(V)} &= +\gamma_{q\bar{q}}^{(V)} \sum_{i,j} \Biggl[+\ \bar{q}_i\ q_j \cdot \bar{q}_i\ q_j - \frac{1}{2}\ \bar{q}_i \gamma_\mu q_j \cdot \bar{q}_j \gamma^\mu q_i \\
&-\frac{1}{2}\ \bar{q}_i \gamma_\mu \gamma_5 q_j \cdot \bar{q}_j \gamma^\mu \gamma^5 q_i -\ \bar{q}_i \gamma_5 q_j \cdot \bar{q}_j \gamma^5 q_i \Biggr].
\end{aligned} \tag{F2}$$

Here, we considered only the flavor-spin Fierzing. [5] The appropriate Fierzing of the color structure is different for diagram (a) and diagram (b) in Fig. 11: (i) For diagram (a) we use the identity [104]

$$(\boldsymbol{\lambda})^\gamma{}_\delta \cdot (\boldsymbol{\lambda})_\alpha{}^\beta = \frac{16}{9} \delta_\alpha^\gamma \delta_\delta^\beta - \frac{1}{3} (\boldsymbol{\lambda})_\alpha^\gamma \cdot (\boldsymbol{\lambda})_\delta^\beta \tag{F3}$$

Since the mesons are colorless, the second term in (F3) may be neglected, and color gives the simple factor 16/9. (ii) In diagram (b) there is in fact a sum over q_1 and q_2. Because the baryons are colorless, we have

$$(\boldsymbol{\lambda}_1)_\alpha{}^\beta + (\boldsymbol{\lambda}_2)_\alpha{}^\beta = -(\boldsymbol{\lambda}_3)_\alpha{}^\beta. \tag{F4}$$

Therefore, for this diagram we have, using (F3), the identity

$$(\boldsymbol{\lambda}_5)^\gamma{}_\delta \cdot \sum_{i=1,2} (\boldsymbol{\lambda}_i)_\alpha{}^\beta = -\frac{16}{9} \delta_\alpha^\gamma \delta_\delta^\beta + \frac{1}{3} (\boldsymbol{\lambda}_5)_\alpha^\gamma \cdot (\boldsymbol{\lambda}_3)_\delta^\beta \tag{F5}$$

Again, for colorless mesons the second term in (F5) may be neglected, and color gives the simple factor $-16/9$. *We find that the direct (a) and exchange (b) diagram give different color factors. Such a difference does not occur in the* $^3P_0$*-model. Now, it appears that the momentum overlap for type (b) is usually much smaller than for type (a), see Ref. [65] for details. This can be traced back to our use of a constant propagator for the (confined) gluon. Therefore, in the following we neglect processes described in diagram (b). Then, the difference between the* $^3P_0$*- and* $^3S_1$*-model is, apart from an overall constant, exclusively given by the different coefficients in the flavor-spin Fierz-identities (F2).*

---

[5] It should be noted that the terms for the couplings of the B-axial $J^{PC} = 1^{+-}$- and tensor $J^{PC} = 2^{++}$mesons are missing on the r.h.s. of (F2). The same is true for the $^3P_0$-interaction (F1).

In the $^3S_1$-model for the interaction Hamiltonian for the pair-creation one uses the one-gluon-exchange (OGE) model [105, 106], see Fig. 11. Considering one-gluon exchange, see Fig. 11, one derives the effective vertex [105, 106] by using a (confined) constant $P_g(ji)$ gluon propagator between quark line i and line j: $P_g(ji) \sim \delta_{ji}/m_g^2$, where the (effective) gluon mass is taken to be $m_g \approx (0.8 fm^{-1}) \approx 250$ MeV [106]. We notice that the color factor for the coupling of colorless mesons to colorless baryons is always the same, and we can include this into an effective coupling γ_S, i.e.

$$\frac{\pi\alpha_s(\boldsymbol{\lambda}_i\cdot\boldsymbol{\lambda}_j)}{m_G^2} \Rightarrow \gamma_{q\bar{q}}^{(V)} . \tag{F6}$$

Here we use for the gluon a constant (confined) propagator $P_g = 1/m_G^2$. As is clear from (F1) $\gamma_{q\bar{q}}$ has the dimension $[\text{MeV}]^{-2}$. Also, we notice that $m_G \approx \Lambda_{QPC}$, therefore $\gamma_{q\bar{q}} \longrightarrow \gamma_{q\bar{q}}/\Lambda_{QPC}^2$. From the momentum conservation rules one now gets different dependences between the momenta as compared to the version of the $^3P_0$-model in [27, 63]. Hence, we have different momentum overlap-integrals.

From the results for the couplings of the mesons in the $^3P_0$-model those for the $^3S_1$–model meson-couplings can be read off by comparing the coefficients in the Fierz-identities (F2) and (F1) for the corresponding operators. Here, we assume that the effect of color in the $^3P_0$- and $^3S_1$-model can be absorbed into $\gamma_{q\bar{q}}^{(S,V)}$, see below. For example, the prediction for the scalar-meson couplings will have the ratio $g_\epsilon(^3S_1) = \left[\gamma_{q\bar{q}}^{(V)}/\gamma_{q\bar{q}}^{(S)}\right] g_\epsilon(^3P_0)$. Apart from an overall constant, the couplings for the $^3S_1$-model can be read off from those of the $^3P_0$-model.

1. Meson-states, Meson- and baryon wave-functions

We list the $\langle B, M|H_{int}|A\rangle$ matrix elements for the different type of mesons. Restriction on the quark-level to process (a) in Fig. 11, using the Fierzed form of the interaction Hamiltonians in (F1). So, below we will give the results for the $^3P_0$-model. Following [107] we write the meson creation operators as

$$\begin{aligned}
J^{PC} = 0^{-+}: \quad d^\dagger_{M,P}(\mathbf{k}) &= i \sum_{r,s=\pm} \int d^3k_1 d^3k_2\ \delta(\mathbf{k}-\mathbf{k}_1-\mathbf{k}_2)\ \cdot \\
&\times \widetilde{\psi}_M^{(L=0)}(\mathbf{k}_1,\mathbf{k}_2)\ \varphi^{(0)}(r,s)\ b^\dagger(\mathbf{k}_1,r)\ d^\dagger(\mathbf{k}_2,s), &\text{(F7)}\\
J^{PC} = 1^{--}: \ d^\dagger_{M,V}(\mathbf{k},m) &= \sum_{r,s=\pm} \int d^3k_1 d^3k_2\ \delta(\mathbf{k}-\mathbf{k}_1-\mathbf{k}_2)\ \cdot \\
&\times \widetilde{\psi}_M^{(L=0)}(\mathbf{k}_1,\mathbf{k}_2)\ \varphi^{(1)}_m(r,s)\ b^\dagger(\mathbf{k}_1,r)\ d^\dagger(\mathbf{k}_2,s), &\text{(F8)}\\
J^{PC} = 0^{++}: \ d^\dagger_{M,S}(\mathbf{k},m) &= \sum_{r,s=\pm} \int d^3k_1 d^3k_2\ \delta(\mathbf{k}-\mathbf{k}_1-\mathbf{k}_2)\ (-)^m\cdot \\
&\times \widetilde{\psi}_{M,m}^{(L=1)}(\mathbf{k}_1,\mathbf{k}_2)\ \varphi^{(1)}_{-m}(r,s)\ b^\dagger(\mathbf{k}_1,r)\ d^\dagger(\mathbf{k}_2,s), &\text{(F9)}\\
J^{PC} = 1^{++}: \ d^\dagger_{M,A}(\mathbf{k},m) &= \sum_{r,s=\pm} \int d^3k_1 d^3k_2\ \delta(\mathbf{k}-\mathbf{k}_1-\mathbf{k}_2)\ C(1,1,1;m_L,m_\sigma,m)\cdot \\
&\times \widetilde{\psi}_{M,m_L}^{(L=1)}(\mathbf{k}_1,\mathbf{k}_2)\ \varphi^{(1)}_{m_\sigma}(r,s)\ b^\dagger(\mathbf{k}_1,r)\ d^\dagger(\mathbf{k}_2,s), &\text{(F10)}\\
J^{PC} = 1^{+-}: \ d^\dagger_{M,B}(\mathbf{k},m) &= \sum_{r,s=\pm} \int d^3k_1 d^3k_2\ \delta(\mathbf{k}-\mathbf{k}_1-\mathbf{k}_2)\ \cdot \\
&\times \widetilde{\psi}_{M,m}^{(L=1)}(\mathbf{k}_1,\mathbf{k}_2)\ \varphi^{(0)}(r,s)\ b^\dagger(\mathbf{k}_1,r)\ d^\dagger(\mathbf{k}_2,s), &\text{(F11)}\\
J^{PC} = 2^{++}: \ d^\dagger_{M,T}(\mathbf{k},m) &= \sum_{r,s=\pm} \int d^3k_1 d^3k_2\ \delta(\mathbf{k}-\mathbf{k}_1-\mathbf{k}_2)\ C(1,1,2;m_L,m_\sigma,m)\cdot \\
&\times \widetilde{\psi}_{M,m_L}^{(L=1)}(\mathbf{k}_1,\mathbf{k}_2)\ \varphi^{(1)}_{m_\sigma}(r,s)\ b^\dagger(\mathbf{k}_1,r)\ d^\dagger(\mathbf{k}_2,s), &\text{(F12)}
\end{aligned}$$

for respectively the pseudoscalar-, vector-, scalar-, axial-vector mesons of the first (A_1 etc.) and second kind (B_1 etc.), and tensor mesons. These representations are the equal-time Bethe-Salpeter wave functions [108]:

$$f_{\mathbf{k},\alpha}(x,y) \equiv \langle 0|T\left[q_i(x)q_j(y)\right]|M(\mathbf{k},\alpha\rangle \stackrel{x^0=y^0}{\longrightarrow} (0|q_i(\mathbf{x})q_j(\mathbf{y})|M(\mathbf{k},\alpha)\,,$$

using the definition $\theta[0]=1/2$. Here, a factor i is included in the definition of the $d^\dagger_{M,P}(\mathbf{k})$-operator. This in order to have under time-reversal $\mathcal{T}|\pi_0(\mathbf{k})\rangle = |\pi_0(-\mathbf{k})\rangle$. The reason is that under time-reversal the spin-components change sign, which implies for the spin-singlet $\varphi^{(0)}(-r,-s) = -\varphi^{(0)}(r,s)$ etc.
The baryon and meson harmonic oscillator wave functions are

$$\begin{aligned}
\widetilde{\psi}_N(\mathbf{k}_1,\mathbf{k}_2,\mathbf{k}_3) &= \left(\frac{\sqrt{3}R_A^2}{\pi}\right)^{3/2} \exp\left[-\frac{R_A^2}{6}\sum_{i<j}(\mathbf{k}_i-\mathbf{k}_j)^2\right] , \\
\widetilde{\psi}^{(L=0)}_M(\mathbf{k}_1,\mathbf{k}_2) &= \left(\frac{R_M^2}{\pi}\right)^{3/4} \exp\left[-\frac{R_M^2}{8}(\mathbf{k}_1-\mathbf{k}_2)^2\right] , \\
\widetilde{\psi}^{(L=1)}_{M,m}(\mathbf{k}_1,\mathbf{k}_2) &= \frac{R_M}{\sqrt{2}}\left(\frac{R_M^2}{\pi}\right)^{3/4} \left[-\boldsymbol{\epsilon}_m\cdot(\mathbf{k}_1-\mathbf{k}_2)\right] .\exp\left[-\frac{R_M^2}{8}(\mathbf{k}_1-\mathbf{k}_2)^2\right] .
\end{aligned}$$

Here we used the spherical unit vectors $\boldsymbol{\epsilon}_{\pm1} = \mp\frac{1}{\sqrt{2}}(\mathbf{e}_1 \pm i\mathbf{e}_2)$, $\boldsymbol{\epsilon}_0 = \mathbf{e}_3$.

2. Coupling-constant Formulas

The matrix elements $\langle B_f(\mathbf{p}')\ M(\mathbf{k})|\mathcal{H}_I^{(S),(V)}|B_i(\mathbf{p})\rangle$ involve the momentum space overlap integrals, which can be performed in a straightforward manner [65]. The summary of the derived formulas in [65], in the case of the ${}^3P_0$-model, for the divers (I=1)-couplings is:

$$\begin{aligned}
g_P &= +\pi^{-3/4}\ \gamma_{q\bar{q}}\ \frac{(m_P R_P)^{1/2}}{(\Lambda_{QPC}R_P)^2}\cdot(6\sqrt{2}) , \\
g_V &= +\pi^{-3/4}\ \gamma_{q\bar{q}}\ \frac{(m_V R_V)^{1/2}}{(\Lambda_{QPC}R_V)^2}\cdot(3/\sqrt{2}) , \\
g_S &= +\pi^{-3/4}\ \gamma_{q\bar{q}}\ \frac{(m_S R_S)^{-1/2}}{(\Lambda_{QPC}R_S)^2}\cdot\frac{9m_S}{M_B} , \\
g_A &= -\pi^{-3/4}\ \gamma_{q\bar{q}}\ \frac{(m_A R_A)^{-1/2}}{(\Lambda_{QPC}R_A)^2}\cdot\frac{6m_A}{M_B},
\end{aligned}$$

with $\Lambda_{QPC} \approx 600$ MeV, and $R_M \approx 0.66$.

---

[1] Th.A. Rijken, in *Proceedings of the XIVth European Conference on Few-Body Problems in Physics*, Amsterdam 1993, edited by B. Bakker and R. van Dantzig, Few-Body Systems, Suppl. **7**, 1 (1994).
[2] M.M. Nagels, T.A. Rijken, and J.J. deSwart, Phys. Rev. D 15 (1977) 2547.
[3] P.M.M. Maessen, Th.A. Rijken, and J.J. de Swart, Phys. Rev. C **40** (1989) 2226.
[4] J.J. de Swart Rev. Mod. Phys. **35**, 916 (1963). Here, the ratio $\alpha \equiv F/(F+D)$ is defined in Eq. (17.7).
[5] Th.A. Rijken, Phys. Rev. **C73**, 044007 (2006).
[6] Th.A. Rijken and Y. Yamamoto, Phys. Rev. **C73**, 044008 (2006).
[7] Th.A. Rijken and Y. Yamamoto, *Extended-soft-core Baryon-Baryon Model, III.* $S=-2$: $\Lambda\Lambda, \Xi N$ *etc. Scattering* , nucl-th/0608074.
[8] Th.A. Rijken, M.M. Nagels, and Y. Yamamoto, Nucl. Phys. **A 835** (2010) 160.
[9] Th.A. Rijken, M.M. Nagels, and Y. Yamamoto, Progres of Theoretical Physics Suppl. No. **185**, 14 (2010).
[10] Th.A. Rijken, V.G.J. Stoks, and Y. Yamamoto, Phys. Rev. C 59 (1999) 21.
[11] V.G.J. Stoks, R.A.M. Klomp, M.C.M. Rentmeester, and J.J. de Swart, Phys. Rev. C 48 (1993) 792.
[12] R.A.M. Klomp, private communication (unpublished).
[13] O. Hashimoto and H. Tamura, *Spectroscopy of* Λ*-hypernuclei*, progress in Particle and Nuclear Physics **57** (2006) 564-653.
[14] H. Takahashi et al., Phys. Rev. Lett. 87 (2001) 212502.
[15] M.M. Nagels, Th.A. Rijken, and Y. Yamamoto, *Extended-soft-core Baryon-baryon Model ESC16. II. Hyperon-Nucleon Interactions*, to be published (referred to as II).
[16] M.M. Nagels, Th.A. Rijken, and Y. Yamamoto, *Extended-soft-core Baryon-baryon Model ESC16. III. Hyperon-Hyperon Interactions*, to be published (referred to as III).
[17] A. Manohar and H. Georgi, Nucl. Phys. **B234** (1984) 189.

[18] G.A. Miller, Phys. Rev. **C 39** (1989) 1563.
[19] P.V. Landshoff and O. Nachtmann, Z. f. Physik, **C 35** (1987) 405.
[20] F.J. Ynduráin, *Quantum chromodynamics* (Springer, Berlin, 1980), see chapter IV for a description and references original literature.
[21] J. Gasser and H. Leutwyler, Nucl. Phys. **B94** (1975) 269.
[22] S. Gasiorowicz and J.L. Rossner, Am. J. Phys. **49** (1981) 954. Here, one uses the constituent quark masses: $m_u = m_d = 310$ MeV and $m_s = 483$ MeV.
[23] B. Povh et al, *Particles and Nuclei* (Springer, Berlin, 1995).
[24] H.D. Politzer, Nucl. Phys. **B117** (1976) 397.
[25] M. Lavelle and D. McMullan, Physics Reports **279** (1997) 1-65. In this reference an extensive discussion of the dressing-problem can be found.
[26] L. Micu, Nucl. Phys. **B10** (1969) 521; R. Carlitz and M. Kislinger, Phys. Rev. D **2** (1970) 336.
[27] A. Le Yaouanc, L. Oliver, O. Péne, and J.-C. Raynal, Phys. Rev. D **8** (1973) 2223; Phys. Rev. D **11** (1975) 1272.
[28] This pair-creation mechanism has been shown to be dominant in Lattice QCD. See: N. Isgur and J. Paton, Phys. Rev. **D31**, 2910 (1985).
[29] J. Schwinger, Phys. Rev. Lett. **18**, 923 (1967); Phys. Rev. **167**, 1432 (1968); *Particles and Sources*, Gordon and breach, Science publishers, Inc., New York, 1969.
[30] S. Weinberg, Phys. Phys. 166 (1968) 1568; Phys. Phys. 177 (1969) 2604.
[31] V. De Alfaro, S. Fubini, G. Furlan, and C. Rosetti, *Currents in Hadron Physics* Ch. 5, North-Holland Pulishing Company, Amsterdam 1973.
[32] C. Patrignani et al (Particle Data Group), Chin. Phys. **C 40**, 100001 (2016).
[33] M. Gell-Mann, Phys. Rev. **125**, 1067 (1962); S. Okubo, Progr. Theor. Phys. **27** 949 (1962); ibid **28** 24 (1962).
[34] V.G.J. Stoks and Th.A. Rijken, Nucl. Phys. **A 613** (1997) 311.
[35] M. Ablikim et al, Phys. Lett. **B 645** (2007) 19. In this analysis of the $J/\psi \to \omega\pi^+\pi^-$ data the ε-pole is at $E(\varepsilon) = (552 - i\ 232)$ MeV, which corresponds to $m_\varepsilon = 620$ MeV, $\Gamma_\varepsilon = 464$ MeV.
[36] M.M. Nagels, Th.A. Rijken, and J.J. de Swart, Phys. Rev. D **17** (1978) 768.
[37] Th.A. Rijken, Ann. Phys. (N.Y.) **208**, 253 (1991).
[38] Th.A. Rijken and V.G.J. Stoks, Phys. Rev. C 54 (1996) 2851;
[39] Th.A. Rijken and V.G.J. Stoks, Phys. Rev. C 54 (1996) 2869;
[40] F.E. Low, Phys. **D 12**, 163 (1975).
[41] S. Nussinov, Phys. Rev. Lett., **34**, 1286 (1975).
[42] J.J. de Swart, T.A. Rijken, P.M. Maessen, and R.G.E. Timmermans, Nuov. Cim. **102 A**, 203 (1989).
[43] S. Otsuki, R. Tamagaki, and W. Wada, Progr. Theor. Phys. **32** (1964) 320; S. Otsuki, R. Tamagaki, and M. Yasuno, Progr. Theor. Phys. Suppl. Extra number (1965), 578.
[44] M. Oka, K. Shimizu, and K. Yazaki, Progr. Theor. Phys. Suppl. **137**, 1 (2000).
[45] Y. Fujiwara, Y. Suzuki, and C. Nakamoto, Progr. in Part. and Nuclear physics, **58** (2007) 439.
[46] M.M. Nagels, T.A. Rijken, and J.J. de Swart, *N-N Potentials from Regge-Pole Theory*, in Few body Systems and Nuclear Forces I, Proceedings Graz 1978, Edited by H.Zingl, M. Haftel, and H. Zankel. Springer-Verlag, Berlin Heidelberg New york.
[47] T.A. Rijken, Ann. Phys. (N.Y.), **164** (1985) 1,23.
[48] A.A. Logunov and A.N. Tavkhelidze, Nuovo Cimento **29**, 380 (1963); R. Blankenbecler and R. Sugar, Phys. Rev. **142**, 1051 (1966); M.H. Partovi and E.L. Lomon, Phys. Rev. **D2**, 1999 (1970).
[49] R.H. Thompson, Phys. Rev. **D1**, 110 (1970).
[50] A. Gersten, P.A. Verhoeven, and JJ.J. de Swart, Nuovo Cimento **A26**, 375 (1975).
[51] A. Klein, Phys. Rev. **90**, 1101 (1952); W. Macke, Z. Naturforsch. **89**, 599 (1953); **89**, 615 (1953).
[52] A. Klein and T-S. H. Lee, Phys. Rev. **D12**, 4308 (1974).
[53] J.J. de Swart, M.M. Nagels, T.A. Rijken, and P.A. Verhoeven, Springer tracts in Modern Physics, Vol. **60**, 137 (1971).
[54] S. Okubo and R.E. Marshak, Ann. Phys. (N.Y.) **4**, 166 (1968).
[55] J.T. Brown, B.W. Downs, and C.K. Iddings, Ann. Phys. (N.Y.) **60**, 148 (1970).
[56] C. Itzykson and J-B Zuber, 'Quantum Field Theory', McGraw-Hill Inc. 1980.
[57] N. Nakanishi, Suppl. Progr. Theor. Phys. **51** (1972) 1
[58] N. Nakanishi and I. Ojima, 'Covariant Operator Formalism of Gauge Theories and quantum Gravity', section 2.4.2, World Scientific Lecture Notes in Physics, Vol. 27, World Scientific Pub. Co 1990.
[59] J.D. Bjorken and S.D. Drell, *Relativistic Quantum Mechanics* and *Relativistic Quantum Fields* (McGraw-Hill Inc., New York, 1965).
[60] A. Le Yaouanc, L. Oliver, O. Péne, and J.-C. Raynal, Phys. Rev. D **12** (1975) 2137; ibid **18**, 1591 (1978).
[61] R. van Royen and V.F. Weisskopf, Nuovo Cimento A **50**, 617 (1967).
[62] E. Leader and E. Predazzi, *An introduction to gauge theories and modern particle physics*, Vol. I, chapter 12, Cambridge Monographs on Particle Physics, Nuclear Physics and Cosmology, Editors T. Ericson and P.V. Landshoff, Cambridge University Press 1996.
[63] M. Chaichian and R. Kögerler,Ann. Phys. **124**, 61 (1980).
[64] *Review of Particle Physics*, Particle Data Group, Phys. Rev. **D 66** 010001-1 (2002).
[65] Th. A. Rijken, *Baryon-baryon Couplings in the* $^3P_0$ *and* $^3S_1$ *QPC-models*, Notes University of Nijmegen, Nijmegen, The Netherlands, *NN-online, THEF 12.01.*

[66] Th.A. Rijken, *Nucleon-Nucleon Interactions*, talk at KITPC workshop on Present Status Nuclear Interaction Theory, Beijin August 2014.
[67] Y. Yamamoto, T. Motoba, and Th.A. Rijken, *G-matrix approach to Hyperon-Nucleus systems*, Progr. Theor. Phys. Suppl. **185** (2010) 72.
[68] R.A. Bryan and A. Gersten, Phys. Rev. D **6** (1972) 341.
[69] D.V. Bugg and R.A. Bryan, Nucl. Phys. **A540** (1992) 449.
[70] V.G.J. Stoks, R.A.M. Klomp, C.P.F. Terheggen, and J.J. de Swart, Phys. Rev. C**49** (1994) 2950.
[71] M.M. Nagels, Th.A. Rijken, J.J. deSwart, G.C. Oades, J.L. Petersen, A.C. Irving, C. Jarlskog, W. Pfeil, H. Pilkuhn, and H.P. Jacob, Nucl. Phys. **B 147** (1979) 189-276.
[72] D.E. Gonzales Trotter et al, Phys. Rev. Lett. **83** (1999) 3788.
[73] V. Huhn et al, Phys. Rev. Lett. **85** (2000) 1190.
[74] G.A. Miller, B.M.K. Nefkens, and I. Šlaus, Phys. Rep. **194**, 1-116 (1990)
[75] E. Epelbaum, H.-W. Hammer, and U.-G. Meissner, Rev. Mod. Phys. **81** (2009) 1773.
[76] A. Andronic, P. Braun-Munzinger, and J. Stachel, Physics Letters B 673 (2009) 142.
[77] R. Kokoski and N. Isgur, Phys. Rev. **D 35** (1987) 907.
[78] S. Kumano and V.R. Pandharipande, Phys. Rev. **D 38** (1988) 146.
[79] R. Navarro Perez, J.E. Amaro, and E. Riu Arriola, Phys. Rev. **C 88** (2013) 024002.
[80] B. von Przewoski *et al*, Phys. Rev. **C 58** (1998) 1897.
[81] C.E. Allgower *et al*, Phys. Rev. **C 62** (2000) 064001.
[82] I.E. Lagaris and V.R. Pandharipande, Nucl. Phys. bf A 359 (1981) 349.
[83] H.-J. Schulze and Th.A. Rijken, Phys. Rev. **C 84** (2011) 035801.
[84] M. Baldo, G.F. Burgio and H.-J. Schulze, Phys. Rev. **C61** (2000), 055801.
[85] I. Vidana, A. Polls, A. Ramos, L. Engvik and M. Hjorth-Jensen, Phys. Rev. **C62** (2000), 035801.
[86] S. Nishizaki, Y. Yamamoto, and T. Takatsuka, Progr. Theor. Phys. **105**, 607 (2001); **108**, 703 (2002).
[87] A.B.Kaidalov and K.A. Ter-Martirosian, Nucl. Phys. B75 (1974), 471.
[88] J.B. Bronzan and R.L. Sugar, Phys. Rev. D16 (1977), 466.
[89] Th.A. Rijken, *Multiple-Pomeron Coupling and the Universal Repulsion in Nuclear/Hyperonic Matter. I. Triple-Pomeron Vertices*, notes Nijmegen 2005 (unpublished).
[90] Th.A. Rijken, *Multi-Pomeron Exchange and the Universal Repulsion in Nuclear/Hyperonic Matter*, NN-online, THEF 08.01.
[91] Y. Yamamoto, T. Furumoto, N. Yasutake, and Th.A. Rijken, Phys. Rev. **C 88**, 022801(R) (2013).
[92] Y. Yamamoto, T. Furumoto, N. Yasutake, and Th.A. Rijken, Phys. Rev. **C 90**, 045805 (2014).
[93] Y. Yamamoto, T. Furumoto, N. Yasutake, and Th.A. Rijken, Eur. Phys. J. **A52** (2016) 19.
[94] Y. Yamamoto, H. Togashi, T. Tamagawa, T. Furumoto, N. Yasutake, and Th.A. Rijken, Phys. Rev. **C 96**, 065804 (2017).
[95] P.B. Cemorest, T. Pennucci, S.M. Ransom, M.S.E. Roberts, and J.W. Hessels, Nature(London) **467** (2010), 1081.
[96] J. Antoniadis et al, Science **340** (2013), 6131.
[97] R.R. Scheerbaum, Nucl. Phys. A257 (1976) 77.
[98] E. Hiyama, M. Kamimura, T. Motoba, T. Yamada, and Y. Yamamoto, Phys. Rev. Lett. 85 (2000) 270.
[99] C.J. Batty, E. Friedman, and A. Gal, Prog. Theor. Phys. Suppl. No.117 (1994) 227.
[100] J. Dabrowski, Phys. Rev. C 60 (1999) 025205.
[101] H. Noumi et al, Phys. Rev. Lett. 89 (2002) 072301.
[102] M. Kohno, Y. Fujiwara, Y. Watanabe, K. Ogata, and M. Kawai, Prog. Theor. Phys. 112 (2004) 895.
[103] Th. A. Rijken, R.A.M. Klomp, and J.J. de Swart, *A Gift of Prophecy*, Essays in celebration of the life of Robert Marshak. Edited by E.C.G. Sudarshan, World scientific publishing Co., 1994.
[104] L.B. Okun, *Leptons and Quarks*, chapter 29, North-Holland Publishing Company 1984.
[105] A. De Rújula, H. Georgi, and S.L. Glashow, Phys. Rev. **D 12**, 147 (1975).
[106] E.M. Henley and Z.-Y. Zhang, Nucl. Phys. **A472**, 759 (1987). **D 12**, 147 (1975).
[107] R. Van Royen and V.F. Weisskopf, Nuovo Cimento **50 A**, 617 (1967).
[108] M. Gell-Mann and F. Low, Phys. Rev. **51**, 350 (1951).